NAVAL POSTGRADUATE SCHOOL
Monterey, California

THESIS

MEASUREMENTS OF DIRECT PATH AND FOLDED PATH OPTICAL SCINTILLATION

by

Bradford Arthur Speer

and

Frederick Hobbs Parker

December 1982

Thesis Advisor: E. A. Milne

Unclassified

SECURITY CLASSIFICATION OF THIS PAGE (When Data Entered)

REPORT DOCUMENTATION PAGE		READ INSTRUCTIONS BEFORE COMPLETING FORM
1. REPORT NUMBER	2. GOVT ACCESSION NO. AD-A126627	3. RECIPIENT'S CATALOG NUMBER
4. TITLE (and Subtitle) Measurements of Direct Path and Folded Path Optical Scintillation		5. TYPE OF REPORT & PERIOD COVERED Master's Thesis December 1982
		6. PERFORMING ORG. REPORT NUMBER
7. AUTHOR(s) Frederick Hobbs Parker Bradford Arthur Speer		8. CONTRACT OR GRANT NUMBER(s)
9. PERFORMING ORGANIZATION NAME AND ADDRESS Naval Postgraduate School Monterey, CA 93940		10. PROGRAM ELEMENT, PROJECT, TASK AREA & WORK UNIT NUMBERS
11. CONTROLLING OFFICE NAME AND ADDRESS Naval Postgraduate School Monterey, CA 93940		12. REPORT DATE December 1982
		13. NUMBER OF PAGES 183
14. MONITORING AGENCY NAME & ADDRESS(if different from Controlling Office)		15. SECURITY CLASS. (of this report) Unclassified
		15a. DECLASSIFICATION/DOWNGRADING SCHEDULE

16. DISTRIBUTION STATEMENT (of this Report)

Approved for public release; distribution unlimited

17. DISTRIBUTION STATEMENT (of the abstract entered in Block 20, if different from Report)

18. SUPPLEMENTARY NOTES

19. KEY WORDS (Continue on reverse side if necessary and identify by block number)

Scintillation Measurements, Atmospheric Optical Scintillation

20. ABSTRACT (Continue on reverse side if necessary and identify by block number)

A theoretical prediction by Dr. Avihu Ze'evi of the correlation between direct path and folded path optical scintillation was developed and published at the Naval Postgraduate School in March 1982. Simultaneously, a method for measuring the scintillation of two laser beams propagating along direct and folded paths was devised and used to record preliminary findings supporting the theoretical

(continued)

DD FORM 1 JAN 73 1473 EDITION OF 1 NOV 65 IS OBSOLETE S/N 0102-014-6601

Unclassified

SECURITY CLASSIFICATION OF THIS PAGE (When Data Entered)

Item 20. (continued)

work. This system has been improved upon to permit a complete experimental verification of the theory to be attempted outside the laboratory. The experimental results do not support Dr. Ze'evi's theory; however, changing turbulence conditions while measuring the scintillation strength may have been the cause. Further attempts at verification will have to control this factor.

Approved for public release; distribution unlimited

Measurements of Direct Path and Folded Path Optical Scintillation

by

Bradford Arthur Speer
Lieutenant, United States Navy
B.S., United States Naval Academy, 1976

and

Frederick Hobbs Parker
Lieutenant, United States Navy
B.S., Cornell University, 1975

Submitted in partial fulfillment of the requirements for the degree of

MASTER OF SCIENCE IN PHYSICS

from the

NAVAL POSTGRADUATE SCHOOL
December 1982

Author: Bradford Arthur Speer

Author: Frederick Hobbs Parker

Approved by: Edmund A. Milne
Thesis Advisor

D. Wayne Radebaugh
Second Reader

Chairman, Department of Physics

William M. Tolles
Dean of Science and Engineering

ABSTRACT

A theoretical prediction by Dr. Avihu Ze'evi of the correlation between direct path and folded path optical scintillation was developed and published at the Naval Postgraduate School in March 1982. Simultaneously, a method for measuring the scintillation of two laser beams propagating along direct and folded paths was devised and used to record preliminary findings supporting the theoretical work. This system has been improved upon to permit a complete experimental verification of the theory to be attempted outside the laboratory. The experimental results do not support Dr. Ze'evi's theory; however, changing turbulence conditions while measuring the scintillation strength may have been the cause. Further attempts at verification will have to control this factor.

TABLE OF CONTENTS

ACKNOWLEDGEMENTS

The authors would like to gratefully acknowledge the help received from a variety of sources. The continued assistance of both Robert C. Moeller and Thomas G. Maris, Model Makers, was invaluable. Their excellent design and fabrication of numerous optical components and precision mountings enabled us to carry out the experimentation phase of our thesis with a high degree of flexibility and accuracy.

The rapid response of Robert A. Sanders,Physical Scientist, in the repair and calibration of a variety of electronic components throughout the course of the experiment saved many hours of delay and allowed our progress to continue.

Finally, the many hours of help and consulation by our thesis advisors, Professors E. C. Crittenden and E. A. Milne, are gratefully acknowledged. Their patience and dedication to this project inspired us, and they willingly gave generously of their time and knowledge throughout the course of our work.

I. INTRODUCTION

A. BACKGROUND

When light from a constant source propagates through the atmosphere, the intensity distribution at a point on the receiver is altered by inhomogeneities in the atmospheric index of refraction along the path. In simple, quantitative models, the index of refraction is primarily a real function of temperature and pressure, and has the following form:

$$n(r) = n_o + n_1(r)$$

where

$n(r)$ is the real index of refraction at a point r,

$n_o = \langle n(r,t) \rangle$ is the time averaged (ensemble) value of $n(r)$ at a point r, usually given the value of 1, and

$n_1(r)$ is the perturbation in refractive index at a point r such that $n_1(r) << n_o$.

If we assume that pressure fluctuations in the atmosphere are small (an isobaric atmosphere) then the index of refraction at a point becomes a function of temperature.

Within the atmosphere near the Earth's surface, point temperature inhomogeneities are caused by convection on a large scale and random molecular motion on the microscale. Large scale vertical temperature gradients in this boundary

layer generate large scale motion of air masses, imparting energy to the velocity field and creating turbulent eddies of a size comparable with the inversion height or height above ground. In the Kolmogorov model of turbulence, these large vortices break down into smaller and smaller vortices until the flow stabilizes at a minimum vortex size where the local Reynolds number within the vortex is less than the critical value for air [Ref. 1]. The outer scale of the turbulence (diameter of the large scale vortex) is termed L_o and the inner scale (diameter of the small scale vortex) is termed ℓ_o. Turbulent vortices throughout the spectrum of sizes from L_o to ℓ_o result in variations in the index of refraction at any given point in the atmosphere as a function of time.

An accepted measure of the turbulence in the atmosphere is the refractive index structure constant, C_n^2 . C_n^2 is proportional to $n_1(r)$ and may be derived from wire probe temperature difference sensors. Typical values for C_n^2 in the lower atmosphere range from 10^{-17} $(m^{-2/3})$ for weak turbulence to 10^{-12} $(m^{-2/3})$ for strong turbulence. As one would expect for a temperature dependent parameter C_n^2 , varies diurnally and reaches a peak during the midday period. [Ref. 2].

Direct path optical scintillation may be defined as fluctuations in the irradiance (common usage is to refer to

the irradiance as intensity) at the receiver, due to inhomogeneities in the index of refraction over the propagation length causing random dispersion of the light as a function of space and time. Because C_n^2 is a direct measure of the level of atmospheric turbulence, it also varies directly with the amount of scintillation observed, and appears in equations describing the strength of the scintillation.

An accepted measure of the scintillation strength is the variance of the normalized intensity, as follows:

$$\frac{\sigma_I^2}{I_o} = \langle (I/I_o)^2 \rangle - \langle I/I_o \rangle^2$$

$$= [\langle I^2 \rangle - \langle I \rangle^2]/I_o^2$$

$$= \sigma_I^2 \ / \ I_o^2$$

where $I = I(r,t)$ is the intensity on the receiver at an instant in time,

$I_o = \langle I(r,t) \rangle$ is the ensemble average, and

$\sigma_I^2 = \langle I^2 \rangle - \langle I \rangle^2$.

Experimentally it has been found that if we restrict ourselves to regions of weak turbulence, then the log intensity of the electromagnetic field is also a random variable with normal distribution [Ref. 3]. It is therefore convenient to describe the scintillation strength as the log intensity variance, as follows:

for $\ell = \log (I/I_o)$

then $\sigma_\ell^2 = \langle \ell^2 \rangle - \langle \ell \rangle^2$

and $\sigma_\ell^2 = \langle [\log (\frac{I}{I_o})^2] \rangle - \langle \log (\frac{I}{I_o}) \rangle^2$

$= \langle (\log I - \log I_o)^2 \rangle - \langle \log I - \log I_o \rangle^2$

$= \langle (\log I)^2 \rangle - 2 \log I_o \langle \log I \rangle +$

$(\log I_o)^2 - \langle \log I \rangle^2 - (\log I_o)^2$

$+ 2 \log I_o \langle \log I \rangle$

$= \langle (\log I)^2 \rangle - \langle \log I \rangle^2$

$= \sigma^2_{\log I}$.

Thus, $\sigma_\ell^2 = \sigma^2_{\log I}$.

In this way the variance of the received signal intensity is seen to have no dependence upon the average signal intensity, and the log normal distribution may be completely described by a single parameter, σ_ℓ^2.

Assuming conditions of homogeneous turbulence with $\ell_o << (\lambda L)^{1/2}$, the log amplitude variance was shown by Tatarski [Refs. 3, 4] to obey the following relations:

Plane Waves $\sigma_x^2 = 0.31\ K^{7/6}\ C_n^2\ L^{11/6}$

Spherical Waves $\sigma_x^2 = .125\ K^{7/6}\ C_n^2\ L^{11/6}$

where $K = 2\pi/\lambda$,

L = path length,

λ is the optical wavelength, and

σ_x^2 = log amplitude variance of the signal.

These equations may be related to the log intensity variance by noting that

$$\sigma_\ell^2 \simeq 4\ \sigma_x^2.$$

We then have the following:

Plane Waves $\sigma_\ell^2 = 1.24\ K^{7/6}\ C_n^2\ L^{11/6}$.

Spherical Waves $\sigma_\ell^2 = 0.52\ K^{7/6}\ C_n^2\ L^{11/6}$.

The restriction that $\ell_o << (\lambda L)^{1/2}$ equates to a minimum vortex size of approximately 0.8 cm for λ = .6328 micrometer (HeNe laser source) with a path length of 100 meters. More recent observations [Ref. 5] report general agreement with these equations for

$$\sigma_x^2 < 0.3$$

and

$$\sigma_\ell^2 < 1.2.$$

This is the criteria we chose to use in defining the weak turbulence regime for our experiment.

Direct path optical scintillation is an important consideration in many practical situations of military interest. Optical laser communication, laser spotting, target illumination, and power transmission are just a few of these. Rigorous theoretical analyses of direct path scintillation by many authors over the last few decades have resulted in a fairly high degree of confidence that the factors involved in direct path scintillation, especially turbulence, are well understood. Theoretical predictions of signal log intensity variance, or scintillation strength, agree reasonably well with experimental findings. The correlation between direct and folded path scintillation strength is less well documented or understood. In his doctoral thesis at the Naval Postgraduate School, Dr. Avihu Ze'evi examined the special case of folded path scintillation using a plane mirror target and a point detector in the vicinity of or at the same location as the optical transmitter. The correlation of the scintillation strength for a folded path with the scintillation strength for a direct path was formulated. It is this correlation that we sought to verify in our experiment.

B. FOLDED PATH THEORY

In his theoretical treatment of the folded path problem, Ze'evi [Ref. 1] bases his work on the following assumptions:

1. The end points of the folded path are close in comparison with the length of the path.

2. The target that folds the path is a specular reflector such that there is no discontinuity of the light rays.

3. An infinite plane mirror or at least a very large mirror is used as the specular reflector so that all of the beam is reflected. This assumption excludes the effect of beam wander and neglects diffraction effects.

He then goes on to state that the basic question that must be addressed in determining any correlation between the direct path and folded path situations is whether or not the two parts of the folded path are statistically independent. If one can assume statistical independence, then the two parts of the folded path can be treated separately, applying the well known results for direct path propagation to each path. Figure 1 illustrates the situation where the light from a laser source is partially reflected and partially transmitted at a specular target. $\langle S_F^2 \rangle$ and $\langle S_{2L}^2 \rangle$ represent the variance of the signal log intensity at a point along the folded and the direct paths, respectively, such that the distances to each point along these respective paths are equal. Then for the two parts of the folded path to be statistically independent,

$$\langle S_F^2 \rangle = \langle S_{2L}^2 \rangle .$$

In his work, Ze'evi shows that

$$\langle S_F^2 \rangle = \langle S_{2L}^2 \rangle \quad (1 + f(y_o, \theta))$$

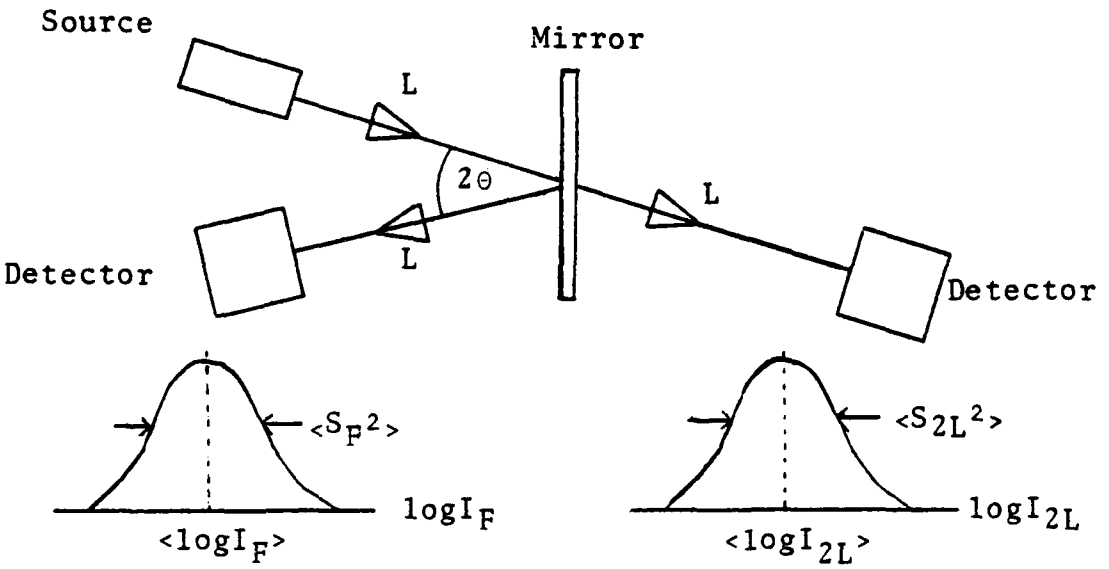

Figure 1. The reflected (folded path) and transmitted distributions at a distance 2L from a point source.

where $f(y_o, \theta)$ is the path dependency function, arrived at by numerical integration. The path dependency function is illustrated in Figure 2. The parameter, y_o, is defined to be

$$y_o = \frac{L \sin(2\theta)}{L_o}$$

$$\simeq D/L_o,$$

where D is the source detector displacement and θ is the half angle between the two parts of the folded path, illustrated in Figure 3. For small angles of θ, the f dependency is relatively weak, and the expression for $\langle S_F^2 \rangle$ then becomes

$$\langle S_F^2 \rangle \simeq \langle S_{2L}^2 \rangle \, (1 + f(y_o)).$$

We then have the following:

$$\lim f(y_o, \theta) = 1 \qquad \text{when } \theta \longrightarrow 0, \quad y_o \longrightarrow \theta$$

$$y_o \longrightarrow 0$$

$$\lim f(y_o, \theta) = 0$$

$$0 \longrightarrow \frac{\pi}{4}$$

then

$$\langle S_F^2(L, \theta) \rangle = \begin{cases} 2\langle S_{2L}^2 \rangle, & \theta = 0 \\ \\ \langle S_{2L}^2 \rangle, & \theta = \frac{\pi}{4} \end{cases}$$

Thus, it is clear that the paths are statistically independent only for $2\theta = \frac{\pi}{2}$; however, because $f(y_o, \theta)$ decreases rapidly

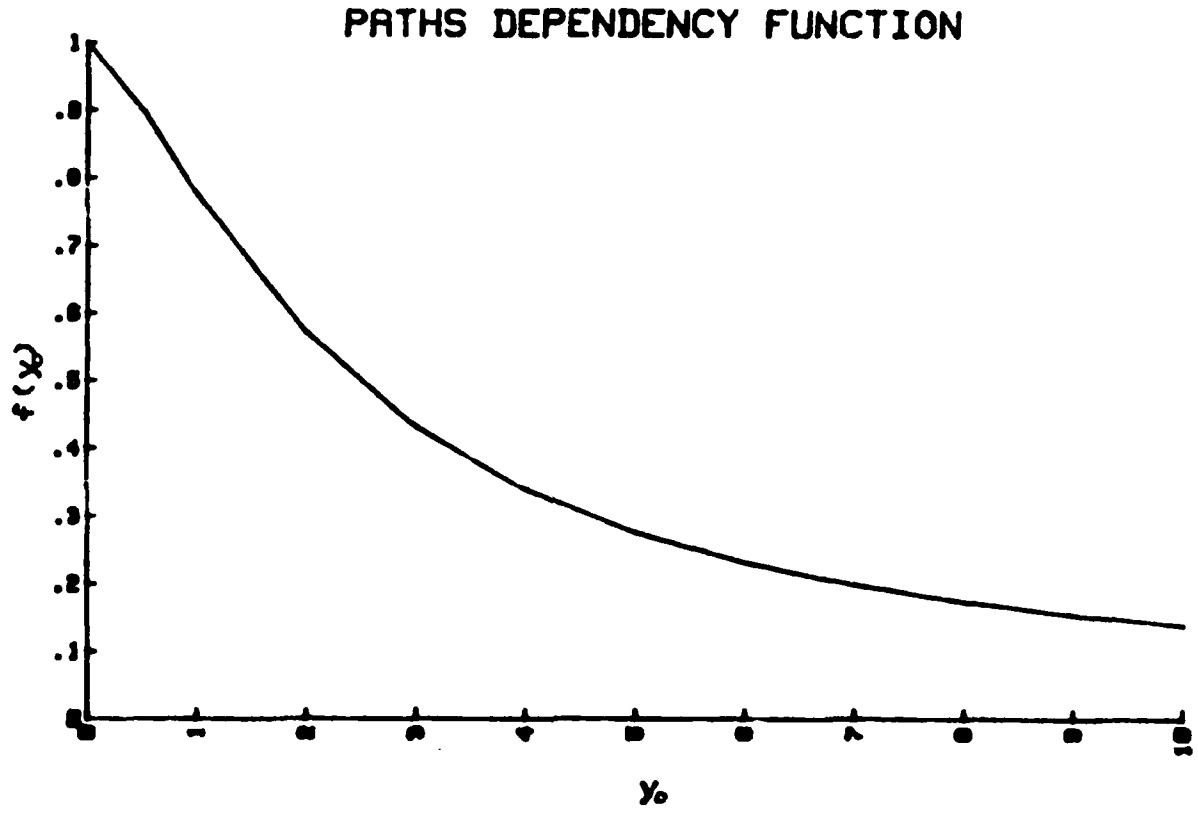

Figure 2. The Behavior of $f(y_o, \theta)$ as a Function of y_o for Small Value of θ

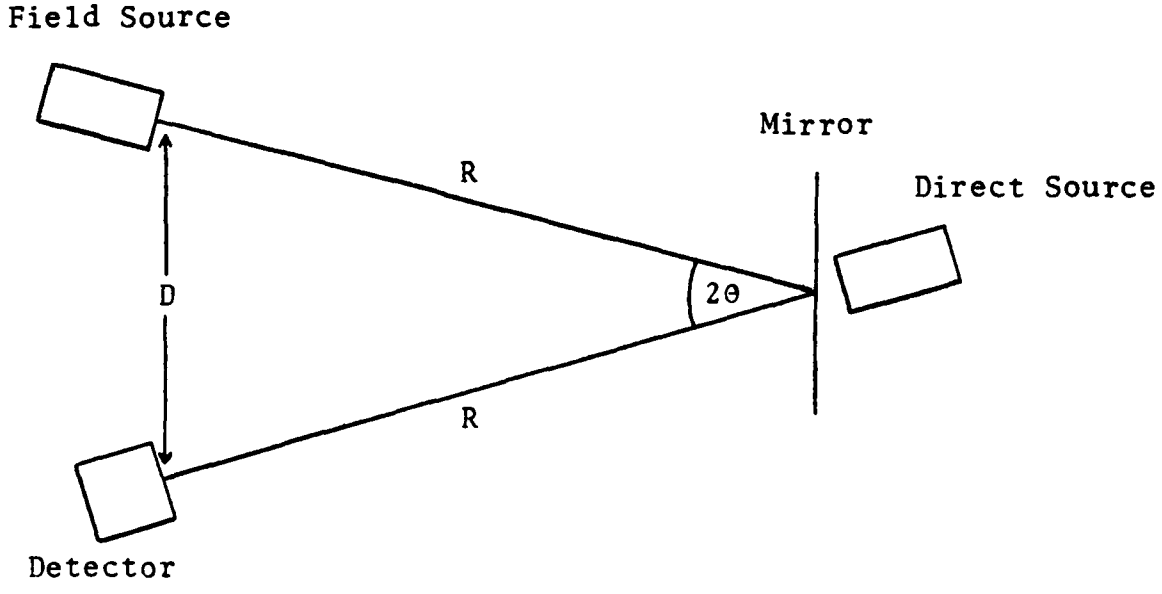

Figure 3. Diagram of the System Geometry Showing the Relationship of the Quantities D, R, and 2θ

for small values of y_o and approaches slowly to zero, Ze'evi defines the region in which statistical independence exists as that where $f(y_o,\theta) = e^{-1}$. This criteria is met for small θ where

$$y_o \geq 4$$

and statistical independence of the folded path now depends solely on the source detector displacement, D.

The next step is to relate the displacement to the variances of the folded path and the direct path, $\langle S_F^2 \rangle$ and $\langle S_L^2 \rangle$, respectively. We are not interested in the case of $\langle S_{2L}^2 \rangle$ in most situations of practical application. It is convenient at this point to remember that the variances we are working with are generally accepted to be taken from log normal distributions in the weak turbulence regime, and so we may adopt the notation $\sigma_\ell^2(L)$ and $\sigma_\ell^2(F)$ for the direct path and folded path variances, respectively. The subscript ℓ indicates a log normal distribution.

Using the results for the log intensity variance of spherical waves calculated by Tatarski [Refs. 3, 4] as follows:

$$\sigma_\ell^2(L) = 0.52\, K^{7/6} C_n^2\, L^{11/6}$$

and

$$\langle S_L \rangle^2 = \frac{A_1 \pi^{1/2}\, \Gamma(5/6)}{2^{2/3}} \left(\frac{L}{L_o}\right)$$

where

$$A_1 = \frac{.033\, 2^{5/3}\, \pi^{3/2}\, K^2\, C_n^2\, L_o^{8/3}}{\Gamma(11/16)},$$

Ze'evi arrives at the following expression for a path of length 2L in the weak turbulence regime:

$$\sigma_\ell^2(2L) = A_1\ 2^{5/6}\ L^{5/6}\ \langle S_{2L}^2 \rangle.$$

Relating this to the expression

$$\langle S_F^2 \rangle = \langle S_{2L}^2 \rangle (1 + f(y_o, \Theta)$$

Ze'evi shows that

$$\sigma_\ell^2(F) = A_1\ 2^{11/6}\ L^{5/6}\ \langle S_L^2 \rangle (1 + f(y_o, \Theta))$$

and finally,

$$R = \frac{\sigma_\ell^2(F)}{\sigma_\ell^2(L)} = 2^{11/6}\ (1 + f(y_o, \Theta).$$

R is the ratio of the folded path scintillation strength to the direct path scintillation strength in the weak turbulence regime ($\sigma_\ell^2 < 1.2$), and is the parameter we attempted to verify during our experiment. The range of R is

$$2^{11/8} \leq R \leq 2^{17/6}$$

or

$$3.56 \leq R \leq 7.12.$$

By restricting ourselves to the weak turbulence regime in these discussions, we have ignored such effects as saturation of the scintillation strength and the transverse

correlation length (the smallest lateral distance at the receiver that would allow independent intensity fluctuations to be recorded) of the signal. In addition, because we intended to measure the scintillation strength from an (approximate) point detector in our experiment, we have also omitted any reference to aperture averaging of the received signal intensity. This is appropriate in keeping with the conditions under which Ze'evi's folded path theory was formulated. With these caveats stated, we may proceed to a discussion of our experimental approach.

II. EXPERIMENTAL APPROACH

A. PROBLEM DESCRIPTION

An initial attempt at verifying Ze'evi's theory was attempted by Hodgini [Ref. 6] in the early part of 1982. This was of benefit to us in our work because much of the equipment necessary to perform the experiment was available, and because several factors involved in the experiment, e.g., the stability and correlation of the helium-neon sources had already been investigated.

In order to compare the correlation between the direct path and folded path variance, it was necessary to construct an electro-optical data collection system that could measure the desired optical parameters (the intensity fluctuations from the two different path geometries) and then store the data in a histogram type of arrangement until the statistics of the intensity distributions could be calculated and recorded. The primary requirement for the experiment in order that the direct path and folded path scintillation strength could be compared, was that the two lasers propagate over the same uniform surface leading to the detector. For the two sources to be subject to the same atmospheric conditions over the path length meant that the lasers would have to be alternately pulsed at a rate high enough that the turbulence along the path was frozen during the length

of time necessary to transmit and receive both pulses. The atmosphere can be considered frozen for time intervals of up to 1 millisecond [Ref. 1]. A basic cycle of 1000 Hertz was chosen giving a one millisecond period wherein first the direct then the folded path lasers would be pulsed and the signals sampled. This allowed a separation of approximately one quarter millisecond between each successive pulse.

The optical setup we devised is illustrated in Figure 4, where both the zero displacement case and an arbitrary displacement example are shown. The target end consists of the direct path laser, whose beam is modulated by a mechanical chopper, expanded by a lens system, and reflected to the detector aperture by a beam splitter. Behind the beam splitter is the mirror for the folded path. The detector end includes both the folded path laser with an optical modulation system (Pockels cell modulator and polarizer), another beam splitter for the case where the folded and direct paths are directly overlayed, and the detector, dewar, and aperture. The signal pulses from the laser at the detector end then propagate down range to the target end, pass through the splitter, reflect off of the mirror, and are returned to the detector via the same path as the direct path laser.

Our two greatest problems in developing the experimental setup were timing and alignment. Timing was of the utmost importance due to the rapidity at which the data was sampled

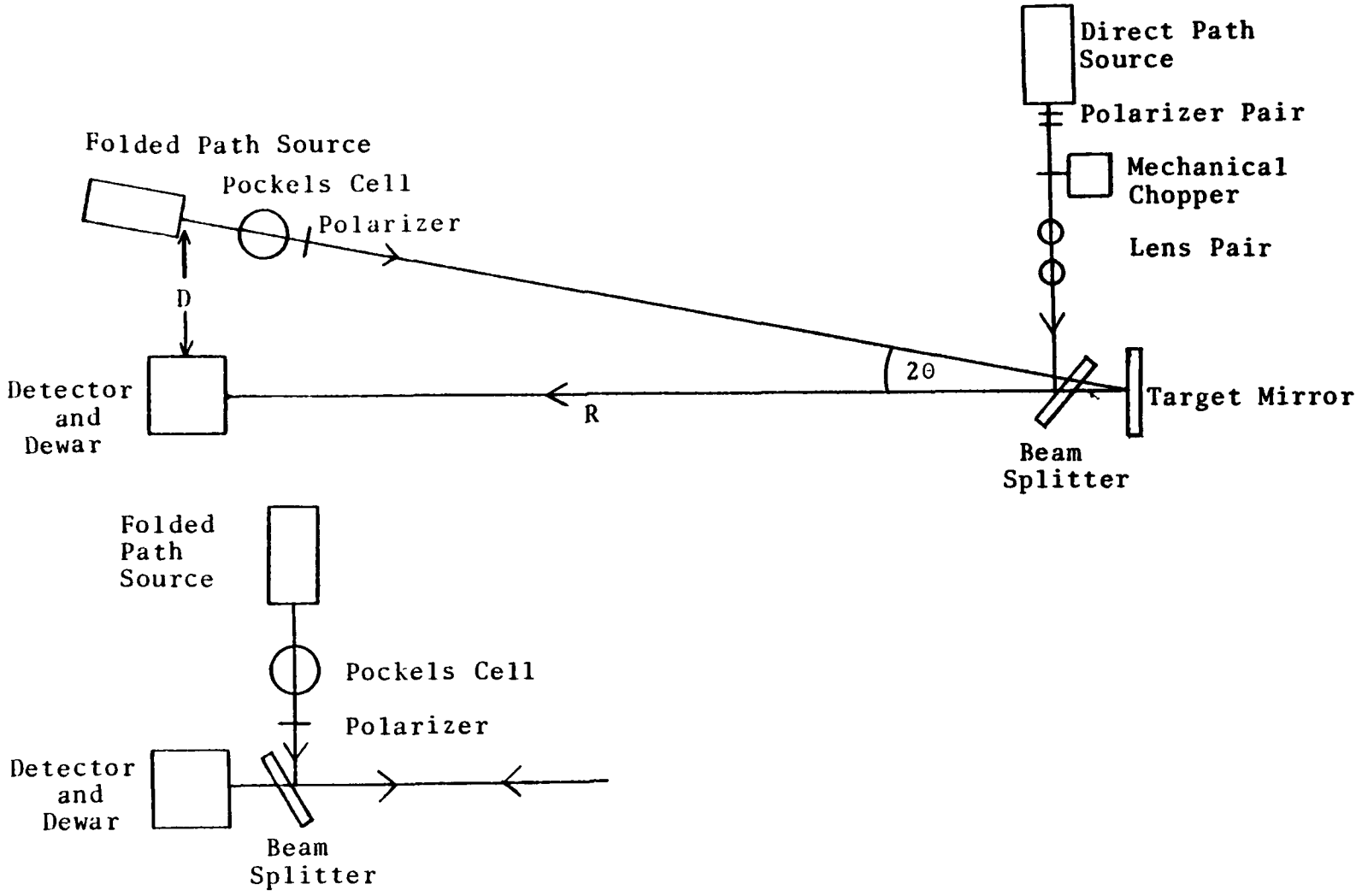

Figure 4. Equipment Diagram for D = Various Displacements (Top) and D = 0 Case (Bottom).

and because of the need to store the sampled data alternately at different locations corresponding to the different intensity distributions from the two paths. Alignment was likewise critical because of the requirement that the optical pulses from the two separate sources traverse the same physical path to the aperture of the detector.

In consideration of these two difficult requirements and the inherent complexity of a large number of electronic and optical components, the system was first assembled and tested in the basement of Spanagel Hall. A laser range running along the ceiling provided a 145 meter path with eight large ventillator ducts delivering heated air into the optical path to provide the necessary turbulence.

Once system development was complete, a variety of interior data runs were conducted for final system checkout. The entire system, exactly as constructed and tested inside, was then relocated to an outside site. This site was a 100 meter long, flat grassy area alongside Spanagel Hall and approximately 30 meters away. All optical components were situated on concrete tables and anchored with lead bricks for stability, while the signal processing equipment and computers were placed on movable tables. Later, another outdoor site atop Spanagel Hall would be tried that provided a shorter path but more scintillation.

B. OPTICAL EQUIPMENT

The final system consisted of one optical configuration for all data runs except the zero displacement run, which incorporated an additional beam splitter at the detector end. Both of these configurations are depicted in Figure 4.

1. Laser Sources

The two lasers utilized throughout the experiment were Spectra Physics HeNe lasers with a wavelength of .6328 micrometer and an output of .95 milliwatt. These lasers were chosen as sources for the following reasons: One, they produce light in the visible range, making alignment easier; two, the output power and therefore the hazard level was relatively low; and three, the correlation between these two lasers when pulsed alternately with a pulse separation of 0.3 millisecond over the same optical path, through the same turbulence was excellent. Hodgini reported source variances for these lasers as less than 3×10^{-4}, and the correlation coefficient (ratio of source variances) for the two HeNe lasers as .996 [Ref. 6]. Although the lasers had a tendency to become unstable with time, the correlation between the two sources did not, and therefore they could be used together in measuring scintillation with some confidence that their internal stability (source variance) would not be a contributor to the scintillation we were measuring.

2. Target End Optics

The target end optics consisted of a beam expanding lens system, a set of adjustable polarizers for fine intensity adjustment of the direct path laser signal intensity, a four inch optical beam splitter, and mirror. The lens system was required in order to expand the direct path laser spot size to the approximate size of the folded path laser spot at the target end beam splitter. This also helped match folded and direct path signal intensities at the detector aperture, and made system alignment easier. Both the direct path signal and the folded path signal would then transit through the same volume of atmosphere in reaching the detector aperture. The first lens, actually a microscope objective, received the laser beam and focused it to a point near the focal point of the second lens, which then collimated the beam entering the beam splitter. Two polarizers, placed ahead of the microscope objective, were used to make final reductions in the direct path signal intensity to closely match the intensity of the folded path signal.

The four inch beam splitter was a critical component because the folded path signal had to pass through it twice and the direct path signal had to be reflected by it enroute to the detector. It was therefore of extreme importance that no structure be imparted to the transiting pulses and also that reflection losses be minimal so that the signal intensities reaching the detector be as high as possible.

To satisfy these conditions, a four inch diameter, half inch thick optical window was acquired with an advertised flatness correct to 1/10 wavelength and parallelism within two seconds of arc. An antireflective coating was applied and one side of the splitter silvered to provide 50 percent transmission, the latter meaning 50 percent of the signal intensity from either source was lost at each pass through the beam splitter. Coating and silvering the splitter also produced the beneficial result that the maximum signal intensity from the direct path laser reflected by the back side of the beam splitter was less than 0.4 percent of the signal intensity reflected from the front of the splitter, and therefore could be neglected. The target mirror utilized was a five inch optical flat. The important qualities required were good optical flatness and large size. The flatness had been previously verified using an interferometer and the five inch diameter proved large enough to accomodate the folded path spot size after its initial 100 meter transit.

C. PULSE FORMING AND DETECTION EQUIPMENT

The pulse forming equipment in our experiment included a mechanical chopper to modulate the direct path laser and and electro-optical modulation system to modulate the folded path laser. After the signals arrived at the aperture, they were converted to an analog voltage signal by the detector and amplified before being log converted and stored.

1. Mechanical Chopper

The mechanical chopper was positioned between the second polarizer and the microscope objective at the target end. A circular wheel with an open to closed ratio of 1:4 was rotated using a 3000 rpm electrical motor, resulting in a chopping frequency of 1000 Hertz. A light emitting diode mounted opposite a detector was also placed on the chopper and provided the reference trigger signal for the entire experimental system. This trigger was led to an Interstate P12 pulse generator which delayed the signal to provide the trigger for the modulation system on the folded path laser.

2. Modulation System

A Coherent Associates Model 3003 modulation system (Pockels cell) was used for pulse forming of the folded path laser. After the pulse of the direct path laser was initiated by the mechanical chopper, a delay of approximately .4 millisecond was provided by the P12 described above, and this delayed trigger was led to the Pockels cell modulation system to initiate the folded path pulse. Folded path pulse width could be matched to that provided by the mechanical chopper by varying the pulse width at the P12.

3. Detector

The detector utilized for our intensity measurements was a Model 50 EHS Silicon Avalanche Detector manufactured by the General Electric Company. When operated at voltages of between 1200 and 1500 volts and cooled in a dewar of

liquid nitrogen, the detector provided an extremely high signal to noise ratio. The high voltage caused high amplification of weak signals by placing the detector into its avalanche region, and the cooling suppressed noise. A high signal to noise ratio was needed because of the extremely low signal power available at the detector aperture from the HeNe sources. Although we did not verify the linearity of this detector over the dynamic range of incident signal intensity available to us, the detector's linear response in the weak signal regime had been previously established by the atmospheric physics group at NPS and we neglected any nonlinearity at this point.

In order to make our detector system a point detector, the aperture needed to be as small as possible and still pass enough light to enable the detector to register a signal. Hodgini [Ref. 6] shows that the Fresnel zone site at the aperture is the most important criteria. Zone size can be determined as follows:

$$\ell_F = (\lambda L)^{1/2}$$

where ℓ_F is the Fresnel zone radius,

λ = .6328 micrometer, and

L is the range.

The Fresnel zone size at 145 meters is 9.58 mm, at 100 meters is 7.95 mm, and at 40 meters is 5.03 mm. This is a smaller length than the lateral coherence length of the light, either outside or in the lab, and therefore an aperture size smaller than the Fresnel zone size for a particular range would approximate a point detector. Using this constraint, Hodgini had settled on a 3 mm diameter aperture and we adopted this size as well. Light passing through this opening was then focused on the detector by a single convergent lens placed a focal length from the detector surface. We did not use any spectral filters between the aperture and the lens as all of our experimental work was done under conditions of very low ambient light.

4. Signal Amplifier

The output from the detector was led directly to a Model 113 Princeton Applied Research (PAR) Low Noise Amplifier. This device provided high signal gain and an adjustable bandwidth with high and low frequency roll-offs. These features were necessary to scale the amplitude of the signal reaching the analog to digital converter on the storage computer, and also to obtain the optimum signal shape. One point in particular should be made regarding the selection of signal bandwidth, and that is this: we had to be very careful that the low frequency roll-off was not set too high, resulting in a dip in the background level following

the signal (removal of too many Fourier components from the wave shape) and leading to an erroneous background sample in the signal processing performed by the demodulators. In other words, we wanted to eliminate as much noise as possible but not damage the optimum signal shape in doing so.

D. SIGNAL PROCESSING EQUIPMENT

Scintillation effects from the atmosphere along the path traveled by the light pulses caused the intensity at the aperture and therefore at the detector to be a function of time. This same effect was also present in the background intensity just before and after the signal. We wanted to be able to sample the largest instantaneous value of the intensity during the pulse, and the value of the background intensity following the pulse. The difference between these two values would be the true signal intensity. This process of sampling and returning the absolute intensity is termed "demodulation", and the equipment we needed to perform this task for both laser signals was available in the form of two demodulators used by the atmospheric physics group at NPS. Additionally, since the actual measure of the scintillation strength is the log intensity variance, the absolute intensity magnitudes had to be converted to logarithmic values prior to being digitized and stored. Our signal processing equipment then consisted of two demodulators, two log converters, and the electronic switch.

1. Demodulators

Two demodulators were utilized in our experiment, one for both the direct path and the folded path signal. The function of each was identical. A demodulator received the signal directly from the PAR low noise amplifier described previously. A trigger pulse activated the demodulator to receive only its respective input signal, after which the demodulator had to accomplish four actions to output a differential signal. Figure 5 illustrates these actions for the direct path signal; the folded path signal was exactly the same, simply occurring about 0.3 millisecond later. The stretch cutoff function took the instantaneous maximum of an incoming signal and held it for an adjustable period of time, allowing the signal sample to be set within this time frame. After the stretch cutoff was released, the demodulator saw only the background signal, and a background sample was taken. The demodulator electronically took the difference between the two values it had sampled and output the difference. This differential signal was held until the next input and input trigger arrived.

2. Log Converters

The differential output of each demodulator was sent to its own Hewlett-Packard 7562A Log Converter. These devices produced a dc output voltage that was proportional to the log of the dc input voltage in the following manner:

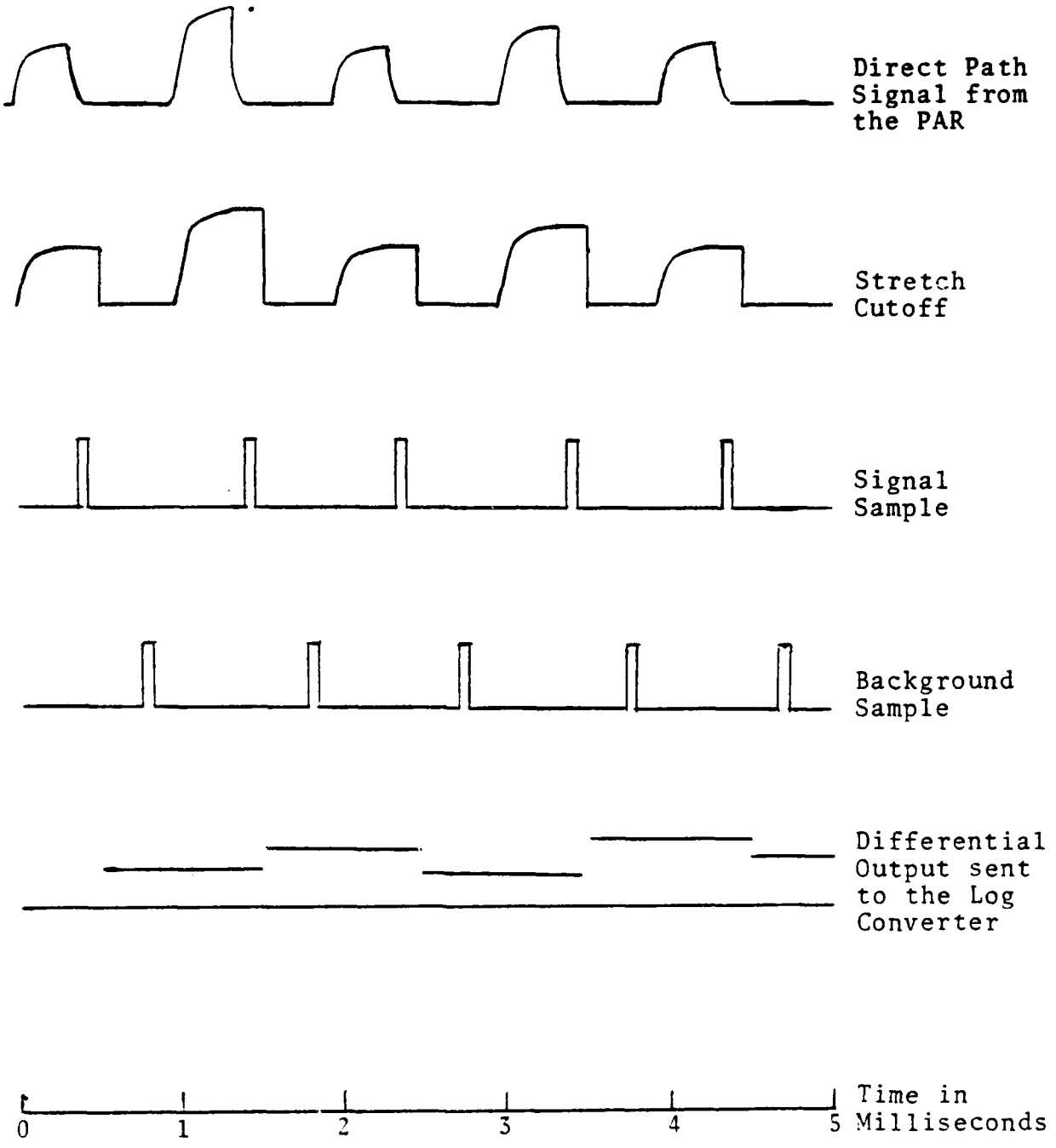

Figure 5. Timing of the Demodulator Waveforms

$$V_L = a + b \log V_D$$

where V_D is the demodulator differential output, V_L is the log output, and a and b were constants determined by the design of the equipment. The constant, a, simply resulted in a shift of the mean of the distribution, and could be different for each log converter. This was identical to a uniform increase in incident signal intensity and did not affect the log variance, as shown in Chapter I. The constant, b, had to be the same for each log converter, or the variance ratio

$$\frac{\sigma_\ell^2(F)}{\sigma_\ell^2(L)}$$

would be multiplied by a gain factor. We measured b for each log converter and found the values to be within .009 of each other. This confirmed the accuracy of the two parallel data lines reaching the electronic switch. The two log converted differential signals corresponding to the direct path and folded path signal intensities were now ready for digitizing and storage in the data storage computer.

3. Electronic Signal Switching

The Nicolet 1080 Stored Program Computer was used for data storage during an experimental run. Each experimental run consisted of collecting sixteen pairs of variance values at a specific value of the displacement, D, and between 10

to 13 displacements comprised an experimental try at validating the folded path theory. Because the NIC-80 had only one analog to digital converter (ADC) port, we time-shared the port between the two input signal trains. A new signal arrived at the ADC every 0.3 millisecond. A switch was required that would receive the output signals from the log converters and sequence these signals to the ADC. Our switch was built using the AD7510D1 analog chip. The function of the electronic switch is illustrated graphically in Figure 6, where the two independent data signals, represented by dotted lines, are shown being sequenced through the electronic switch to the NIC-80. The solid lines represent system timing signals. An Interstate Electronics Corporation P25 Pulse Generator was synchronized to the delayed trigger of the folded path optical modulation system and output two continuous pulse trains, one the complement of the other. Both the positive and negative pulse trains went to the electronic switch and controlled the transmission of the alternating signals to the ADC. In addition, the positive pulse train went to the port on the NIC-80 labeled "Sense 2" to tell the computer in which data storage area to assign the incoming data point. When a positive value was present at the switch and Sense 2, the folded path log intensity signal was allowed to transit the switch, be digitized in the ADC, and enter the folded

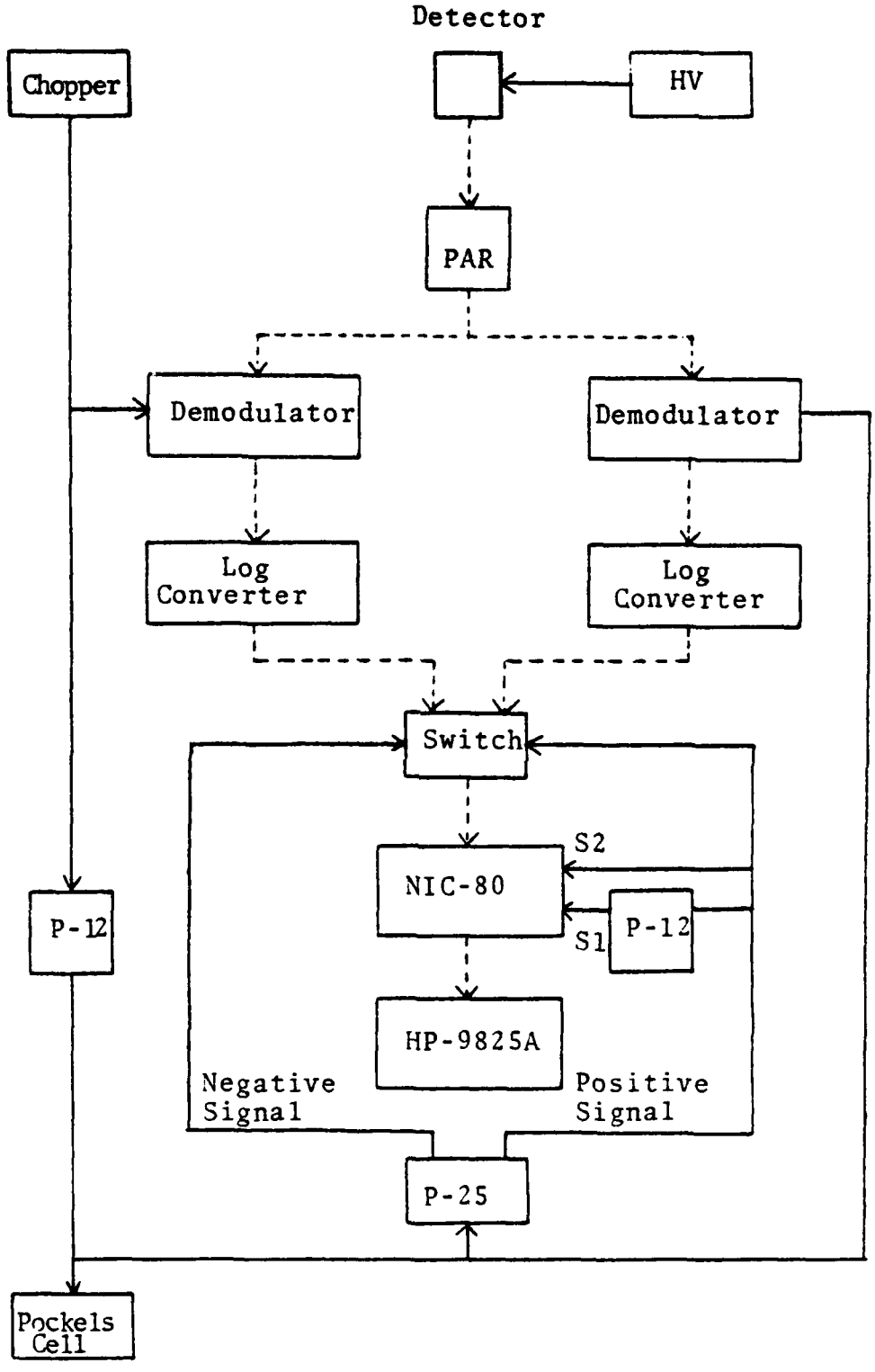

Figure 6. Diagram of the Data Acquisition and Reduction System

path storage area in the computer. The relationship of these signals in time is shown in Figure 7.

E. COMPUTERS

The computer system which we needed for our experiment was available and already adapted by the atmospheric physics group at NPS for the express purpose of storing and processing the high speed analog signals from direct path scintillation measurements. This system consisted of three components, the Nicolet Instrument Corporation Model NIC-80, the Hewlett-Packard (HP) 9825A Calculator, and the HP 9871A Printer. To these three we added a fourth component, the HP 9862A Calculator Plotter, to obtain a graphical output of the data as an aid in determining its validity. Each component of the system is discussed in detail in the paragraphs that follow.

1. NIC-80

The NIC-80 is a general purpose computer, highly suited to the role of high speed data storage and manipulation. It is configured for use with a CRT and has a hardwired analog to digital converter (ADC) as well as several ports for the purpose of timing and control. Signals from both laser sources were sent to the NIC-80 via the electronic switch, arriving at the ADC where they were converted to a digital value. This value was scaled by the stored program to correspond to a range of memory addresses in the machine,

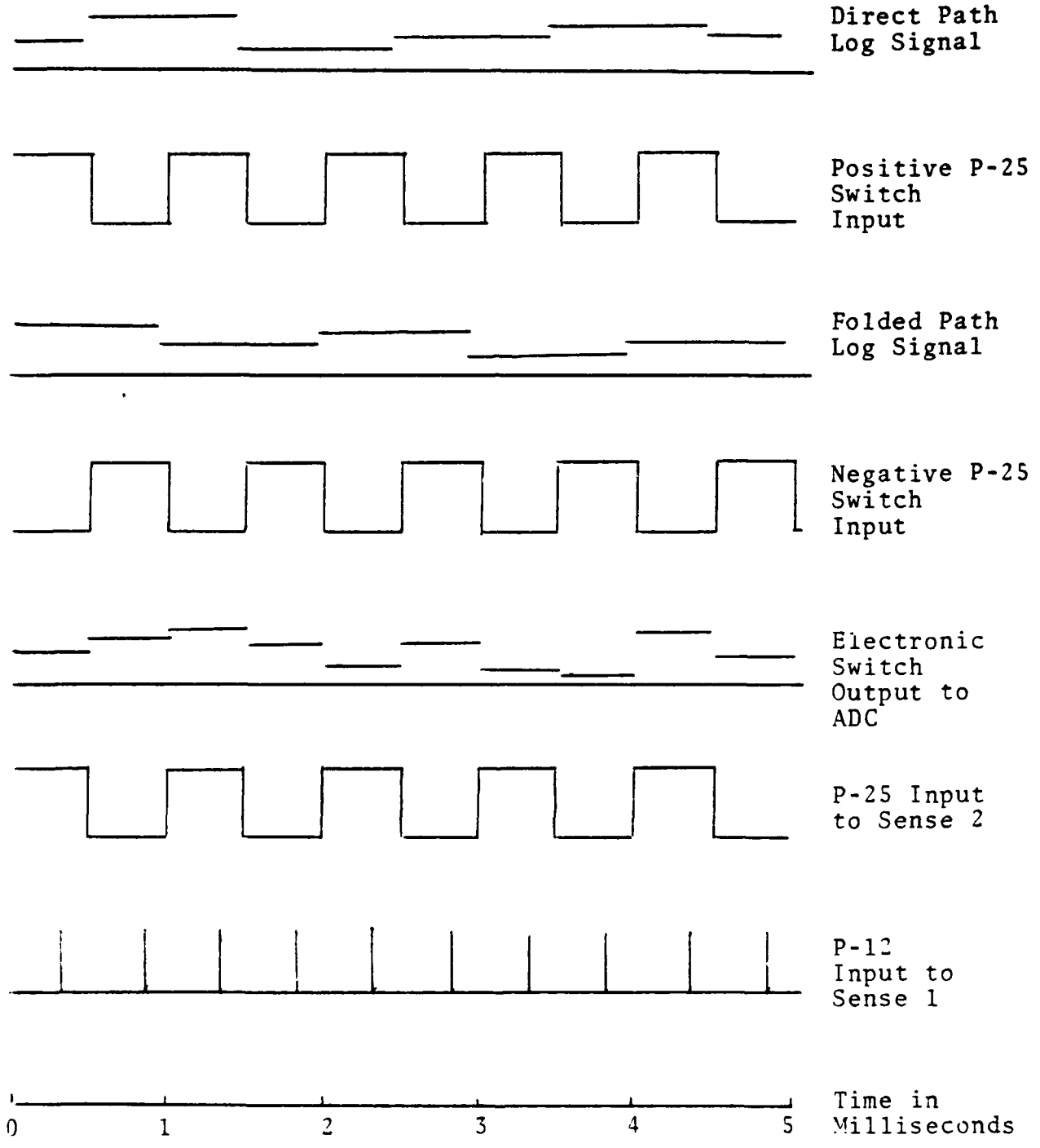

Figure 7. Interlacing, Coordination, and Sampling of Output Signals

and each time the value occurred, a count was added at the corresponding memory address. Only positive values from the ADC were counted by the stored program, which helped smooth out the tail regions of each distribution. During a data collection period, each source had its own block of memory addresses and thus a histogram of counts versus point signal intensity at the detector was developed for each laser source. The range of each histogram (intensity distribution) in the NIC-80 was 256 memory spaces or "bins", corresponding to a range of 0 to 256 from the ADC. Through tests run on artificial data, it was determined that the bin widths at the ADC, that is, the analog signal range per value (or bin) at the ADC was so close to a constant value, that for the purposes of our statistical analysis of each source's histogram, we could assume equal bin widths of signal intensity. This proved to be an excellent assumption, and enormously simplified the statistical calculations that followed. The smoothness of the intensity distribution that we got from this process of digitizing and storage was almost entirely a function of the average bin width in the ADC. Our average bin width was 33.169 millivolts, and this proved adequate for the range of signal intensities that we used. The value of the original signal intensity at the detector was, of course, not important, simply the variance of mean signal intensity. Each run consisted of 16,384 samples per laser source or 32,768 samples total, and took approximately 15 seconds to

complete. After completing a data run, the NIC-80 program would reassign a new block of memory for each laser source and the process would be repeated until 16 runs or 32 data pairs had been recorded. The entire 16 run period took approximately four minutes, during which time it was possible to monitor visually on the CRT the building up of the histogram for each source. In other words, we had a real time picture of the scintillation data during each run. This was very useful for monitoring the relative variances of each source, as well as their relative mean intensities, with the result that the quality of the data was immediately apparent and could be assessed before devoting too much time to a run. Such factors as poor alignment and faulty system timing could be spotted immediately from the nature of the intensity distributions displayed on the CRT.

The NIC-80 was programmed entirely in assembly language, compiled and loaded from the HP-9825A. The assembly language program for the NIC-80 is included in Appendix A. Timing pulses arriving at the ports labeled Sense 1 and Sense 2 were interpreted by the computer program to tell the machine which source's signal was currently present at the ADC and thus the program directed the storage of the data count at the proper memory address. For example, a high voltage present at Sense 2 meant that the signal from the direct path source was ready for digitizing, and a low voltage meant that the signal was from the folded path source.

A concurrent trigger pulse at Sense 1 then allowed the signal at the ADC to be digitized. Sense 1 therefore had to be triggered at twice the frequency of the data rate from either source. At first glance this seems redundant with the function of Sense 2, but it really is not; Sense 1 paced the digitizing and Sense 2 determined which laser source was being digitized.

2. HP-9825A Calculator

The HP-9825A Calculator was the operator-machine interface for our experiment, and the program for the 9825A controlled the function of the NIC-80, the printer, and the plotter. Control of the NIC-80 was accomplished through a computer interface built by Processor Edmund Milne at NPS, and the control signals consisted of pairs of binary values exchanged as initiation and answer "handshakes" at critical points to control the execution of the NIC-80 program. The 9825A program was written in HPL and was initially structured to collect all the data for a given value of D in the NIC-80 then transfer the data to the 9825A for processing and graphing immediately after the run. Approximately 30 minutes was then required to print and graph the data for all 16 pairs; this was the method used to collect the data for experimental results one and two, discussed in Chapter III. A copy of this program for the 9825A appears in Appendix B. For reasons to be discussed later, we decided late in the project to try a different method of data collection and processing

in which it was desired to shorten the elapsed time between runs, time which previously had been devoted to printing and graphing. Our goal was to try and collect fewer numbers of data pairs at each value of D, and to try and collect all the data for all values of D that we intended to use --12 or 13 points usually--in 30 minutes or less by recording the data from the NIC-80 on magnetic tape and moving to the next displacement without processing the data. This was the method used to record the data from our third experiment, and the program to do this is also included in Appendix B. One final note needs to be made regarding the 9825A interface with the NIC-80. The NIC-80 data word is 20 bits long, but the parallel input/output bus is 16 bits long. This necessitated the transfer of data from the NIC-80 to the 9825A in two 10 bit segments, which is two transfers per word of data. The first transfer included the 10 highest bits from the word and the second transfer included the 10 lowest bits from the word; the first part was multiplied by 1024 in the 9825A and added to the second part to form the complete data value. This process was repeated for all the values in each intensity distribution from both laser sources in a given run.

After loading all the values in a pair of intensity distributions from a run, the 9825A was now ready to calculate the statistical parameters that we desired. This was accomplished in a straightforward manner, using the

accepted formulas for mean, variance, standard deviation, and chi-square shown in Appendix C. No curve fits were used and no data points were excluded to reduce the effect of noise in the tails of the log normal distributions. Even so, the values of the variance calculated by our program and another program from Professor Edmund Milne that used a curve fit to determine the variance were within one percent of each other. This strengthened our confidence in our approach. In order to determine how closely the log normal curves corresponded to a true Gaussian curve, we chose the chi-square calculation with a goodness of fit parameter of 288.87 for a 95% confidence interval, derived from the number of degrees of freedom (253) in our data histograms. This portion of the calculation required that we use values from the Standard Normal Table, and we interpolated linearly between values in the table out to the sixth decimal place to obtain a smooth, continuous true normal for each set of data. Test runs conducted with data points derived from the equation of a Gaussian curve were used to verify the statistical values arrived at by our program, including the chi-square value, which in theory would be zero for a true Gaussian distribution. Different runs utilized different values for the mean, variance, and maximum ordinate; in all cases the program determined the correct values and returned a chi-square value less than 0.3. A sample test run is shown in Figure 8. After performing this software validation, we had complete confidence in the programs.

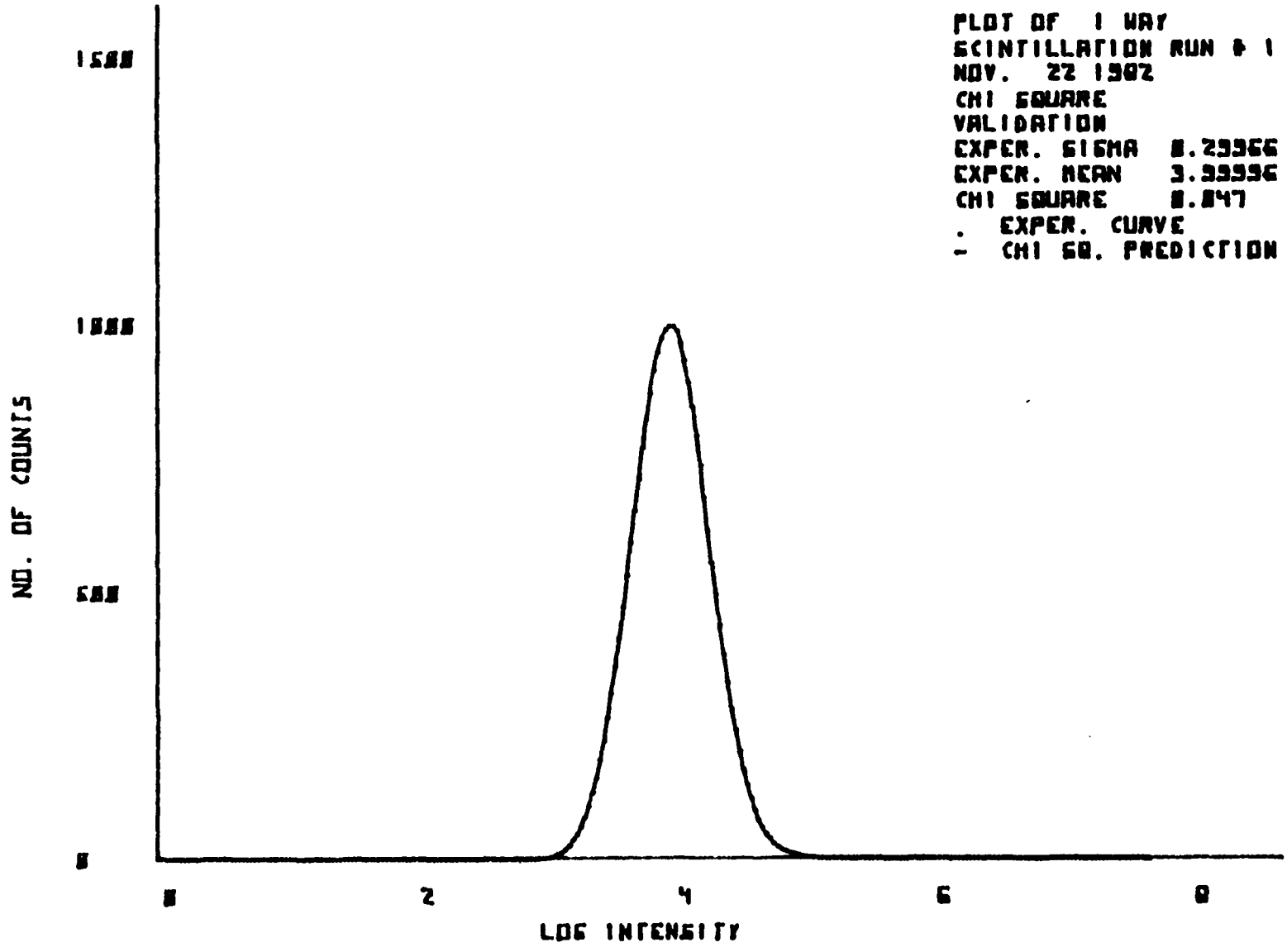

Figure 8. Chi-Square Validation Run

3. The HP-9871A Printer

The HP-9871A Printer is an impact printer controlled by the 9825A. We programmed the 9825A to print automatically the standard deviation and chi-square value for each intensity distribution in a run. These printouts appear in Appendices D through F, along with representative plots from the runs. A header on each page lists the date the data was recorded, whether or not the detector was cooled with the aperture in place, what the gain was, the avalanche voltage, bandpass, and the value of the displacement in cm for that particular run. In the columns below this are listed the number of data points that actually made it into the histogram, the variance, and the chi-square value. In each case, the direct path parameters are displayed first, then the folded path parameters.

4. HP-9862A Calculator Plotter

The last component in our computer system was the HP-9862A calculator plotter. We used the plotter to display graphically the data points from each histogram, as well as the true normal curve calculated by the chi-square approach. The smoothness of the latter curve was a result of the linear interpolation of the normal table referred to earlier. Plotting the data allowed us to judge easily the quality of the log normal assumption for the scintillation, and also discover where the data differed

from the true normal curve if the chi-square value was in excess of our goodness of fit parameter. Plotting the data was not automatic for each run as was the printout; instead, we took one representative set of curves for each value of the displacement that we measured. These plots are arranged with their respective printouts in Appendices D through F. The printout for a run overlays the two plots that go with it. Note that we did not always take the best set of data from a run (the lowest chi-square values), but instead we chose to keep plots that were representative of the entire run as a whole. Again, each plot includes a header coded as in the printout.

III. EXPERIMENTAL WORK

A. GOALS

There were three main goals of our experiment. First, we wanted to design a system that would allow us to simultaneously record the scintillation over both a direct and a folded path. Second, we wanted to calculate the scintillation strength for each path, which meant that we needed to calculate the variance of the received intensity. In addition, we wanted to know after we had the variance how accurate had been our assumption of a log normal distribution. Our third goal was to compare our experimental results of the relationship between the direct path and folded path variances to the theoretical prediction by Ze'evi.

B. PREPARATION

In order to perfect alignment procedures and timing sequences, a large number of runs were conducted on our inside range in the basement of Spanagel Hall. Due to the unknown turbulence conditions in the basement and the differences between operating in the open atmosphere and in the building, these runs were only useful for checking out the optics, timing, and data reduction techniques. No data from these runs is included in this report. We should mention at this point that we did not undertake to measure

the overall system's dynamic range or linearity before concluding our test phase. The reason for this is that all of the component equipment comprising our system, including the detector, was operated well within the linear regime for each. We thus felt that further investigation of these factors was neither profitable nor necessary.

C. FIRST OUTSIDE EXPERIMENT

We transferred our entire system, including the target end equipment, detector end equipment, signal processing equipment, and the computers, outside to a 100 meter range on the South side of Spanagel Hall approximately 30 meters from the building. We arbitrarily selected 100 meters as the range because we felt that we would need a long distance in the relatively sheltered area south of the building in order to get enough scintillation to have variances above the source variance regime of 10^{-4}. We went out 30 meters from the base of the building to try to get away from any nonuniform turbulence effects near the Hall. It quickly became evident that daylight runs utilizing the HeNe sources would not be possible. The power available from each source was not enough to be detectable by the eye, making system alignment almost impossible. Hodgini notes in his thesis that optical alignment proved to be of extreme importance in obtaining accurate results, and for this reasons we wanted to be absolutely certain that the alignment was correct and

that both spots from the laser sources were centered on the detector aperture while running the experiment. Because of the small size of the aperture (3mm) and the presence of the optical splitter that further reduced laser signal intensity, our ability to align the system visually was critical; for this reason we decided to do the experiment at night.

The direct path laser source was collimated to produce a constant spot size. This was done in order to match approximately the direct and folded path spot sizes at the target end splitter so that pulses from the direct path source would be traveling through the same volume of atmosphere, and hence subject to the same turbulence conditions as the folded path pulses on their return to the detector. The variance in the log normal curve resulting from the direct path source would then be larger than if the light had been allowed to diverge normally because the pulse wave fronts would be plane instead of spherical. We corrected for this effect when analyzing the data.

The first time that we ran the experiment outside, 11 different displacements were sampled from D = 0 to D = 100 cm in intervals of 10 cm. The data was recorded over a period of eight hours the night of 3 November between 8:30 PM and 4:30 AM. Pictures of the equipment and the range alongside Spanagel Hall appear in Figures 9 through 15. The weather

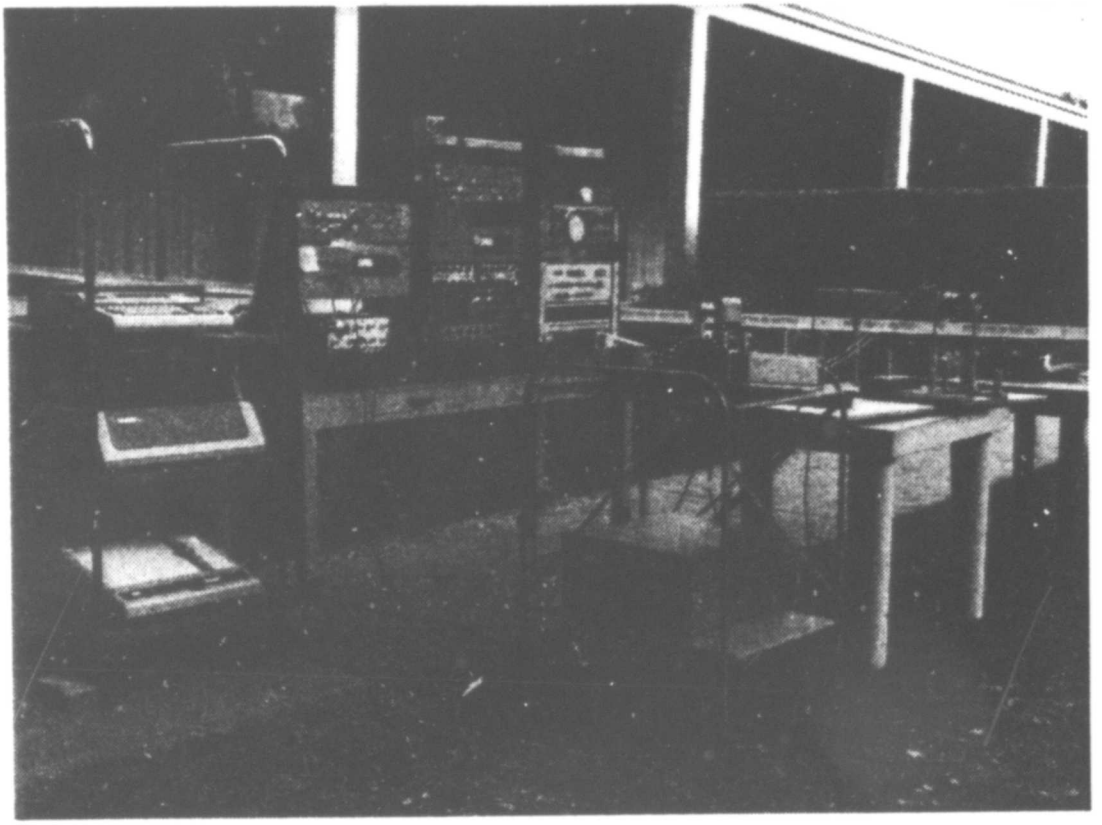

Figure 9.

An Overview of the Data Reduction, Signal Processing, Folded Path Source Equipment, and Detector Assembly. The leftmost bay contains (from top to bottom) the HP-9825A Calculator, HP-9871A Printer, and HP-9862A Calculator Plotter. To the right, this table contains the signal processing equipment which is further identified in Figure 10. The optical equipment and detector are also further detailed in Figure 11. The centermost table supports the PAR amplifier (top, left), the high voltage power supply for the detector (top, right), and the modulation system power supply (bottom).

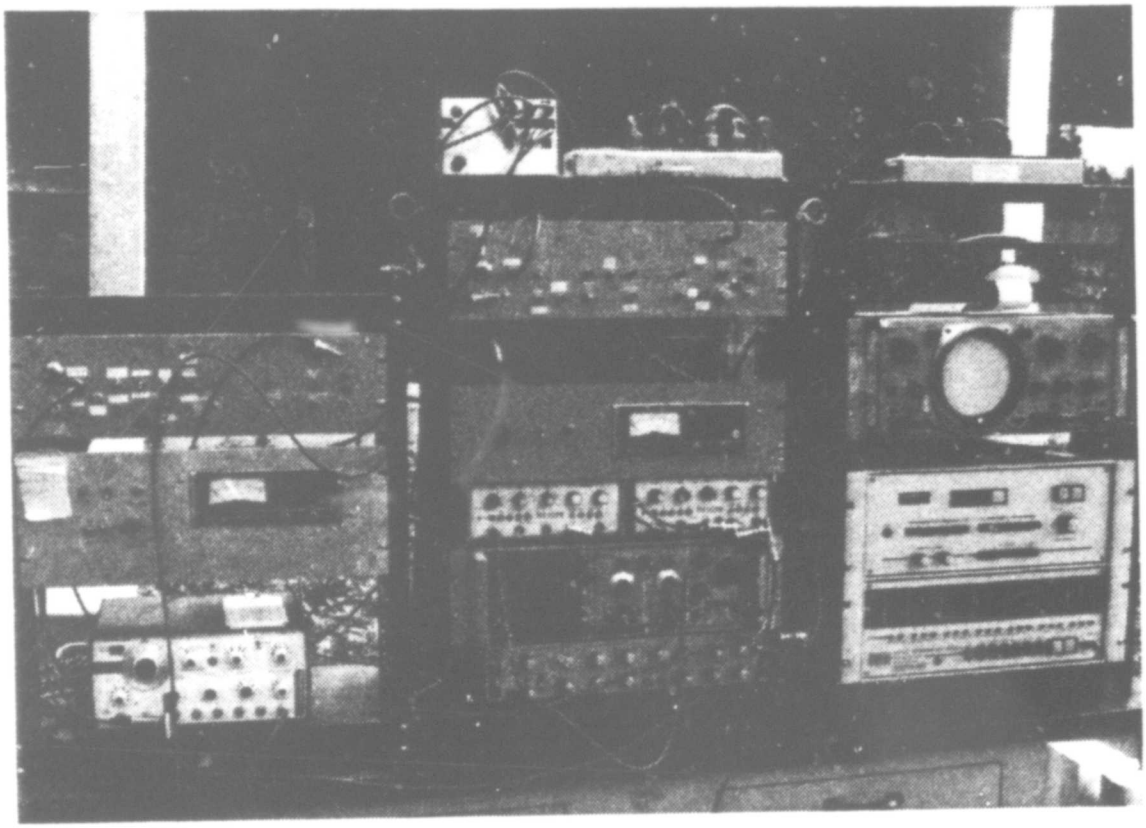

Figure 10.

Left bay, top to bottom: Direct path demodulator, direct path log converter, and signal generator.
Middle bay, top to bottom: Electronic switch, folded path demodulator, folded path log converter, two P-12's (leftmost sent to Sense 1, rightmost is delayed trigger for Pockels cell, oscilloscope, and P-25.
Right bay, top to bottom: HP-9825 to Nicolet 1080 Interface, oscilloscope for Nicolet 1080 display, and Nicolet 1080.

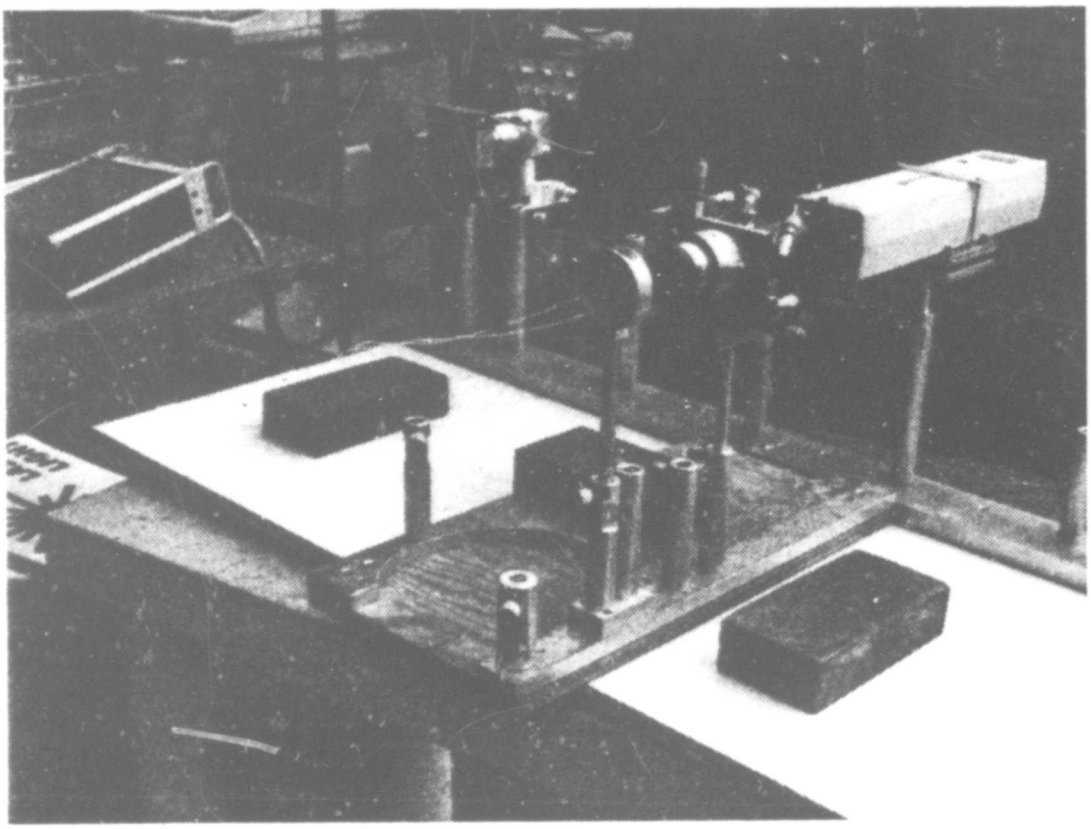

Figure 11.

Left to right on optical bench: detector and dewar assembly with 3 mm aperture installed; folded path Spectra Physics HeNe laser with pulse modulation system (Pockels Cell) in front

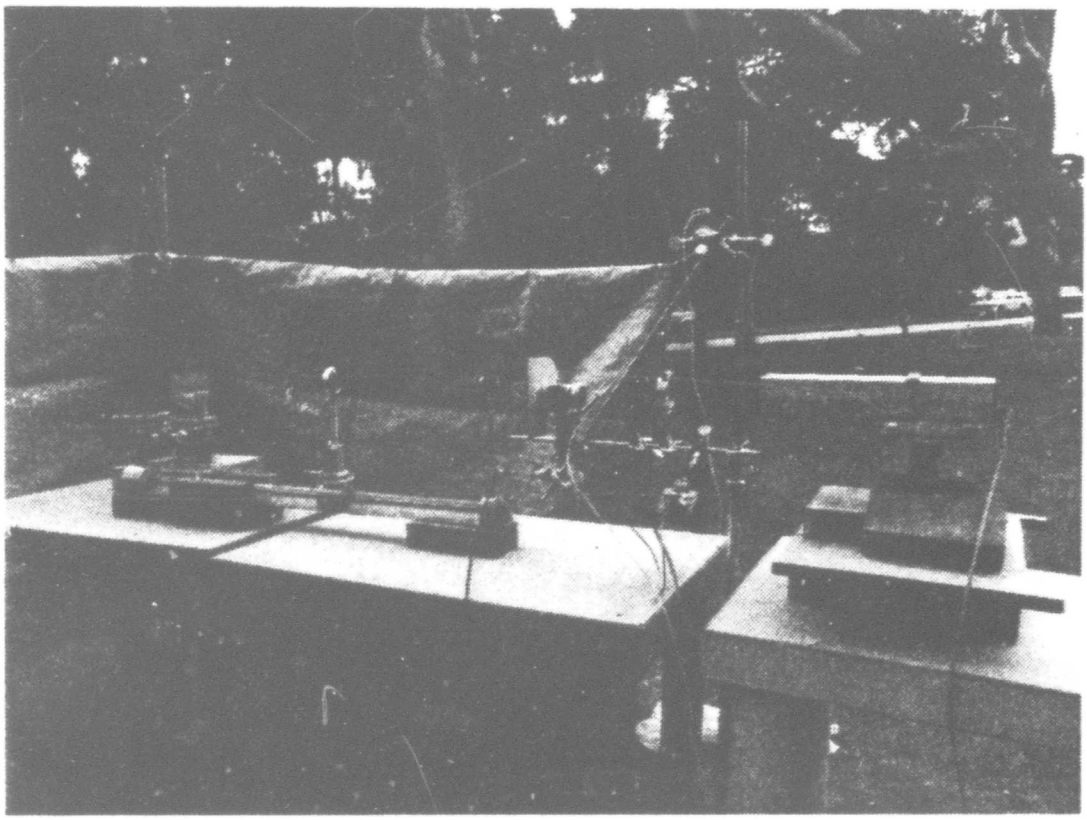

Figure 12.

From right to left: direct path Spectra Physics laser, polarizer pair, mechanical chopper, microscope objective, collimating lens, and optical splitter with target mirror behind it.

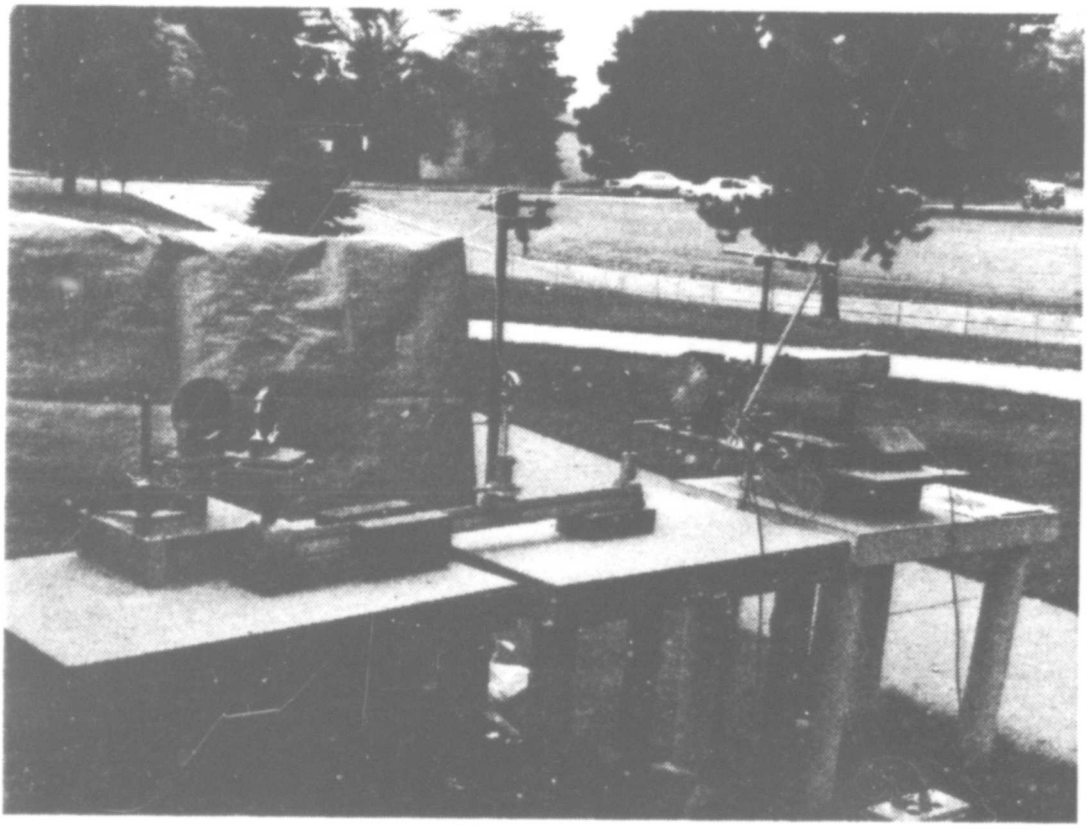

Figure 13. Another View of Direct Path End Highlighting the Optical Splitter and Target Mirror Arrangement

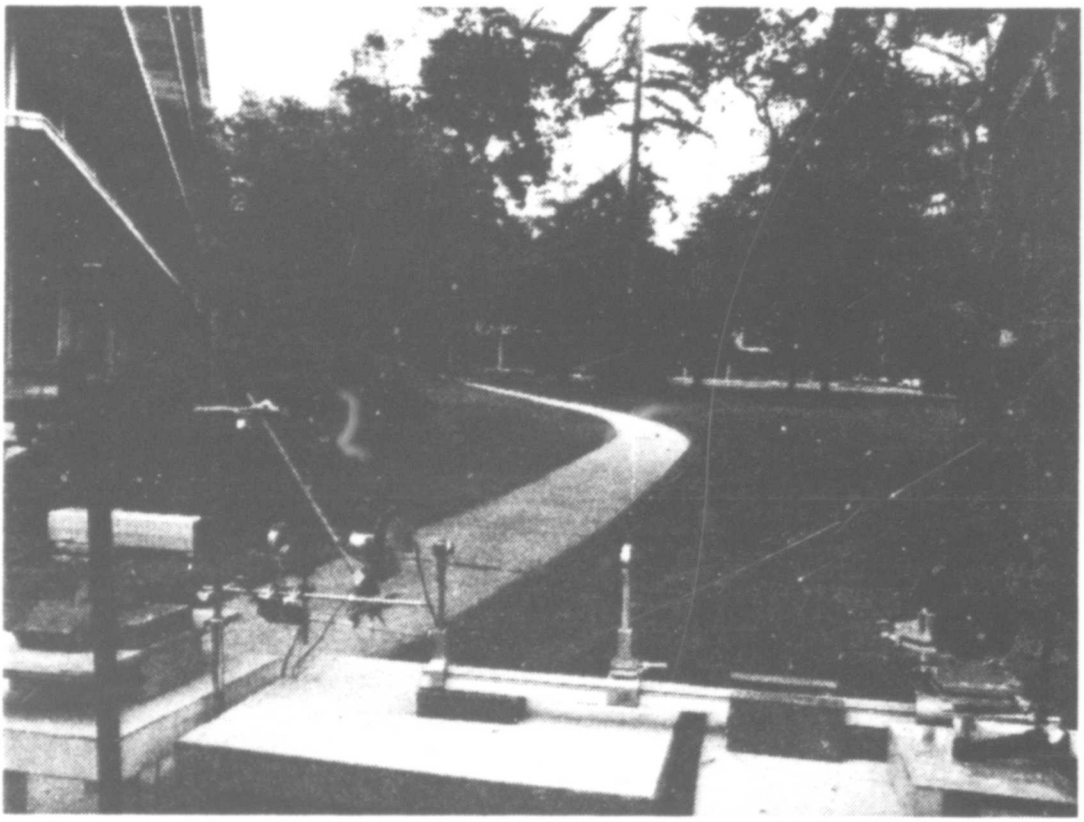

Figure 14. View of 100 Meter Outside Range From Direct Laser to Detector

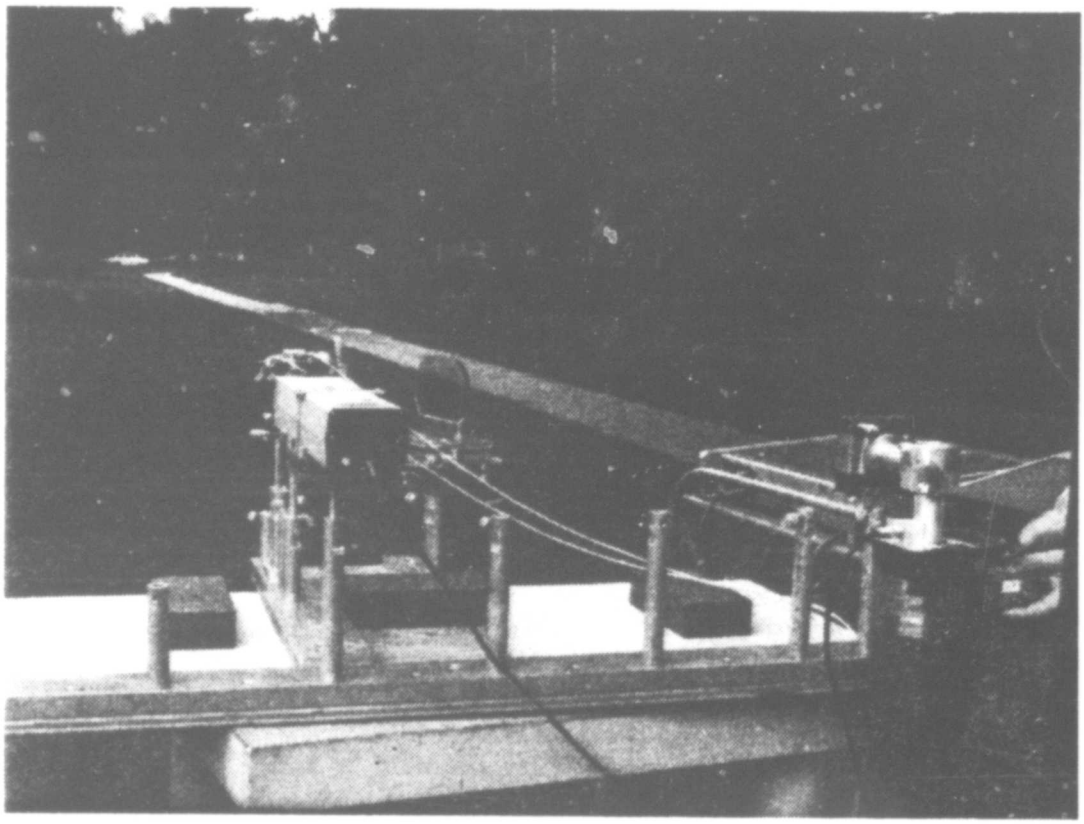

Figure 15. View of 100m Outside Range from Folded Path Source to Target Mirror

was clear and cool with a very slight wind, and no problems were encountered in system alignment or operation. The log normal distributions for each run appeared very reasonable, in that they were all approximately Gaussian, with a chi-square value close to and in some cases less than the required goodness of fit value of 288.87. Note that though the standard deviations of the direct path sources were usually greater than those of the folded path source, it must be remembered that the direct path data was collected from plane wave pulses, and the folded path data was collected from spherical wave pulses. The relationship of plane wave scintillation variance to spherical wave scintillation variance can be deduced from the ratio of the equations by Tatarski in Chapter I, and is 0.52/1.24 or .4194. In order to take the ratio of the folded path variance to the direct path variance, we first converted the direct path variances by multiplying each value by .4194, with the result that the direct path variances were then less than those for the folded path, as expected.

A plot of the average ratios

$$\frac{\sigma_{\ell}^2(F)}{\sigma_{\ell}^2(L)} \quad \text{versus} \quad y_o \left(\frac{D}{L_o}\right)$$

for this experiment is presented in Figure 16. The variance ratio for each displacement was obtained by first determining the ratio of each variance pair in the run, then averaging

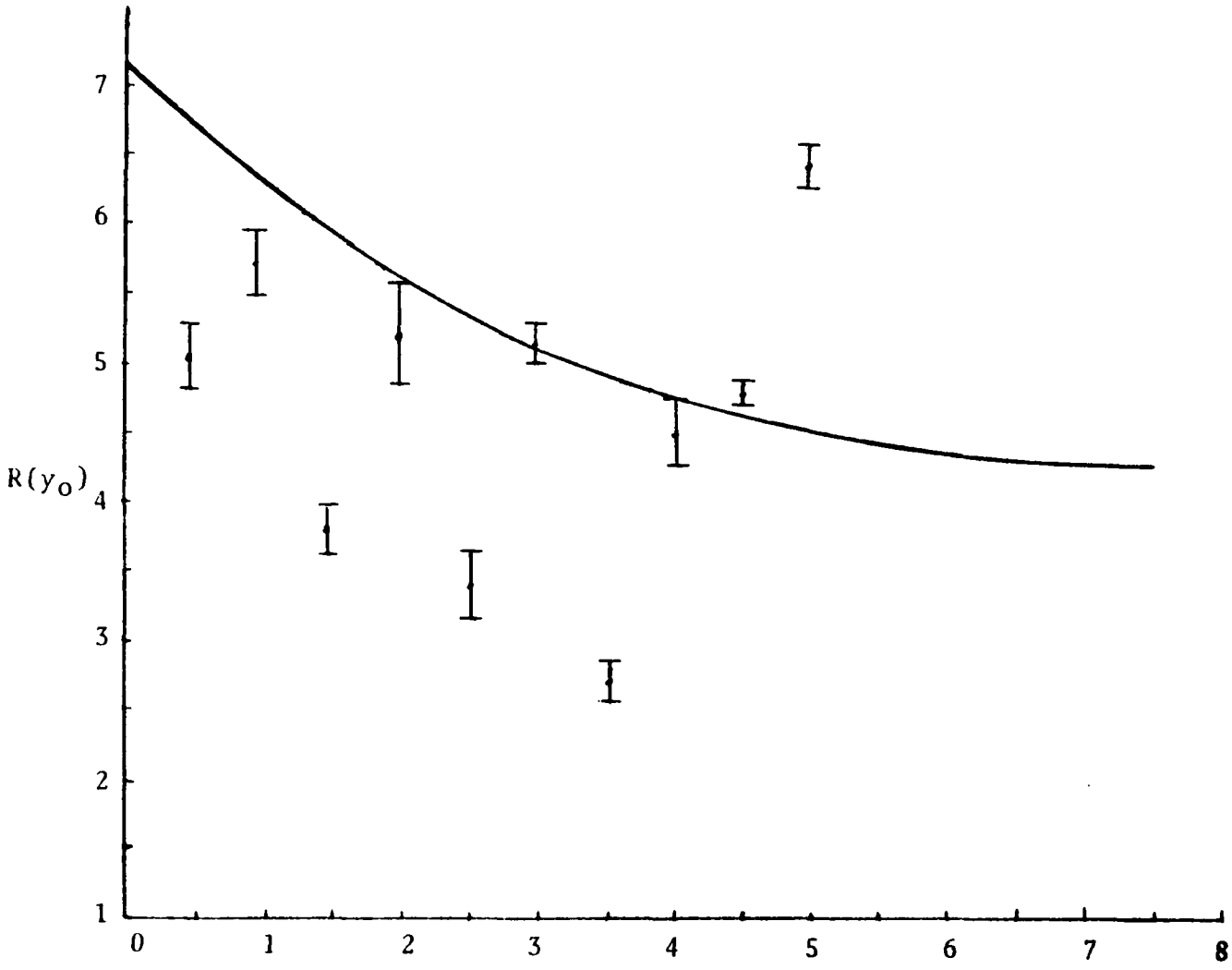

Figure 16. Experiment One Variance Ratios $\frac{\sigma_{\ell}^2(F)}{\sigma_{\ell}^2(L)}$ plotted as a function of $y_o(\frac{D}{L_o})$. The solid line represents the theoretical prediction for $L_o = 20cm$.

these together. Very few variance pairs were excluded, only those having variance ratio values an order of magnitude different than the variance ratio mean, and those whose variances were inverted. The solid line represents the theoretical relationship advanced by Ze'evi for the case of L_o = 20 cm, which seemed to provide the best fit of the experimental data to the theoretical curve. We were relatively free to scale the outer turbulence L_o as desired, as long as it did not exceed the height of the optics above the ground, which was 90 cm.

Although the average ratios plotted in Figure 16 do not conform closely to the theoretical prediction, several reasons for this disparity are possible. First, the technique of projecting a plane wave front for the direct path source and then converting the data to compare with the folded path intensity variance may not have been strictly valid. Moreover, the collimating lens introduced a pronounced Fresnel zone structure in the direct path spot, which could have introduced error into the variance values. Second, the overall strength of the scintillation may have been too low on that particular evening for consistent data to be recorded, given the cumulative effect of the system errors inherent in our equipment. It can be seen from the data that the average strength of the scintillation that night was within the range for weak turbulence, but remained at the low end throughout the night.

D. SECOND OUTSIDE EXPERIMENT

In order to correct for the possible deficiencies in our first experiment, we introduced two changes to both improve the system and increase the strength of the scintillation. We removed the collimating lens pair to eliminate the need to convert the direct path variance to a spherical wave scintillation variance, and allowed the direct path laser pulses to expand naturally upon leaving the laser and passing through the splitter. Then we moved the entire experiment to a new location on the roof of Spanagel Hall. A 40 meter range was chosen that was free of any ventillation ducts or other structures that might change the uniform characteristics of the path. We expected that uniform heating of the red bricks on the roof during the day would result in greater scintillation values at night than at our original location.

During the second experiment, data was sampled for 13 different values of D from D = 10 to D = 110 cm, in intervals of 10 cm. Two additional displacements of D = 5, and D = 150 cm were also used. Once again, the data was taken at night, and no problems were experienced in system alignment or operation. The data was collected over a period of eight hours on 13 November between 8:30 PM and 4:30 AM, and the weather was clear, cool, and with a slight wind present.

The increase in scintillation strength on the roof is definitely present in the increased values of both the direct

path and folded path variance. In addition, the removal of the collimating lens pair eliminated the need for converting of the direct path data. In general, the range of average ratios of the variances is much greater too, and a plot of the ratio

$$\frac{\sigma_{\ell}^2(F)}{\sigma_{\ell}^2(L)} \quad \text{versus} \quad y_o \left(\frac{D}{L_o} \right)$$

for all displacements is presented in Figure 17. As in the results from the first experiment, the solid line represents the proposed relationship advanced by Ze'evi. An outer turbulence scale of L_o = 20 cm was chosen as the best fit of the data to the theoretical prediction. Once again, however, the correlation was not as close as had been hoped.

The points plotted in Figure 17 are labeled for the order in which they were taken during the night. Upon closer examination, it appeared that perhaps some relationship existed between when the data for a particular displacement was collected and the resulting value of the variance ratio. This lead us to the conclusion that perhaps the outer turbulence scale of the range was changing during time required to sample the scintillation at all values of displacement. This would make it impossible to reconcile all our variance ratios to one plot with a single characteristic value of L_o. Therefore, we decided to try to reduce the total time required to sample the scintillation at a significant number of values of the displacement D, in order to try and construct the

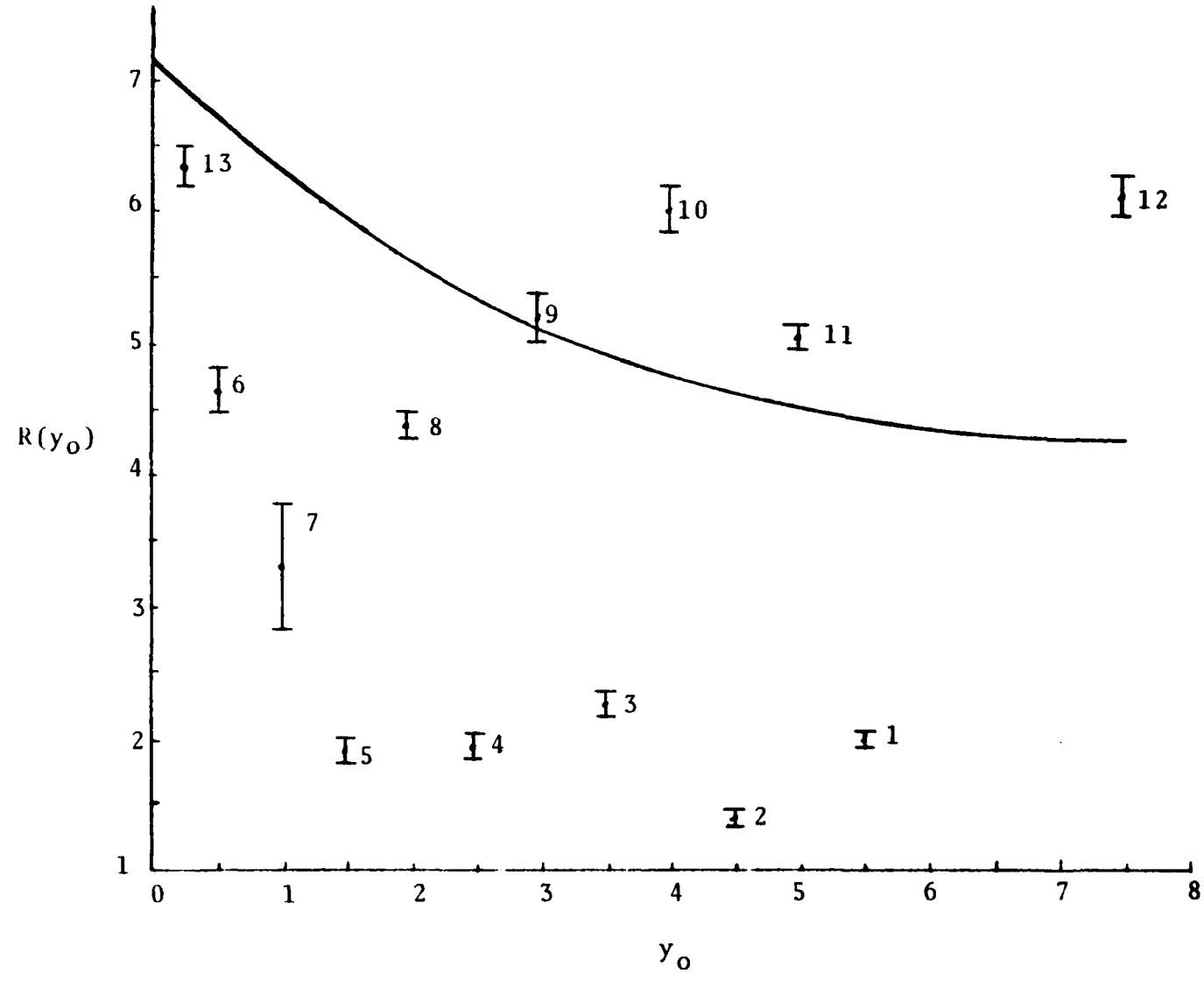

Figure 17. Experiment Two Variance Ratios $\frac{\sigma_{\ell}^2(F)}{\sigma_{\ell}^2(L)}$ Plotted as a Function of $y_o(\frac{D}{L_o})$. The solid line represents the theoretical prediction for L_o= 20 cm.

first part of Ze'evi's curve experimentally. It was also possible that even this would not help because the turbulence may not be uniform throughout the length of the range.

E. THIRD OUTSIDE EXPERIMENT

In this our third experiment, we set out to collect as many variance ratios as possible in the shortest time, beginning with small values of D and working outward from the detector. In this way we hoped to correlate our data with the most critical part of Ze'evi's theoretical curve. To do this required several changes in our scintillation measuring technique, the most important of which was to alter the computer program in the HP-9825A to record fewer data pairs and store them automatically on magnetic tape while aligning the system for a new value of displacement. We chose to record 4 data pairs at each value of D, and we arbitrarily set a time limit of 30 minutes to collect as much data as possible. Additionally, we made a minor change to the folded path source configuration, arranging the laser, Pockels cell, and polarizer on a single base that could be slid as a unit away from the detector, simplifying and shortening realignment time at each successive value of D. Previously the components for the folded path source had been independently mounted and aligned.

During this experiment, we were not able to collect the full range of 13 points as we had done earlier, but

were able to collect five variance ratios in the first 28 minutes. Setup and alignment for each value of D was very rapid, requiring about 4 minutes at each position, and the alignment of each spot from both sources was checked visually each time to ensure that both remained centered on the detector aperture. The data was recorded during the night of 21 November, beginning two hours after sunset. The actual recording of the 4 scintillation pairs on in the NIC-80 required less than a minute, compared to 4 minutes in our two previous experiments when we were collecting 16 scintillation pairs at each value of D.

More scintillation was experienced during this experiment than on the other two nights. A plot of the ratio

$$\frac{\sigma_{\ell}^2(F)}{\sigma_{\ell}^2(L)} \quad \text{versus} \quad y_o \left(\frac{D}{L_o}\right)$$

for the five displacements sampled is shown in Figure 18. An outer turbulence scale of L_o = 20 cm was chosen as a best fit to the theoretical prediction; however, the correlation was again poor.

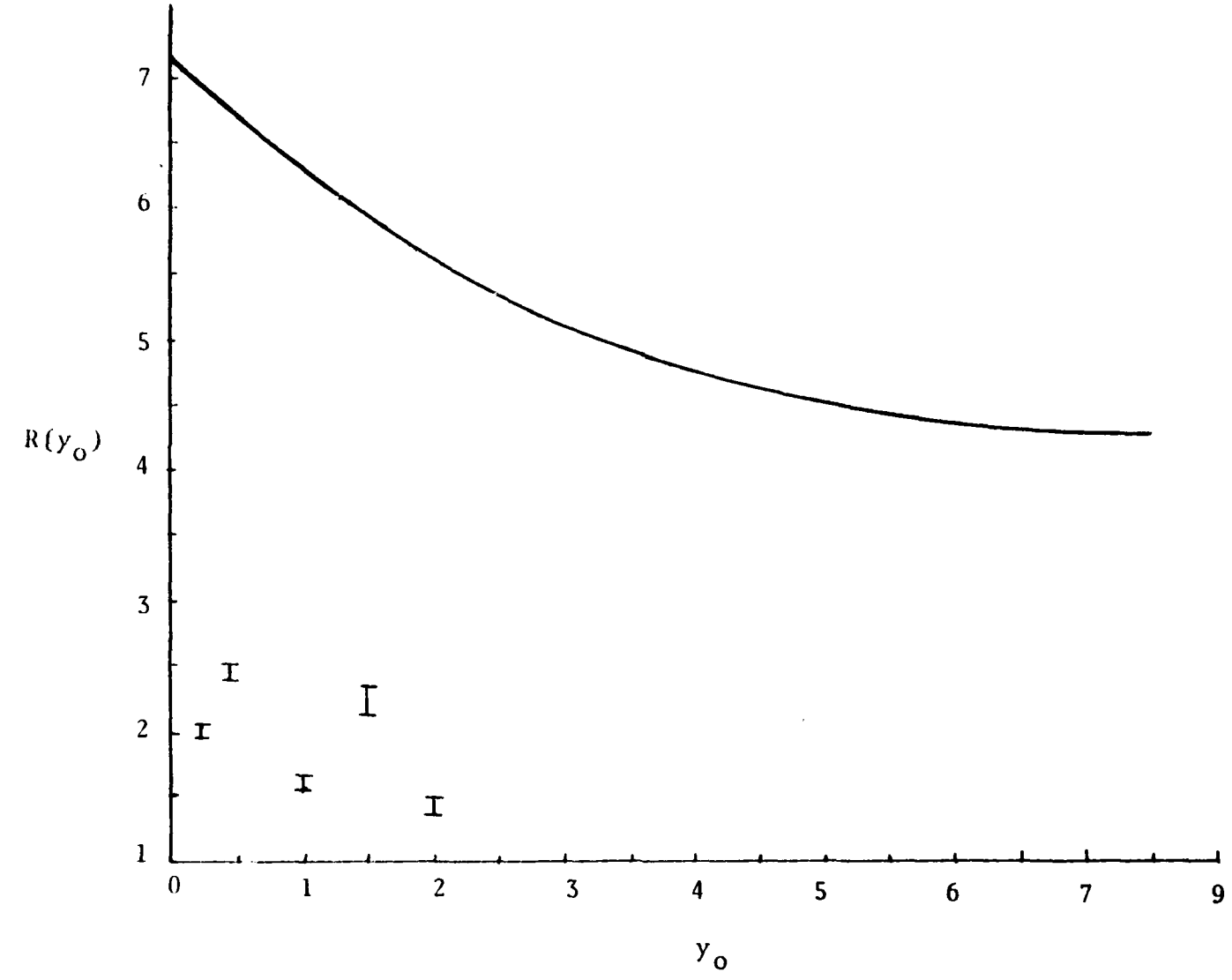

Figure 18. Experiment Three Variance Ratios $\frac{\sigma_\ell^2(F)}{\sigma_\ell^2(L)}$ Plotted as a Function of $y_o(\frac{D}{L_o})$. The solid line represents the theoretical prediction for L_o= 20 cm.

IV. CONCLUSIONS

A. FINDINGS

The findings of this work, based upon our experimental results and analysis of the problem, are as follows:

1. The system as employed in this experiment is suitable for the comparison of directed and folded path scintillation in the weak turbulence regime.

2. Based upon the results of our chi-square analysis of the log normal data, both the direct and folded path intensities are log normally distributed above $\sigma_\ell^2 \approx 0.9$. Below this value, both distributions became severely weighted about the mean and departed markedly from a Gaussian distribution.

3. The scattering of the variance ratios that we measured at various values of displacement does not support the theoretical work by Ze'evi.

B. SUMMARY

As we worked with the equipment and came to understand the problem better, we realized that the business of accurately measuring direct and folded path scintillation was rich in potentially puzzling effects, hard to identify and even harder to eliminate. Even if all other effects are understood, the very nature of performing an experiment

outside the laboratory where you are subject to wind-induced vibrations of your optics or refractive inhomogeneities in the atmosphere, limits your ability to obtain precise data. When we began this experiment, we set for ourselves the following three goals:

1. Construct a system that would allow us to simultaneously record the scintillation over both a direct and a folded path.
2. After recording the scintillation, calculate the scintillation strength for each path and obtain a measure of its validity based upon the accuracy of a log normal assumption distribution.
3. Compare our experimental results of the ratios of folded path variance to direct path variance at various values of displacement in an attempt to verify the theoretical work of Dr. Ze'evi.

Of these three, the first two were achieved and the third requires further work. We were able to construct and test a system that accurately and simultaneously measured direct path and folded path scintillation. This system was successfully tested and produced data that was in agreement with the accepted log normal distribution for scintillation. As expected, folded path variance was consistently greater than the direct path variance during all three outside experiments utilizing two different optical configurations, and the range of the variance ratios was between 2 and 7 in magnitude. Applicability of the weak turbulence scintillation theory was valid, based upon the fact that all log intensity variances were well below 1.2. Additionally,

the statistics program that we wrote for the HP-9825A worked well, and the chi-square test proved to be an accurate measure of the data's correlation to a Gaussian.

What we were not able to do in our experiment was to conclusively prove or disprove the folded path theory. As can be seen from the summary plots of experiments one and two depicted in Figures 16 and 17, there is a fairly wide scattering of the variance ratios at all displacements, and the entire collection of variance ratios from experiment three depicted in Figure 18 lies well below the theoretical curve. Taken at face value, the data does not support the theory; however, the wide range of variables in this experiment that must be controlled to obtain valid results certainly leaves open the possibility that the theory is correct and that the experimental method was not precise enough.

C. EXPLANATIONS

To answer the question of what factors may have been responsible for the scattered nature of the data, it is necessary to look at the data collection techniques that we employed. The first factor that may have played a part is the quality of the sources that we used. In Chapter II we stated that the correlation and variance of the HeNe sources had been examined by Hodgini and found satisfactory. It is possible though that with time and usage, especially

considering the amount of moving about from place to place that we subjected the lasers to, that their internal stability may have been affected. The light from these lasers is randomly polarized, with a source intensity variance of approximately 10^{-4}. If this could have increased with time, then it is certainly possible that the sources would have contributed to the overall scintillation that we measured.

The second factor that may have played a part is that of changing atmospheric conditions, specifically the outer turbulence scale length L_o. This could occur during the collection of a pair of path distributions, during the collection of an entire set of 16 pairs at a given displacement, or during the time required for a set of displacement values to be measured. If any inhomogeneities in the turbulence were present, or if the turbulence was nonuniform throughout the length of the folded path, then this would certainly have affected the data as well. Looking at the first two experiments together since they both employed the same general technique of long periods devoted to the collection of the data, it seems reasonable to assume that non-steady state atmospheric conditions were probably the dominant effect involved in destabilizing the data. This is partially borne out by the results of our third experiment, in which the variance ratios resulting from a much shorter period of time are significantly more consistent.

Taken in the aggregate, the data is extremely inconclusive. No general factor or pattern of the variance ratios emerged. One fact does stand out however, and that is this: future work in this area will absolutely have to control the uniformity and magnitude of the turbulence in the path geometries to accurately verify the folded path theory. Ideally, all 12 or 13 displacements of the folded path should be measured simultaneously in a wind tunnel of controlled, uniform turbulence in order to be absolutely certain that the same factors present in one measurement will be present in all. Any past attempts to correlate folded path scintillation with that of direct path scintillation, and which did not take into account this variable nature of the turbulence must be considered suspect.

D. FUTURE WORK

This experiment needs to be repeated using better sources and an optical configuration that will allow the nearly simultaneous measurement of the folded path scintillation for several values of displacement under uniform conditions. If better and higher power sources were employed, the source stability problem could be eliminated, and the experiment could be performed during the daytime utilizing a narrow bandpass filter in front of the receiver and neutral density filters to control the intensity of the direct path signal.

A broader data base should be constructed, including comparison of direct and folded path scintillation at various heights above the ground. Further investigation into the effects of aperture averaging, different weighting functions, and target interaction as they relate to direct and folded path scintillation is needed. The effect on direct versus folded path correlation if real world variables such as vibration are included needs to be investigated as well. These areas must all be addressed if the theory is to be usable to predict optical system performance under realistic field conditons.

APPENDIX A

NIC-80 COMPUTER PROGRAM

On the pages that follow is listed the computer program we used for the Nicolet Instrument Corporation Model NIC-80. The program is written in the assembly code for the machine which is given in the operating manual, and is compiled on and loaded from the HP-9825A. The 9825A program to perform these functions is an in-house program written by Professor Edmund Milne at the Naval Postgraduate School.

Scintillation File # 9 Track # 0

Address	Content	Mnemonic
0	2110034	MEM A 34
1	4304	LCW
2	110001	MEM A(1
3	4312	LDE
4	110021	MEM A(21
5	4311	LDW
6	4302	SET
7	5220	STO
10	6464	HSR
11	0	JMP 0
12	44463	RHS
13	110000	MEM A(0
14	41	JMP 41
15	227	JMP 227
16	2405666	ACC M 1666 L1
17	405032	RIS 12
20	6474	HSP
21	20	JMP 20
22	4473	PHS
23	2111666	MEM A 1666 L1
24	11777	AND A(1777
25	6474	HSP
26	25	JMP 25
27	4473	PHS
30	1000015	JMP@ 15
31	50017	MCP A(17
32	50217	MCP A(217
33	50617	MCP A(617
34	50417	MCP A(417
35	54017	
36	70000	MNG A(0
37	54217	
40	54417	
41	2110031	MEM A 31
42	4304	LCW
43	2111700	MEM A 1700 B00
44	2405652	ACC M 1652
45	2405671	ACC M 1671 I1
46	2000240	JMS 240
47	6464	HSR
50	46	JMP 46
51	44463	RHS
52	2402000	ACC Z 0
53	302	JMP 302
54	2110037	MEM A 37
55	4304	LCW
56	2165677	ZER M 1677 I
57	3001723	JMS@ 1723 RES

Scintillation File # 9 Track # 0

Address	Content	Mnemonic
60	111000	MEM A(1000
61	2325652	M-A M 1652
62	111000	MEM A(1000
63	2505652	A+M M 1652
64	111000	MEM A(1000
65	5006	LAS 6
66	2405676	ACC M 1676 J
67	2111652	MEM A 1652
70	6114	SE2
71	510400	A+M A(400
72	2405671	ACC M 1671 I1
73	2000240	JMS 240
74	2707676	MMO MZ 1676 J
75	67	JMP 67
76	2135677	MPO AM 1677 I
77	6474	HSP
100	77	JMP 77
101	4473	PHS
102	4032	ASC
103	6464	HSR
104	103	JMP 103
105	44463	RHS
106	2463677	A-M Z 1677 I
107	0	JMP 0
110	462020	A-M Z(20
111	62	JMP 62
112	110001	MEM A(1
113	3405727	ACC M@ 1727 DSK
114	2165677	ZER M 1677 I
115	4031	RSC
116	2111700	MEM A 1700 B00
117	2405676	ACC M 1676 J
120	2111676	MEM A 1676 J
121	4032	ASC
122	3405726	ACC M@ 1726 DSA
123	3001725	JMS@ 1725 DSP
124	44463	RHS
125	405160	EZA
126	0	JMP 0
127	2125677	MPO M 1677 I
130	2471677	A-M A 1677 I
131	6474	HSP
132	131	JMP 131
133	4473	PHS
134	2402000	ACC Z 0
135	5220	STO
136	110400	MEM A(400
137	2405675	ACC M 1675 K

Scintillation File # 9 Track # 0

Address	Content	Mnemonic
140	2110162	MEM A 162
141	2405674	ACC M 1674 L
142	5000	LAS 0
143	111000	MEM A(1000
144	2405672	ACC M 1672 N
145	3111676	MEM A@ 1676 J
146	154	JMP 154
147	4354	TAM
150	3111672	MEM A@ 1672 N
151	2404153	ACC M 153
152	505320	MUL
153	1663460	MULTIPLIER
154	3405674	ACC M@ 1674 L
155	2125676	MPO M 1676 J
156	2125674	MPO M 1674 L
157	2125672	MPO M 1672 N
160	2707675	MMO MZ 1675 K
161	145	JMP 145
162	5000	LAS 0
163	2000224	JMS 224
164	2110162	MEM A 162
165	2405670	ACC M 1670 J1
166	111000	MEM A(1000
167	2405672	ACC M 1672 N
170	110400	MEM A(400
171	2405674	ACC M 1674 L
172	6464	HSR
173	172	JMP 172
174	44463	RHS
175	2402000	ACC Z 0
176	177	JMP 177
177	2111676	MEM A 1676 J
200	2405675	ACC M 1675 K
201	3111675	MEM A@ 1675 K
202	210	JMP 210
203	4354	TAM
204	3111672	MEM A@ 1672 N
205	2404207	ACC M 207
206	505320	MUL
207	1663460	MULTIPLIER
210	3405670	ACC M@ 1670 J1
211	2125676	MPO M 1676 J
212	2125675	MPO M 1675 K
213	2125670	MPO M 1670 J1
214	2125672	MPO M 1672 N
215	2707674	MMO MZ 1674 L
216	201	JMP 201
217	2000224	JMS 224

Scintillation File # 9 Track # 0

Address	Content	Mnemonic
220	2111677	MEM A 1677 I
221	462020	A-M Z(20
222	350	JMP 350
223	0	JMP 0
224	163	JMP 163
225	2110162	MEM A 162
226	2405660	ACC M 1660 L2
227	110400	MEM A(400
230	2405674	ACC M 1674 L
231	3111660	MEM A@ 1660 L2
232	2000015	JMS 15
233	2125660	MPO M 1660 L2
234	5000	LAS 0
235	2707674	MMO MZ 1674 L
236	231	JMP 231
237	1000224	JMP@ 224
240	47	JMP 47
241	6112	SE1
242	241	JMP 241
243	4373	RST
244	2111671	MEM A 1671 I1
245	2405670	ACC M 1670 J1
246	110000	MEM A(0
247	44374	RDG
250	5021	RAS 1
251	510010	A+M A(10
252	5144	EA1
253	1000240	JMP@ 240
254	2505670	A+M M 1670 J1
255	330377	M-A A(377
256	5144	EA1
257	1000240	JMP@ 240
260	330377	M-A A(377
261	5006	LAS 6
262	214001	TAC
263	3135670	MPO AM@ 1670 J1
264	105000	VDS 0
265	4013	TYS
266	1000240	JMP@ 240
267	350	JMP 350
270	2111700	MEM A 1700 B00
271	2405677	ACC M 1677 I
272	110400	MEM A(400
273	2405676	ACC M 1676 J
274	3111677	MEM A@ 1677 I
275	2000015	JMS 15
276	2125677	MPO M 1677 I
277	2707676	MMO MZ 1676 J

Scintillation File # 9 Track # 0

Address	Content	Mnemonic
300	274	JMP 274
301	1000267	JMP@ 267
302	3001723	JMS@ 1723 RES
303	2000240	JMS 240
304	6464	HSR
305	303	JMP 303
306	44463	RHS
307	405160	EZA
310	0	JMP 0
311	110003	MEM A(3
312	3405727	ACC M@ 1727 DSK
313	2111700	MEM A 1700 B00
314	3405726	ACC M@ 1726 DSA
315	3001725	JMS@ 1725 DSP
316	44463	RHS
317	405160	EZA
320	0	JMP 0
321	472001	A-M AZ(1
322	2162000	ZER Z 0
323	302	JMP 302
324	472001	A-M AZ(1
325	2162000	ZER Z 0
326	347	JMP 347
327	462001	A-M Z(1
330	350	JMP 350
331	2000267	JMS 267
332	111000	MEM A(1000
333	2405677	ACC M 1677 I
334	110400	MEM A(400
335	2405676	ACC M 1676 J
336	6464	HSR
337	336	JMP 336
340	44463	RHS
341	5004	LAS 4
342	3405677	ACC M@ 1677 I
343	2125677	MPO M 1677 I
344	2707676	MMO MZ 1676 J
345	336	JMP 336
346	0	JMP 0
347	2000267	JMS 267
350	2111676	MEM A 1676 J
351	471000	A-M A(1000
352	3405726	ACC M@ 1726 DSA
353	3001725	JMS@ 1725 DSP
354	44463	RHS
355	120	JMP 120

APPENDIX B

HEWLETT-PACKARD 9825A CALCULATOR PROGRAMS

Two programs for the HP-9825A are listed in this appendix. The first program does not give the operator the option of storing the data run (at a specific displacement) on magnetic tape before advancing to the next displacement. The second program does contain this option, as well as the choice of how many data pairs (pairs of direct and folded path scintillation distributions) to record at each displacement. Note, however, that the number of data pairs selected in this program MUST correspond to the number of data pairs specified in steps 110 and 221 of the NIC-80 program.

FIRST PROGRAM

```
0: "SPEER/PARKER SCINTILLATION PROGRAM 8/82":
1: dsp "SCINT PROGRAM: push contin";stp
2: dim D$[13],M$[2,60],Q[10]
3: dim A$[39,40],B$[7],P[256],G[256];716→F;701→E
4: dim S[256];dev "E",E,"F",F;on err "er1"
5: dim N$[12,3],R[256],I[256]
6: fxd 0;ldf 2,A$;mdec;" meters"→B$[1,7]
7: time 250;on err "er1"
8: if rds(701)#17;dsp "Printer is not ready";stp
9: 6.328e-7→X;33.169→r0;1→Q[1];5→Q[2];9→Q[3];13→Q[4];17→Q[5]
10: wtb E,27,69,27,84,27,76,13,32,32,32,32,32,32,32;21→Q[6]
11: wtb E,32,32,32,32,32,27,77
12: 25→Q[7];29→Q[8];33→Q[9];37→Q[10];if rds(2)#296;cll "er2"
13: 0→L;1/r0→r25;for J=1 to 256;(J+L)r25/2→S[J];J→L;next J
14: "JAN"→N$[1];"FEB"→N$[2];"MAR"→N$[3]
15: "APR"→N$[4];"MAY"→N$[5];"JUN"→N$[6];"JUL"→N$[7]
16: "AUG"→N$[8];"SEP"→N$[9]
17: "OCT"→N$[10];"NOv"→N$[11];"DEC"→N$[12]
18: on err "er2";wtb 2,1;gto "scint"
19: "er2":beep;dsp "NIC 80 DOWN";wait 250;dsp " ";jmp 0
20: "er1":beep;dsp "error ",char(rom),ern," line ",er1
21: wait 1000
22: if ern=66;wrt "E","Division by zero occured in line",er1
23: stp ;gto r20
24: "input":ent "Enter the number of the month",N
25: ent "Enter the day",T
26: N$[N,1,3]→D$[1,3];". "→D$[4,5];str(T)→D$[6,8]
27: " 1982"→D$[9,13]
28: rlt 3;dsp "Enter wavelength",X;ent "",X;fxd 0
29: ent "Enter run comments",M$[1,1,60]
30: ent "Enter weather comments",M$[2,1,60];ret
31: "scint":on err "er1";time 30000
32: ent "Enter 0 for cal. or 0 for data",M;if M#0;gto "cal"
33: ent "Enter range",R
34: cll "input";dsp "set tcp of form on printer";stp
35: wtb 2,M;wtb E,27,69,27,84,27,76,13,32,32,32,32,32,27,77
36: for I=1 to 16;dsp I,"Scint accumulation"
37: rdb(2)→J;if J#I;wtb 2,I;beep;dsp "OUT OF SYNC";stp
38: wtb 2,I;next I
39: ent "Enter 0=abort, 1=output",B;if B=0;wtb 2,B;gto 0
40: fmt 1,c13,/,c60,/,c60,/,"Wavelength= ",e10.2,c7,/,/,/
41: fmt 2,"    # pts       Sigma    Chi Square",/
42: fmt 3,f4.0,":",f5.0,x,f10.4,x,le10.2
43: fmt 4,f4.0,":",f5.0,x,f10.4,x,le10.2,"**"
44: fmt 6,"Fixed range=",f6.0,c7,/
45: wrt "E.1",D$,M$[1,1,60],M$[2,1,60],X,B$
46: wrt "E","Scintillation measurements of Sigma"
*23317
```

```
47: wrt "E","16384 samples for each measurement"
48: wrt "E.6",R,B$
49: wrt "E.2";gto 50
50: for I=1 to 16;wtb 2,I;rdb(2)→B
51: if B#0;beep;dsp "NOT IN SYNC";wait 2000;gto 0
52: for J=1 to 256;1024*rdb(2)+rdb(2)→R[J];next J
53: wtb 2,1;for J=1 to 256;1024*rdb(2)+rdb(2)→I[J]
54: next J;0→r20→r21
55: for J=1 to 256;r20+R[J]→r20;r21+I[J]→r21;next J;0→B→A
56: dsp "Statistics Calculations"
57: for J=1 to 256;A+R[J]*S[J]→A;B+I[J]*S[J]→B
58: next J;A/r20→A;B/r21→B;0→S→V
59: for J=1 to 256;S+R[J](S[J]-A)(S[J]-A)→S
60: V+I[J](S[J]-B)(S[J]-B)→V;next J
61: √(V/r21)→V;√(S/r20)→S;S→r18;r20→Z;r25/2→r6
62: for K=1 to 2;0→r17;for J=1 to 256;S[J]-r6→r7
63: S[J]+r6→r8;(r7-A)/r18*100→r9;(r8-A)/r18*100→r10
64: frc(abs(r9))→r30;frc(abs(r10))→r26;r9/10→r9;r10/10→r10
65: for Y=1 to 2
66: int(abs(r9))→r11;int(abs(r10))→r12;if r9<0;-r11→r11
67: if r10<0;-r12→r12
68: if r11>38;38-r11+r9→r9;38→r11
69: if r11<-38;(r11+38)(-1)+r9→r9;-38→r11
70: if r12>38;38-r12+r10→r10;38→r12
71: if r12<-38;-(r12+38)+r10→r10;-38→r12
72: int(frc(abs(r9))*10+1)→r13;int(frc(abs(r10))*10+1)→r14
73: Q[r13]→r13;Q[r14]→r14
74: if r11>0;stf(A$[r11,r13,r13+3])→r15
75: if r11=0;stf(A$[39,r13,r13+3])→r15;if r9<0;1-r15→r15
76: if r11<0;abs(r11)→r11;1-stf(A$[r11,r13,r13+3])→r15
77: if r12>0;stf(A$[r12,r14,r14+3])→r16
78: if r12=0;stf(A$[39,r14,r14+3])→r16;if r10<0;1-r16→r16
79: if r12<0;abs(r12)→r12;1-stf(A$[r12,r14,r14+3])→r16
80: if Y=1;r16→r28;r15→r27;gto 82
81: gto 86
82: if r9<0;r9-.1→r9;gto 84
83: r9+.1→r9
84: if r10<0;r10-.1→r10;gto 86
85: r10+.1→r10
86: next Y;(r15-r27)*r30+r27→r15;(r16-r28)*r26+r28→r16
87: prnd(Z*(r16-r15),0)→P[J]
88: if P[J]>0;(R[J]-P[J])^2/P[J]+r17→r17
89: next J;if K=2;gto 92
90: if r17>287.88;wrt "E.4",I,Z,S,r17;cll "Plot";gto 94
91: wrt "E.3",I,Z,S,r17;cll "Plot";gto 94
92: if r17>287.88;wrt "E.4",I,Z,V,r17;cll "Plot";gto 95
93: wrt "E.3",I,Z,V,r17;cll "Plot";gto 95
*22051
```

```
94: r21→Z;B→A;V→r18;ara I→R
95: next K
96: wtb 2,1;next I
97: wtb E,12;gto 7
98: "cal":wtb 2,1
99: ent "0-abort,1-display",D;wtb 2,D;if D=0;gto 0
100: ent "0-abort,1-reset,2-c out,3-bin",D
101: if D=1;wtb 2,D;jmp -2
102: if D=0;wtb 2,D;gto 0
103: if D=2;wtb 2,1;gto "c out"
104: if D=3;wtb 2,D;gto "bin"
105: "c out":dsp "DON'T USE W/O DIGITAL VOLTMETER!"
106: stp ;dsp "Set V1,push continue";stp
107: red 722,K;red 722,K;dsp "Set V2,push continue";stp
108: red 722,L;red 722,L
109: for I=1 to 256;1024*rdb(2)+rdb(2)→A
110: if A>10;fxd 3;prt A+I/1000;fxd 0
111: next I
112: ent "Enter X1",r2,"Enter X2",r3
113: (r3-r2)/(ln(L)-ln(K))→r0;gto 0
114: "bin":0→A;for J=1 to 256;1024*rdb(2)+rdb(2)→I[J];next J
115: min(I[*])→A
116: for J=1 to 256;int(32000*A/I[J])→E;wtb 2,E;next J
117: gto 7
118: "Plot":ent "PLOT type 1,continue 0",r22;if r22#1;gto 143
119: csiz 1.7,1.7,.71,0
120: fxd 0;scl -1.3,8.9,-150,1600;plt 6.2,1550,1
121: lbl "Plot of ";lbl K
122: lbl " way";cplt -14,-1
123: lbl "Scintillation Run #";lbl I;plt 6.2,1455,1;lbl D$
124: cplt -13,-1;lbl M$[1,1,60];fxd 5
125: plt 6.2,1360,1;lbl M$[2,1,60];plt 6.2,1313,1
126: lbl "Exper. Sigma ";lbl r18
127: plt 6.2,1265,1
128: lbl "Exper. Mean  ";lbl A;fxd 3;plt 6.2,1217,1
129: lbl "Chi Square  ";lbl r17;fxd 0;pen
130: plt 0,0,1;plt 8.7,0,2;plt 0,0,1;plt 0,1600,2;pen
131: for X=0 to 8 by 2;plt X,-9,1;cplt -.5,-1.5;lbl X;next X
132: 0→Y
133: plt -.3,Y,1;cplt -2,-.3;lbl Y;Y+500→Y;if Y=2000;gto 135
134: gto 133
135: plt 3,-150,1;lbl "Log Intensity";plt -1,500,1
136: csiz 1.7,1.7,.71,90;lbl "No. of Counts"
137: csiz 1.7,1.7,.71,0;for J=1 to 256
138: plt S[J],R[J],-2;pen;next J;pen;plt 0,0,-2
139: for J=1 to 256;plt S[J],P[J];next J
140: plt 6.2,1169,1;lbl ".  Exper. Curve"
141: plt 6.2,1123,1;lbl "-  Chi Sq. Prediction"
142: plt 8,1500,1
143: ret
144: end
```

```
0: "SPEER/PARKER SCINTILLATION PROGRAM 8/82":
1: dsp "SCINT PROGRAM: push contin";stp
2: dim D$[13],M$[2,60],X,B$[7],R,Q[10]
3: dim A$[39,40],P[256],G[256];716→F;701→E
4: dim S[256];dev "E",E,"F",F;on err "er1"
5: dim N$[12,3],R[256],I[256]
6: fxd 0;lat 11,A$;mdec;" meters"→B$[1,7]
7: time 250;on err "er1"
8: if ras(701)#17;dsp "Printer is not ready";stp
9: 6.328e-7→X;33.169→r0;1→Q[1];5→Q[2];9→Q[3];13→Q[4];17→Q[5]
10: wtb E,27,69,27,84,27,76,12,32,32,32,32,32,32,32,32,32,32
11: wtb E,32,32,27,77
12: 21→Q[6];25→Q[7];29→Q[8]
13: 33→Q[9];37→Q[10];if ras(2)#296;cll "er2"
14: 0→L;1/r0→r25;for J=1 to 256;(J+L)r25/2→S[J];J→L;next J
15: "JAN"→N$[1];"FEB"→N$[2];"MAR"→N$[3]
16: "APR"→N$[4];"MAY"→N$[5];"JUN"→N$[6];"JUL"→N$[7]
17: "AUG"→N$[8];"SEP"→N$[9]
18: "OCT"→N$[10];"NOV"→N$[11];"DEC"→N$[12]
19: on err "er2";wtb 2,1;gto "scint"
20: "er2":beep;dsp "NIC 80 DOWN";wait 250;dsp " ";jmp 0
21: "er1":beep;dsp "error ",char(rom),ern," line ",erl
22: wait 1000
23: if ern=66;wrt "E","Division by zero in line",erl;stp
24: gto 21
25: "input":ent "Enter the number of the month",N
26: ent "Enter the day",T
27: N$[N,1,3]→D$[1,3];". "→D$[4,5];str(T)→D$[6,8]
28: " 1982"→D$[9,13]
29: flt 3;dsp "Enter wavelength",X;ent "",X;fxd 0
30: ent "Enter run comments",M$[1,1,60]
31: ent "Enter weather comments",M$[2,1,60]
32: ent "Enter pair counter",r36;0→r31
33: ent "Enter record file",r32;r32→r34
34: ent "Enter track number",r35;ret
35: "scint":on err "er1";time 30000
36: ent "Enter 1 for cal. or 0 for data",M;if M#0;gto "cal"
37: ent "Enter range",R
38: cll "input";dsp "set top of form on printer";stp
39: wtb 2,M;wtb E,27,69,27,84,27,76,12,32,32,32,32,32,32,32
40: wtb E,32,32,32,32,27,77
41: for I=1 to r36;dsp I,"Scint accumulation"
42: rdb(2)→J;if J#I;wtb 2,I;beep;dsp "OUT OF SYNC";stp
43: wtb 2,I;r31+1→r31;next I
44: dsp "Recording Data";trk r35;clg ;rcr r32,D$,M$,X,B$,R
45: r32+1→r32
46: for I=1 to r36;wtb 2,I;rdb(2)→B
```

```
47: if B#0;beep;asp "NOT IN SYNC";wait 2000;gto 0
48: for J=1 to 256;1024*rab(2)+rab(2)→R[J];next J
49: wtb 2,1;for J=1 to 256;1024*rab(2)+rab(2)→I[J];next J
50: rcf r32,R[*],I[*];r32+1→r32;wtb 2,1;next I
51: ent "Enter 0 next run,1 for calc",r33
52: if r33=0;dsp "READY: Push Cont.";stp ;gto 38
53: for M=1 to r31;ent "Enter start file",r34
54: ent "Enter track number",r35;trk r35
55: laf r34,D$,M$,X,B$,R;r34+1→r34
56: fmt 1,c13,/,c60,/,c60,/,"Wavelength= ",e10.2,c7,/,/,/
57: fmt 2,"    # pts       Sigma    Chi Square",/
58: fmt 3,f4.0,":",f5.0,x,f10.4,x,le10.2
59: fmt 4,f4.0,":",r5.0,x,r10.4,x,le10.2,"**"
60: fmt 6,"Fixed range=",f6.0,c7,/
61: wrt "E.1",D$,M$[1,1,60],M$[2,1,60],X,B$
62: wrt "E","Scintillation measurements of Sigma"
63: wrt "E","16384 samples for each measurement"
64: wrt "E.6",R,B$
65: wrt "E.2"
66: for I=1 to r36;laf r34,R[*],I[*]
67: 0→r20→r21
68: for J=1 to 256;r20+R[J]→r20;r21+I[J]→r21;next J;0→B→A
69: dsp "Statistics Calculations";for J=1 to 256;A+R[J]*S[J]→A
70: B+I[J]*S[J]→B;next J;A/r20→A;B/r21→B;0→S→V
71: for J=1 to 256;S+R[J](S[J]-A)(S[J]-A)→S
72: V+I[J](S[J]-B)(S[J]-B)→V;next J
73: √(V/r21)→V;√(S/r20)→S;S→r18;r20→Z;r25/2→r6
74: for K=1 to 2;0→r17;for J=1 to 256;S[J]-r6→r7
75: S[J]+r6→r8;(r7-A)/r18*100→r9;(r8-A)/r18*100→r10
76: frc(abs(r9))→r30;frc(abs(r10))→r26;r9/10→r9;r10/10→r10
77: for Y=1 to 2
78: int(abs(r9))→r11;int(abs(r10))→r12;if r9<0;-r11→r11
79: if r10<0;-r12→r12
80: if r11>38;38-r11+r9→r9;38→r11
81: if r11<-38;(r11+38)(-1)+r9→r9;-38→r11
82: if r12>38;38-r12+r10→r10;38→r12
83: if r12<-38;-(r12+38)+r10→r10;-38→r12
84: int(frc(abs(r9))*10+1)→r13;int(frc(abs(r10))*10+1)→r14
85: Q[r13]→r13;Q[r14]→r14
86: if r11>0;stf(A$[r11,r13,r13+3])→r15
87: if r11=0;stf(A$[39,r13,r13+3])→r15;if r9<0;1-r15→r15
88: if r11<0;abs(r11)→r11;1-stf(A$[r11,r13,r13+3])→r15
89: if r12>0;stf(A$[r12,r14,r14+3])→r16
90: if r12=0;stf(A$[39,r14,r14+3])→r16;if r10<0;1-r16→r16
91: if r12<0;abs(r12)→r12;1-stf(A$[r12,r14,r14+3])→r16
92: if Y=1;r16→r28;r15→r27;gto 94
93: gto 98
```

```
94: if r9<0;r9-.1→r9;gtc 96
95: r9+.1→r9
96: if r10<0;r10-.1→r10;gtc 98
97: r10+.1→r10
98: next Y;(r15-r27)*r30+r27→r15;(r16-r28)*r26+r28→r16
99: prnd(Z*(r16-r15),0)→P[J]
100: if P[J]>0;(R[J]-P[J])^2/P[J]+r17→r17
101: next J;if K=2;gtc 104
102: if r17>287.88;wrt "E.4",I,Z,S,r17;cll "Plot";gto 106
103: wrt "E.3",I,Z,S,r17;cll "Plot";gto 106
104: if r17>287.88;wrt "E.4",I,Z,V,r17;cll "Plot";gto 107
105: wrt "E.3",I,Z,V,r17;cll "Plot";gto 107
106: r21→Z;B→A;V→r18;ara I→R
107: next K
108: r34+1→r34;next I
109: wtb E,12;next M
110: wtb E,12;gto 0
111: "cal":wtb 2,1
112: ent "0-abort,1-display",D;wtb 2,D;if D=0;gto 0
113: ent "0-abort,1-reset,2-c out,3-bin",D
114: if D=1;wtb 2,D;jmp .-2
115: if D=0;wtb 2,D;gto 0
116: if D=2;wtb 2,1;gto "c out"
117: if D=3;wtb 2,D;gto "bin"
118: "c out":asp "DON'T USE ROUTINE W/O DIGITAL VOLTMETER!"
119: stp ;asp "Set v1,push continue";stp
120: red 722,K;red 722,K;asp "Set V2,push continue";stp
121: red 722,L;red 722,L
122: for I=1 to 256;1024*rab(2)+rab(2)→A
123: if A>10;rxd 3;prt A+I/1000;rxd 0
124: next I
125: ent "Enter X1",r2,"Enter X2",r3
126: (r3-r2)/(ln(L)-ln(K))→r0;gto 0
127: "bin":0→A;for J=1 to 256;1024*rab(2)+rab(2)→I[J];next J
128: min(I[*])→A
129: for J=1 to 256;int(32000*A/I[J])→B;wtb 2,B;next J
130: gto 7
131: "Plot":ent "PLOT input 1,continue 0",r22;if r22#1;gto 154
132: csiz 1.7,1.7,.71,0
133: rxd 0;scl -1.3,8.9,-150,1600;plt 6.2,1550,1
134: lbl "Plot of ";lbl K;lbl " way";cplt -14,-1
135: lbl "Scintillation Run #";lbl I;plt 6.2,1455,1;lbl D$
136: cplt -13,-1;lbl M$[1,1,60];rxd 5
137: plt 6.2,1360,1;lbl M$[2,1,60];plt 6.2,1313,1
138: lbl "Exper. Sigma ";lbl r18;plt 6.2,1265,1
139: lbl "Exper. Mean  ";lbl A;rxd 3;plt 6.2,1217,1
140: lbl "Chi Square  ";lbl r17;rxd 0;pen
```

```
141: plt 0,0,1;plt 8.7,0,2;plt 0,0,1;plt 0,1600,2;pen
142: for X=0 to 8 by 2;plt X,-9,1;cplt -.5,-1.5;lbl X;next X
143: 0→Y
144: plt -.5,Y,1;cplt -2,-.3;lbl Y;Y+500→Y;if Y=2000;gto 146
145: gto 144
146: plt 3,-150,1;lbl "Log Intensity";plt -1,500,1
147: csiz 1.7,1.7,.71,90;lbl "No. of Counts";csiz 1.7,1.7,.71,0
148: for J=1 to 256
149: plt S[J],R[J],-2;pen;next J;pen;plt 0,0,-2
150: for J=1 to 256;plt S[J],P[J];next J
151: plt 6.2,1169,1;lbl ".  Exper. Curve"
152: plt 6.2,1122,1;lbl "-  Chi Sq. Prediction"
153: plt 8,1500,1
154: ret
155: end
*32056
```

APPENDIX C

CHI-SQUARE GOODNESS OF FIT TESTING TO THE DISTRIBUTION HYPOTHESIS

The following discussion will illustrate the rationale behind our selection of the chi-square test to examine the assumed log normal intensity distributions in our experiments. It will also describe the methodology utilized in the actual determination of the chi-square value that was calculated for each log intensity distribution. Two theorems are necessary in order to begin. [Ref. 7].

Theorem 1: Assume that Y has distribution function F_y, which is either discrete or continuous, and that Y_1, Y_2, Y_n is a random sample of Y. Then if we define

$$I_1 = (y: y \leq a), \quad I_2 = (y: a_1 < y \leq a_2) \ldots,$$

$$I_{k-1} = (y: a_{k-2} < y \leq a_{k-1}), \quad I_k = (y: a_{k-1} < y),$$

and let X_i be the number of sample values that fall in I_i, $i = 1,2,\ldots,k$, $(X_1, X_2, \ldots, X_k)$ is the multinomial random variable with parameters $n, p_1, p_2, \ldots, p_k$, where n is the sample size (for the sample of Y) and

$$p_i = P[Y \text{ falls in } I_i], \quad i = 1,2,3,\ldots,k.$$

Theorem 2: Assume that Y has distribution function F_y which satisfies certain regularity conditions and which is indexed by r unknown parameters, Θ_1, Θ_2, ..., Θ_r, and that

$Y_1, Y_2, \ldots, Y_n$ is a random variable of Y. Let $\hat{\theta}_1, \hat{\theta}_2, \ldots, \hat{\theta}_r$ be the maximum likelihood estimators for $\theta_1, \theta_2, \ldots, \theta_r$, respectively, and define $I_1, I_2, \ldots, I_k$ and $X_1, X_2, \ldots, X_k$ as in Theorem 1. Then, if we define

$$\hat{P}_i = P[Y \text{ falls in } I_i], \quad i = 1,2,\ldots,k$$

where $\hat{\theta}_1, \hat{\theta}_2, \ldots, \hat{\theta}_r$ replace $\theta_1, \theta_2, \ldots, \theta_r$ in F_Y, the distribution of the statistic

$$V = \sum_{i=1}^{k} \frac{(X_i - n P_i)^2}{n \hat{P}_i}$$

tends to that of a chi-square random variable with k-r-1 degrees of freedom as n gets large.

Therefore, when it is desired to test the hypothesis that F_y has a specified form, the actual data is used to estimate the parameters and then the chi-square test is initiated. That is, the observed value of V is computed and then compared with the $100(1 - \alpha)$ percentile of the chi-square distribution with k-r-1 degrees of freedom. If the value of V exceeds this latter value, then the hypothesis that F_Y has the specific form is rejected.

In practice, Larson [Ref. 7] states that there is general agreement that the length of the finite intervals should be equal. In addition, he states that many authors agree that the chi-square approximation specified in Theorem 2 is quite good when the number of intervals used is

as large as possible, consistent with the constraint that $n\,p_i \geq 5$ for $i=1,2,\ldots,k$.

For the purposes of this experiment, it was desired to test the hypothesis that the log intensity distribution for a given path configuration could be described by a normal distribution. Therefore, the hypothesis was that the log intensity was a normal random variable.

To accomplish this, the points in a specific signal distribution (from a given path geometry in a run) were first counted then used to compute the observed values of the maximum likelihood estimators for the normal distribution. These were the mean, $\hat{M}$, and the variance, $\hat{\sigma}^2$, and they were determined as follows:

$$\hat{M} = \frac{1}{n} \sum_{\ell=1}^{n} \text{count}(\ell)$$

and

$$\hat{\sigma}^2 = \frac{1}{n} \sum_{\ell=1}^{n} (\text{count}(\ell) - \hat{M})^2$$

where

n = total number of points in a distribution, and

$\text{count}(\ell)$ = intensity value of a single point.

For our experiment, and subject to the constraints discussed previously as well as the dynamic range of the ADC in the NIC-80, 256 intervals of equal length were used with $n \approx 16{,}384$. The index k denotes a particular interval or bin. Because the data was stored in a histogram of counts

per bin, we used the following expressions, which are equivalent to those listed above, to compute M and $\hat{\sigma}^2$:

$$\hat{M} = \frac{1}{n} \sum_{k=1}^{256} (\overline{\text{bin } k}) \text{ (freq (K))}$$

$$\hat{\sigma}^2 = \frac{1}{n} \sum_{k=1}^{256} \text{(freq (K))} (\overline{\text{bin } K} - \hat{M})^2$$

where $\overline{\text{bin } k}$ = mean value of the Kth bin interval,

freq(k) = number of counts in bin K.

Once these two values were calculated, they were used to compute the observed values of the estimators of the probabilities of individual log intensity values falling into the 256 bins used to summarize the distribution. To compute these values, denoted $\hat{P}_1$, $\hat{P}_2$,..., $\hat{P}_{256}$, the probability that a normal random variable with mean and standard deviation $\hat{\sigma}$ would exist in each of the 256 intervals was calculated.

This was easily accomplished for the normal distribution by using the standard normal table and the expressions

$$\hat{P}_k = N_z \left(\frac{\text{bin } k_h - \hat{M}}{\hat{\sigma}} \right) - N_z \left(\frac{\text{bin } k_L - \hat{M}}{\hat{\sigma}} \right)$$

where bin k_h = upper value for bin k, and

bin k_L = lower value for bin k.

The next step required the calculation of the statistic V, using the expression

$$V = \sum_{k=1}^{256} \frac{[\text{freq}(k) - n(\hat{P}_k)]^2}{n(\hat{P}_k)}$$

The expression for degrees of freedom from Theorem 2 is degrees of freedom = k-r-1, where k = 256, the number of bins, and r = 2, for the parameters $\hat{M}$ and $\hat{\sigma}$ that were estimated. Therefore, there were 253 degrees of freedom for this process. With this information, the final step was to determine the value for the desired percentile of the chi-square distribution with 253 degrees of freedom and compare this to the statistic V. We chose the 95th percentile, with a value of 287.88. For any given log intensity distribution, if the value calculated for V was less than 287.88, then the hypothesis that the distribution was normal was accepted. If V was greater than this value, then the hypothesis was rejected.

APPENDIX D

DATA FROM THE FIRST EXPERIMENT

D(cm)	$\langle R \rangle \left(\langle \frac{\sigma_F^2}{\sigma_S^2} \rangle \right)$	Error $\left(\pm \frac{\sigma}{N} \right)$	Runs Utilized	Comments
0	2.77	.109	All sixteen	Two splitters
10	5.02	.207	All	(Decreasing ratios throughout the run)
20	5.70	.260	All	
30	3.77	.156	excl. #3	
40	5.16	.360	All	
50	3.40	.249	All	
60	5.17	.123	All	
70	2.68	.166	excl. #4	
80	4.54	.211	excl. #6,12	
90	4.70	.063	All	
100	6.39	.173	All	

NOV. 3 1982
Ap,1500,2k,1k,300k,0
Night,still,cir,outsd
Wavelength= 6.33E-07 meters

Scintillation measurements of Sigma
16384 samples for each measurement
Fixed range= 100 meters

# pts	Sigma	Chi Square
1:16385	0.2321	1.17E 03**
1:16383	0.1755	8.92E 02**
2:16385	0.2109	1.17E 03**
2:16383	0.1544	1.13E 03**
3:16385	0.2159	1.29E 03**
3:16383	0.1598	1.34E 03**
4:16385	0.2162	1.09E 03**
4:16383	0.1622	9.98E 02**
5:16385	0.2162	1.10E 03**
5:16383	0.1516	1.17E 03**
6:16385	0.2154	1.06E 03**
6:16383	0.1437	1.56E 03**
7:16385	0.2043	1.19E 03**
7:16383	0.1291	1.37E 03**
8:16385	0.2206	1.27E 03**
8:16383	0.1443	1.27E 03**
9:16385	0.2017	1.24E 03**
9:16383	0.1182	1.36E 03**
10:16385	0.2038	1 37E 03**
10:16383	0.1289	1.59E 03**
11:16385	0.2076	1.58E 03**
11:16383	0.1366	1.49E 03**
12:16383	0.2070	1.13E 03**
12:16383	0.1478	1.38E 03**
13:16383	0.2015	1.22E 03**
13:16385	0.1447	1.27E 03**
14:16383	0.2057	1.20E 03**
14:16385	0.1553	1.07E 03**
15:16383	0.2094	1.14E 03**
15:16385	0.1411	1.29E 03**
16:16382	0.1957	1.21E 03**
16:16385	0.1510	1.70E 03**

Figure 19. Scintillation Statistics

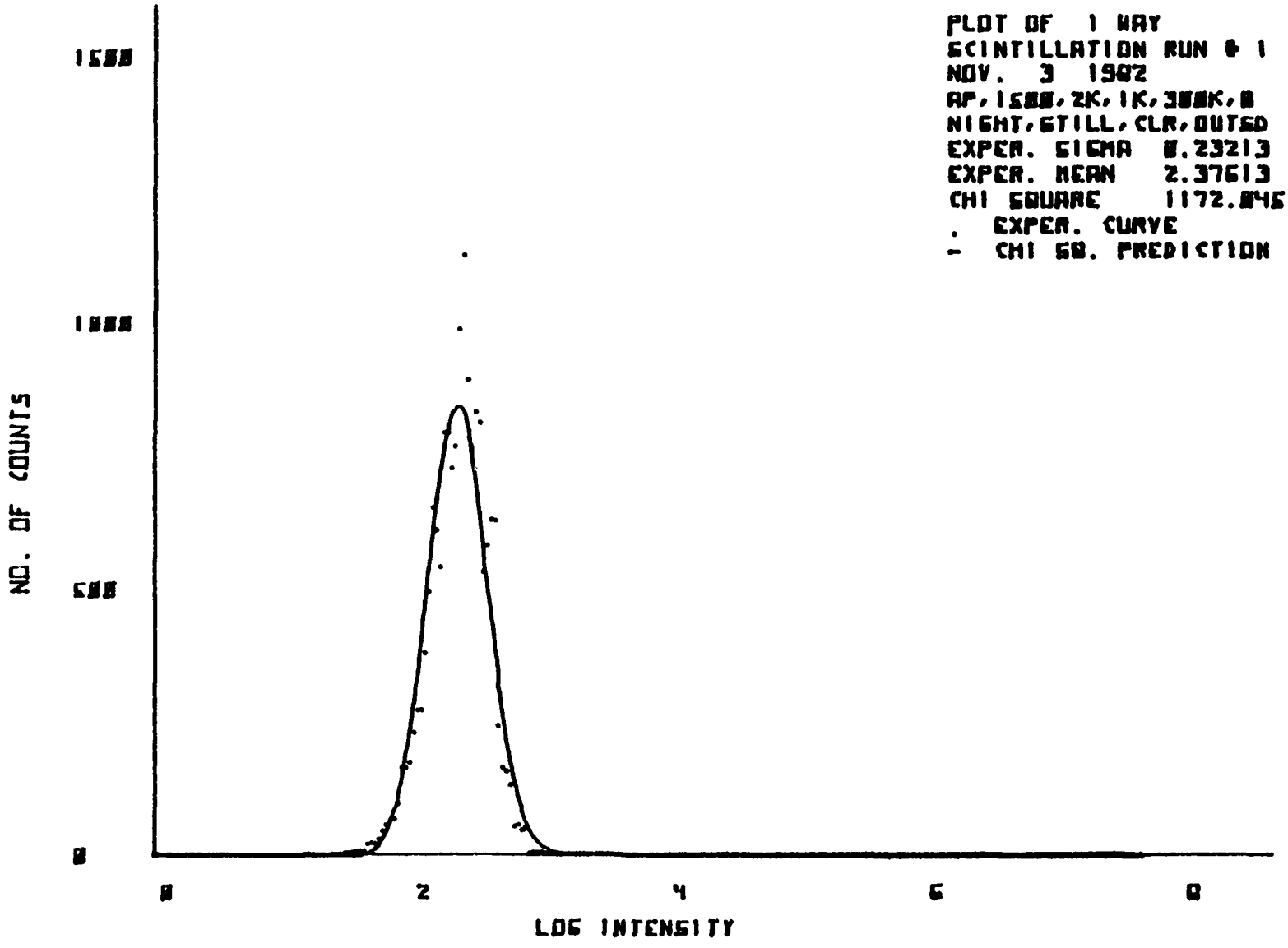

Figure 20. Scintillation Data and Theoretical Curve

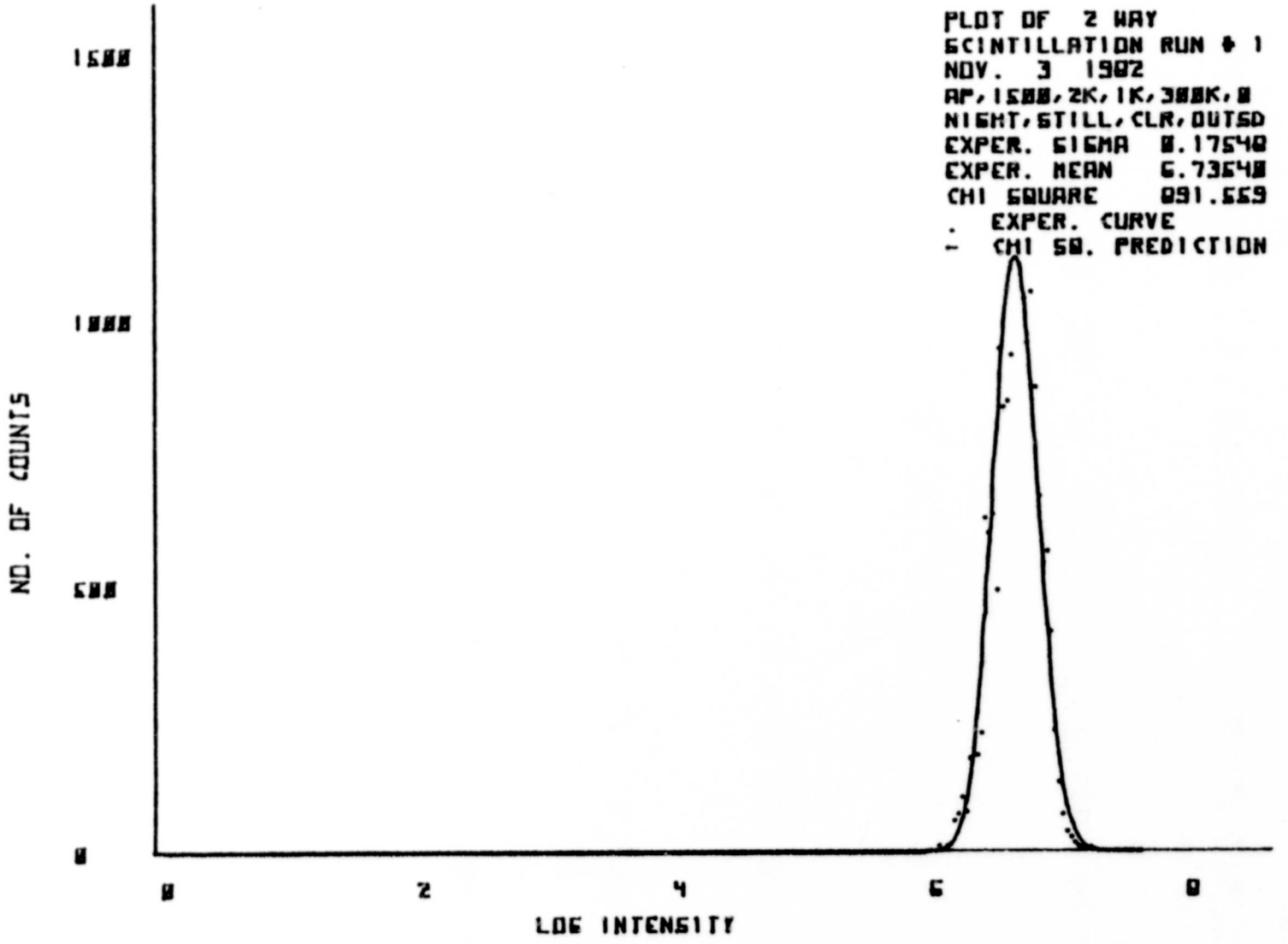

Figure 21. Scintillation Data and Theoretical Curve

NOV. 3 1986
Ap,1400,500,1k,300k,10
Night,clr,slwd,outsd
Wavelength= 6.33E-07 meters

Scintillation measurements of Sigma
16384 samples for each measurement
Fixed range= 100 meters

# pts	Sigma	Chi Square
1:16385	0.1076	7.99E 02**
1:16383	0.1027	7.67E 02**
2:16385	0.1108	9.77E 02**
2:16383	0.1037	1.12E 03**
3:16385	0.1018	1.23E 03**
3:16383	0.1037	7.62E 02**
4:16385	0.1000	7.80E 02**
4:16383	0.1041	7.19E 02**
5:16385	0.1030	5.98E 02**
5:16383	0.0961	8.17E 02**
6:16385	0.1056	5.10E 02**
6:16383	0.0828	1.55E 03**
7:16385	0.1081	4.89E 02**
7:16383	0.0837	1.24E 03**
8:16385	0.1097	5.14E 02**
8:16383	0.1018	8.33E 02**
9:16385	0.1133	6.19E 02**
9:16383	0.1180	6.23E 02**
10:16385	0.1023	8.66E 02**
10:16383	0.1050	7.54E 02**
11:16385	0.0995	5.96E 02**
11:16383	0.0906	1.25E 03**
12:16385	0.0991	7.87E 02**
12:16383	0.0964	1.35E 03**
13:16385	0.1044	8.08E 02**
13:16383	0.1028	9.40E 02**
14:16385	0.1101	1.21E 03**
14:16383	0.0978	9.26E 02**
15:16385	0.1077	5.41E 02**
15:16383	0.0924	1.06E 03**
16:16385	0.0993	6.25E 02**
16:16383	0.0868	1.36E 03**

Figure 22. Scintillation Statistics

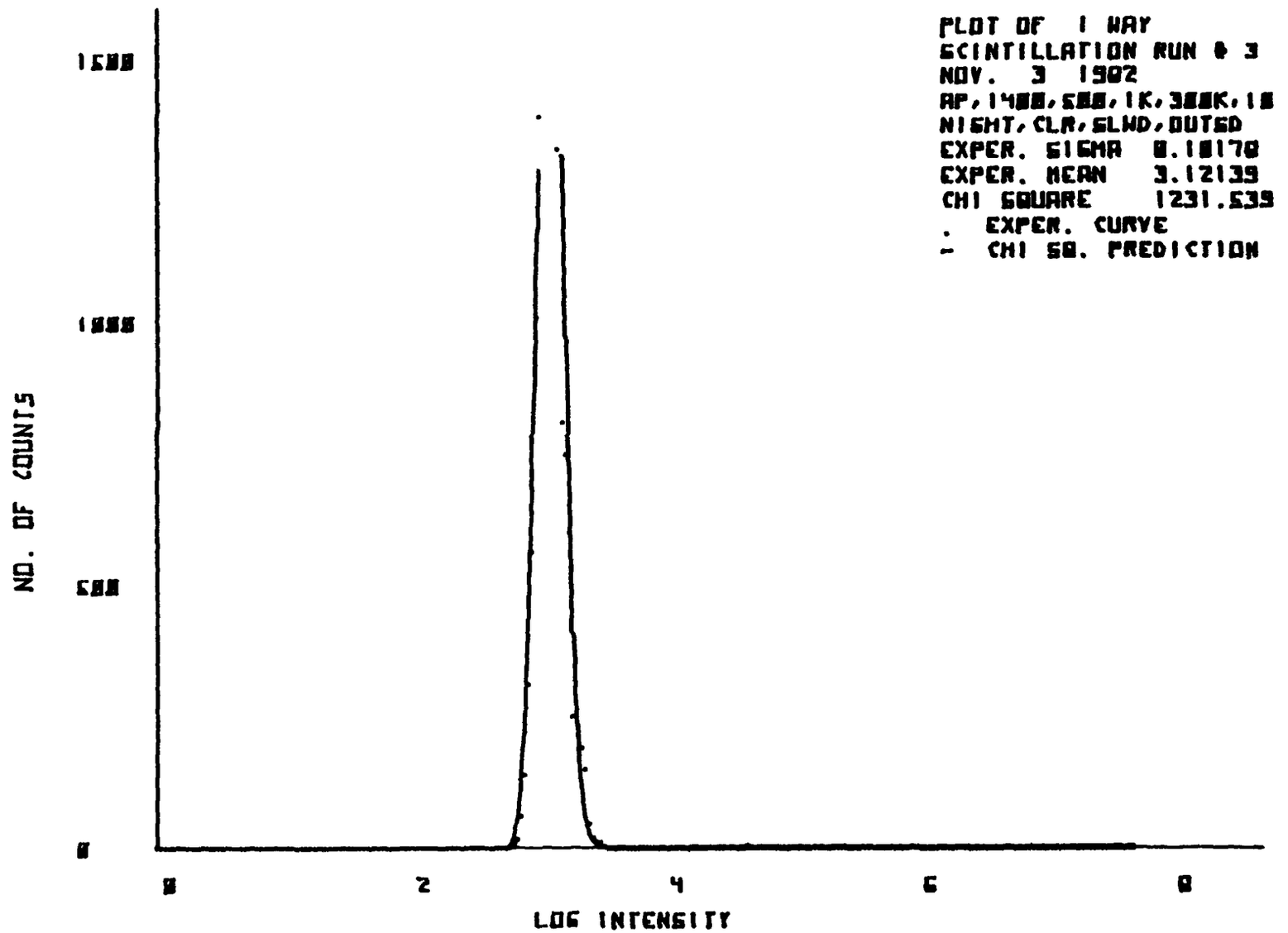

Figure 23. Scintillation Data and Theoretical Curve

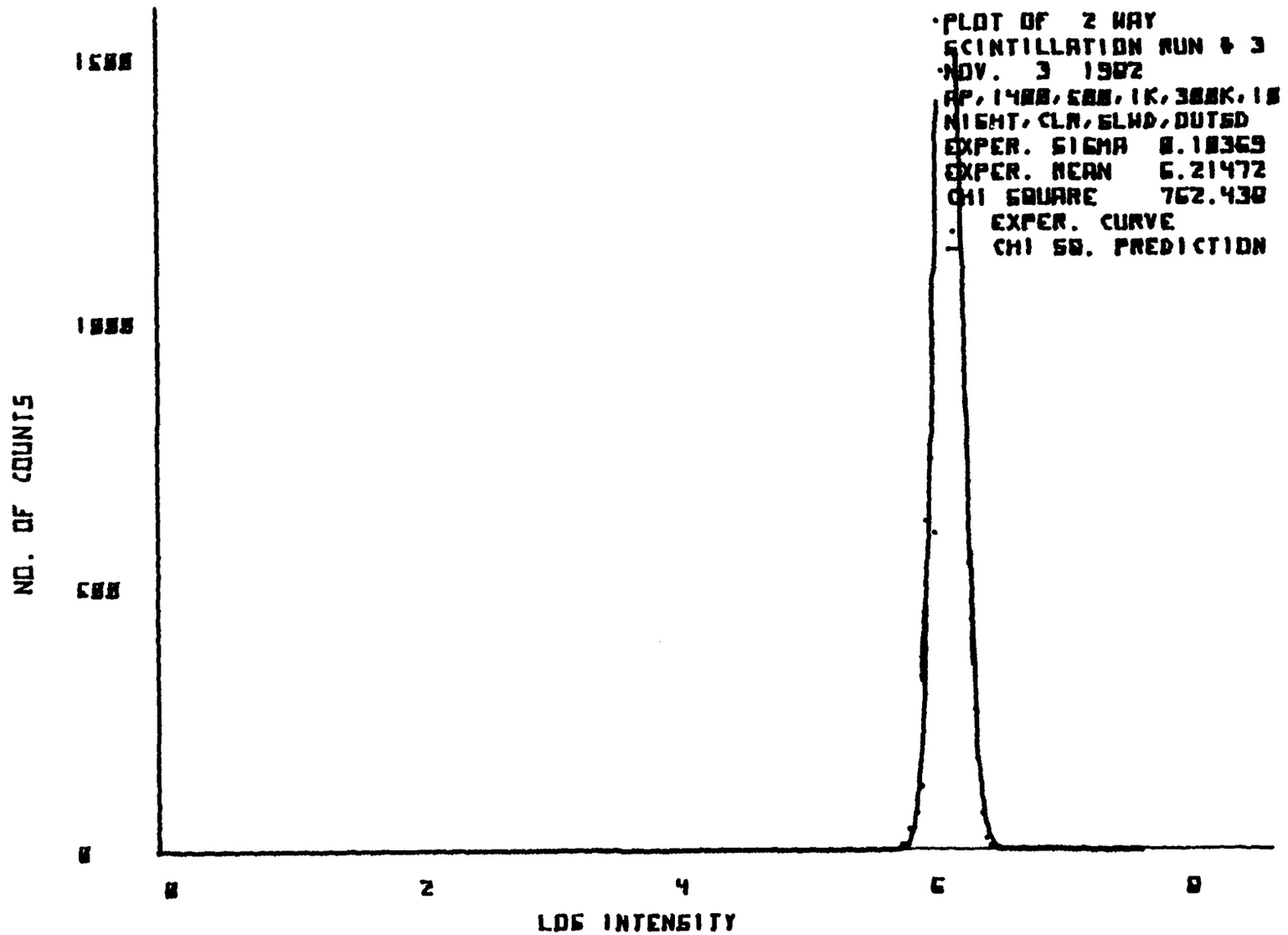

Figure 24. Scintillation Data and Theoretical Curve

NOV. 3 1982
Ap,1500,G100,1k,300k,20
Night,outsd,clr,wdy
Wavelength= 6.33E-07 meters

Scintillation measurement or Sigma
16384 samples for each measurement
Fixed range= 100 meters

# pts	Sigma	Chi Square
1:16385	0.0764	4.18E 02**
1:16383	0.0833	6.27E 02**
2:16385	0.0663	5.36E 02**
2:16383	0.0717	1.03E 03**
3:16385	0.0652	4.57E 02**
3:16383	0.0710	9.02E 02**
4:16385	0.0642	6.40E 02**
4:16383	0.0689	1.27E 03**
5:16385	0.0614	5.56E 02**
5:16383	0.0603	1.54E 03**
6:16385	0.0751	5.31E 02**
6:16383	0.0719	1.07E 03**
7:16385	0.0636	5.58E 02**
7:16383	0.0683	1.26E 03**
8:16385	0.0609	4.74E 02**
8:16383	0.0674	1.39E 03**
9:16385	0.0824	6.88E 02**
9:16383	0.0781	7.01E 02**
10:16385	0.0800	5.65E 02**
10:16383	0.0787	1.16E 03**
11:16385	0.0829	4.83E 02**
11:16383	0.0836	9.38E 02**
12:16385	0.0979	3.72E 02**
12:16383	0.1015	6.53E 02**
13:16385	0.1125	2.96E 02**
13:16383	0.0936	5.69E 02**
14:16385	0.1116	5.32E 02**
14:16383	0.1081	5.90E 02**
15:16385	0.1069	5.48E 02**
15:16383	0.0957	6.14E 02**
16:16385	0.1423	5.97E 02**
16:16383	0.1152	5.88E 02**

Figure 25. Scintillation Statistics

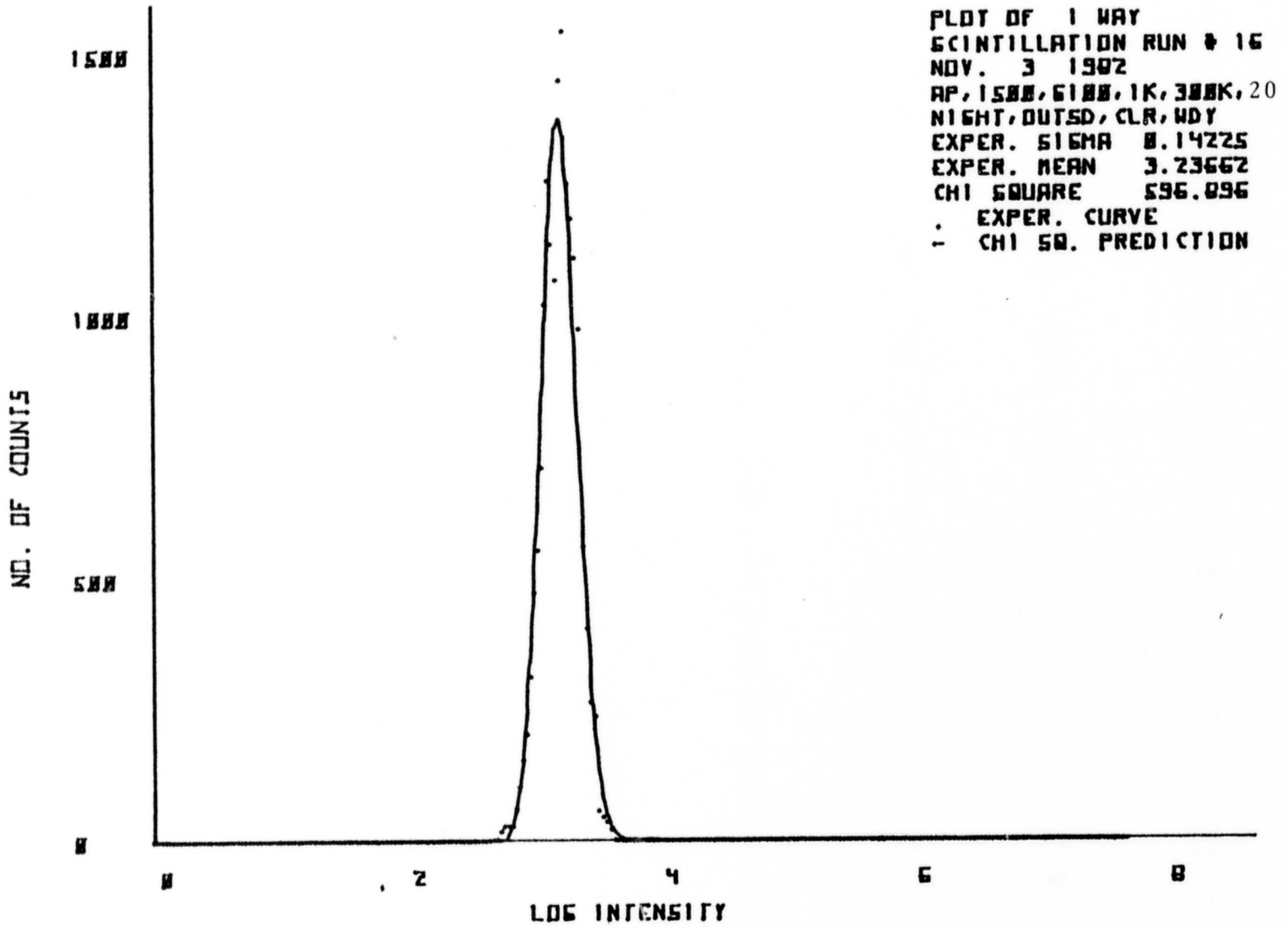

Figure 26. Scintillation Data and Theoretical Curve

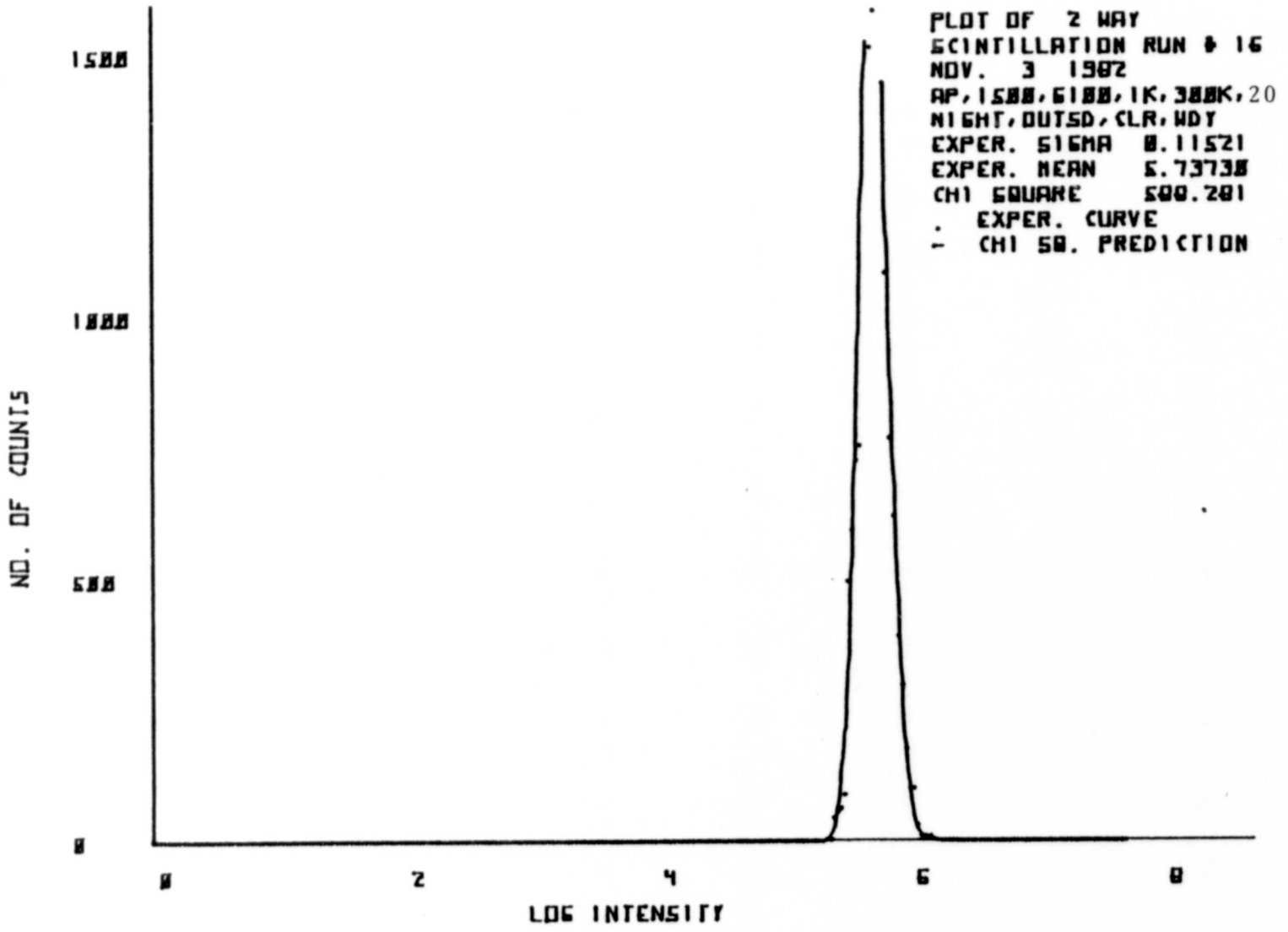

Figure 27. Scintillation Data and Theoretical Curve

NOV. 3 1982
AP,1500,500,1k,10k,30
Night,still,clr,outsd
Wavelength= 6.33E-07 meters

Scintillation measurements of Sigma
16384 samples for each measurement
Fixed range= 100 meters

# pts	Sigma	Chi Square
1:16385	0.1013	6.24E 02**
1:16383	0.0808	8.30E 02**
2:16385	0.1022	6.22E 02**
2:16383	0.0799	9.29E 02**
3:16385	0.0997	3.85E 02**
3:16383	0.0700	8.61E 02**
4:16385	0.0948	3.86E 02**
4:16383	0.0741	7.99E 02**
5:16385	0.0919	6.22E 02**
5:16383	0.0716	8.67E 02**
5:16385	0.1066	4.26E 02**
6:16383	0.0876	8.92E 02**
7:16385	0.1006	3.74E 02**
7:16383	0.0864	1.18E 03**
8:16385	0.1195	5.80E 02**
8:16383	0.0918	7.36E 02**
9:16385	0.1193	5.62E 02**
9:16383	0.0969	1.64E 03**
10:16385	0.1120	4.34E 02**
10:16383	0.0918	9.05E 02**
11:16385	0.1012	4.69E 02**
11:16383	0.0844	1.21E 03**
12:16385	0.0990	4.78E 02**
12:16383	0.0954	1.02E 03**
13:16385	0.1163	6.21E 02**
13:16383	0.1018	1.16E 03**
14:16385	0.1104	5.69E 02**
14:16383	0.0877	2.71E 03**
15:16385	0.0977	1.18E 03**
15:16383	0.0841	2.61E 03**
16:16385	0.0990	6.18E 02**
16:16383	0.0755	5.10E 03**

Figure 28. Scintillation Statistics

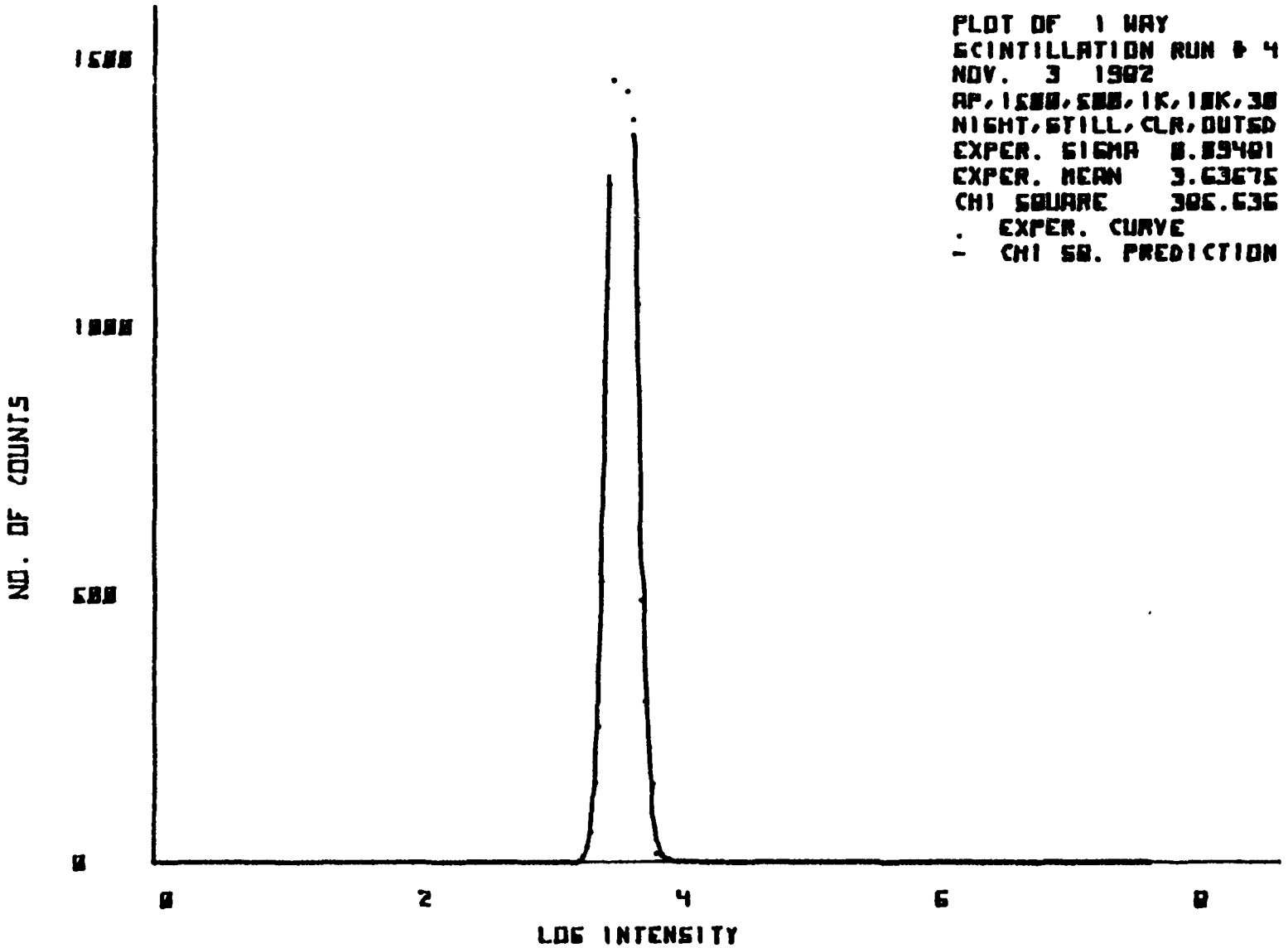

Figure 29. Scintillation Data and Theoretical Curve

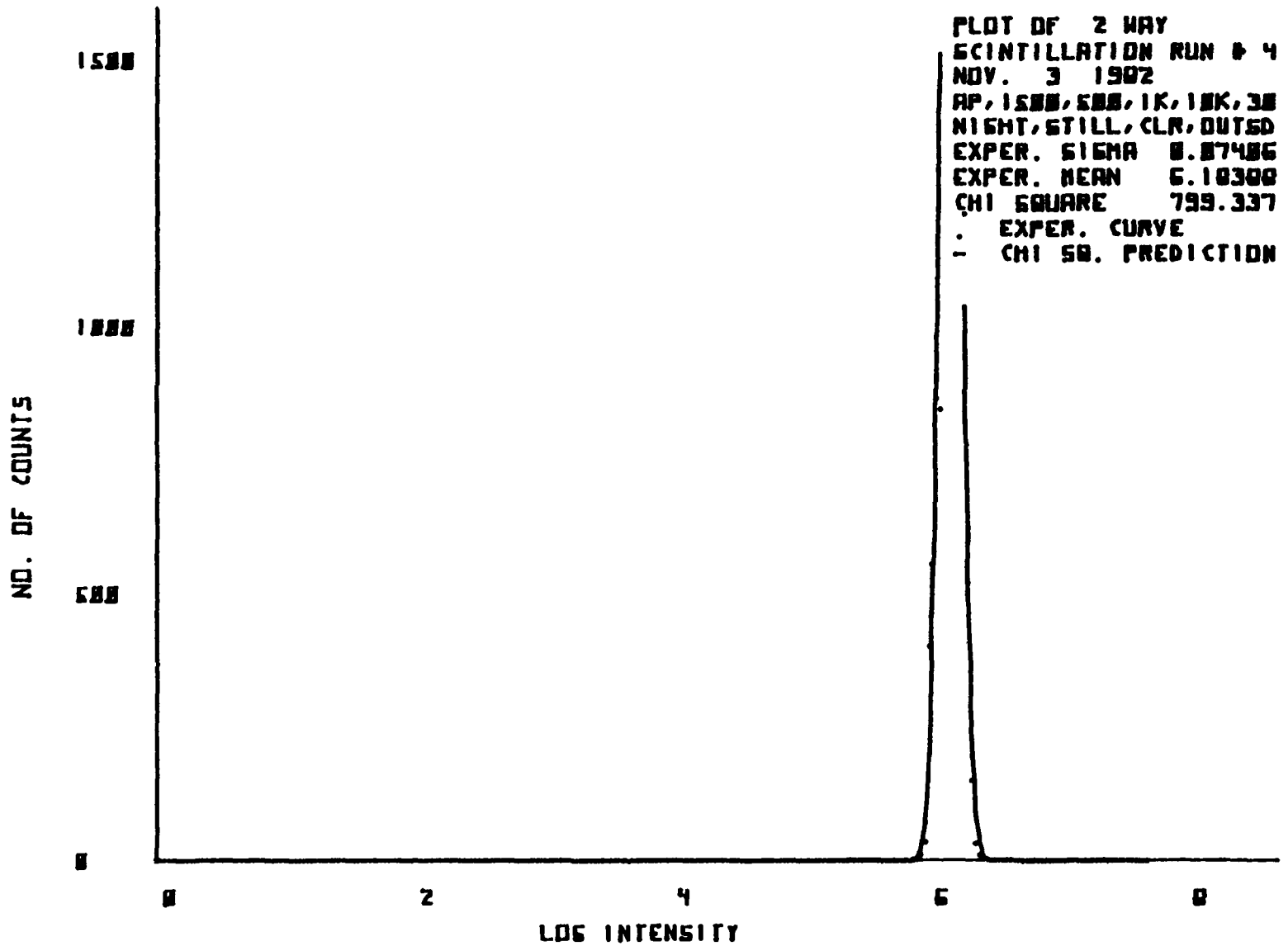

Figure 30. Scintillation Data and Theoretical Curve

NOV. 3 1982
Ap,1500,200,1k,300k,40
Night,outsd,clr,still
Wavelength= 6.33E-07 meters

Scintillation measurements of Sigma
16384 samples for each measurement
Fixed range= 100 meters

# pts	Sigma	Chi Square
1:16383	0.1219	8.49E 02**
1:16385	0.0806	1.20E 03**
2:16383	0.1260	6.64E 02**
2:16385	0.0956	1.51E 03**
3:16383	0.0962	4.88E 02**
3:16385	0.0772	1.57E 03**
4:16383	0.0870	6.01E 02**
4:16385	0.0774	1.29E 03**
5:16383	0.1022	4.40E 02**
5:16385	0.0843	1.21E 03**
6:16383	0.1067	5.64E 02**
6:16385	0.0797	1.67E 03**
7:16383	0.0788	5.18E 02**
7:16385	0.0835	9.98E 02**
8:16383	0.0739	7.22E 02**
8:16385	0.0793	1.00E 03**
9:16383	0.0767	8.63E 02**
9:16385	0.0807	2.40E 03**
10:16383	0.0800	7.29E 02**
10:16385	0.0756	2.33E 03**
11:16383	0.0677	7.42E 02**
11:16385	0.0651	1.33E 03**
12:16383	0.0673	6.45E 02**
12:16385	0.0687	1.11E 03**
13:16383	0.0623	6.42E 02**
13:16385	0.0635	2.15E 03**
14:16383	0.0657	5.59E 02**
14:16385	0.0671	1.98E 03**
15:16383	0.0604	1.31E 03**
15:16385	0.0679	2.86E 03**
16:16383	0.0596	6.59E 02**
16:16385	0.0667	1.94E 03**

Figure 31. Scintillation Statistics

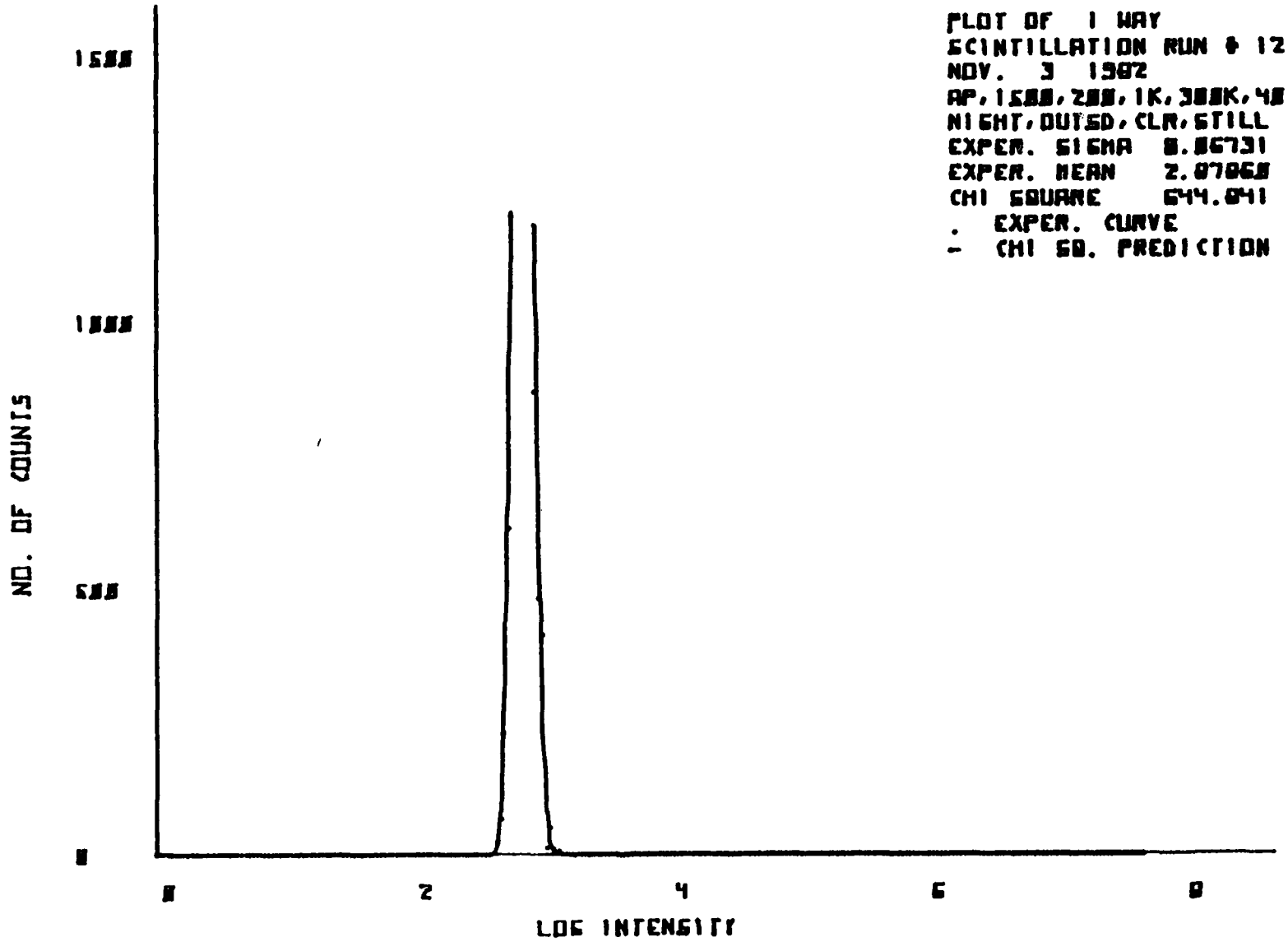

Figure 32. Scintillation Data and Theoretical Curve

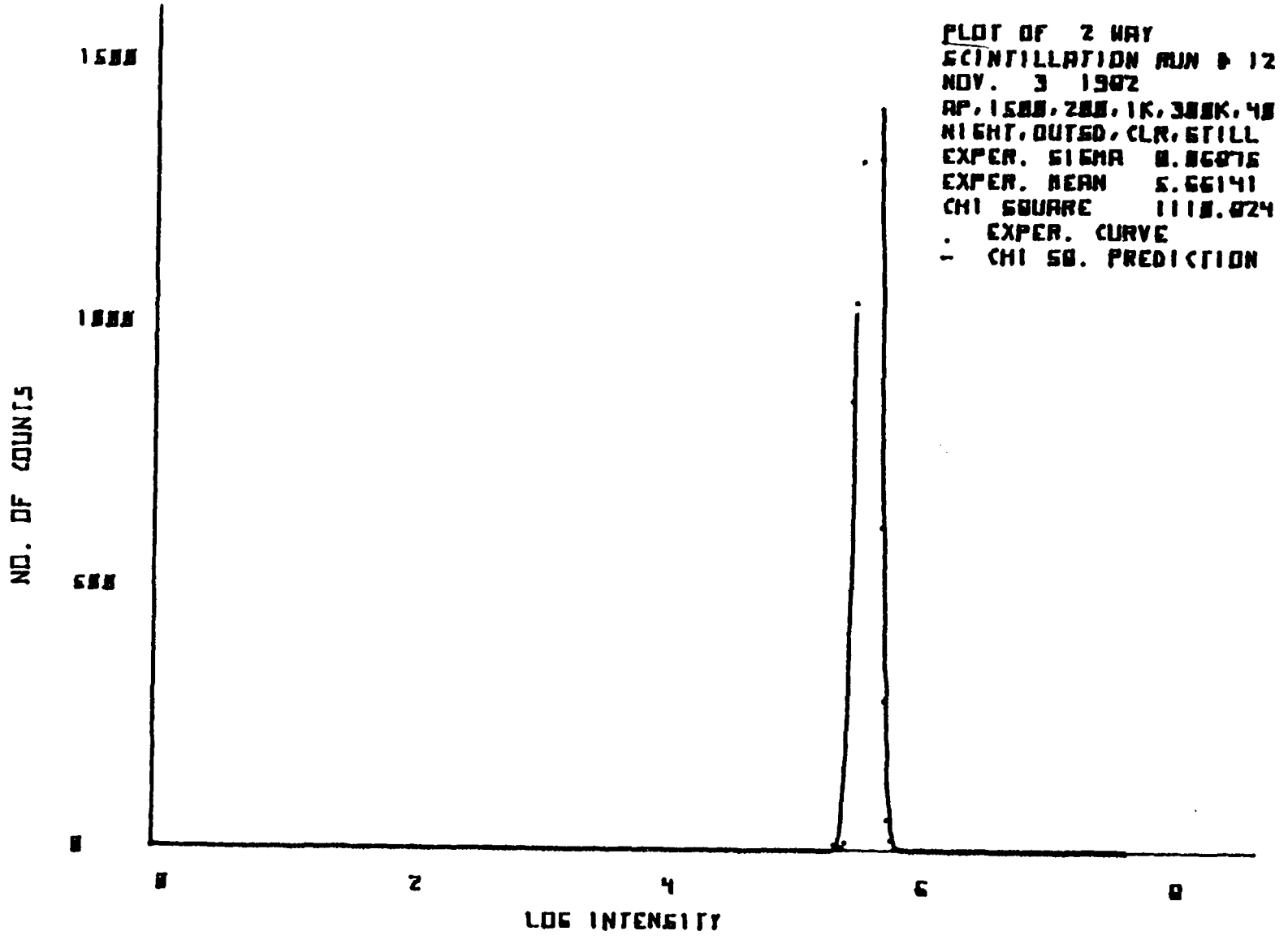

Figure 33. Scintillation Data and Theoretical Curve

NOV. 3 1982
Ap,1500,50,1k,300k,50
Night,outsd,still,cir
Wavelength= 6.33E-07 meters

Scintillation measurements of Sigma
16384 samples for each measurement
Fixed range= 100 meters

# pts	Sigma	Chi Square
1:16384	0.1048	4.86E 02**
1:16384	0.0673	3.95E 03**
2:16385	0.1145	9.24E 02**
2:16383	0.0898	1.78E 03**
3:16385	0.1110	5.66E 02**
3:16383	0.0956	1.17E 03**
4:16385	0.1098	4.69E 02**
4:16383	0.0944	1.35E 03**
5:16385	0.1256	5.01E 02**
5:16383	0.1106	6.41E 02**
6:16385	0.1095	6.65E 02**
6:16383	0.1077	9.43E 02**
7:16385	0.1066	7.36E 02**
7:16383	0.0949	9.48E 02**
8:16385	0.1045	5.49E 02**
8:16383	0.0691	2.56E 03**
9:16385	0.1213	7.46E 02**
9:16383	0.1050	9.07E 02**
10:16385	0.0991	5.59E 02**
10:16383	0.0782	1.47E 03**
11:16385	0.1034	9.33E 02**
11:16383	0.0775	2.59E 03**
12:16385	0.1149	5.72E 02**
12:16383	0.0804	1.63E 03**
13:16385	0.1134	6.37E 02*8
13:16383	0.0701	2.21E 03**
14:16385	0.0969	8.77E 02**
14:16383	0.0602	6.83E 03**
15:16385	0.0911	8.16E 02**
15:16383	0.0621	6.61E 03**
16:16385	0.0930	7.44E 02**
16:16383	0.0619	7.91E 03**

Figure 34. Scintillation Statistics

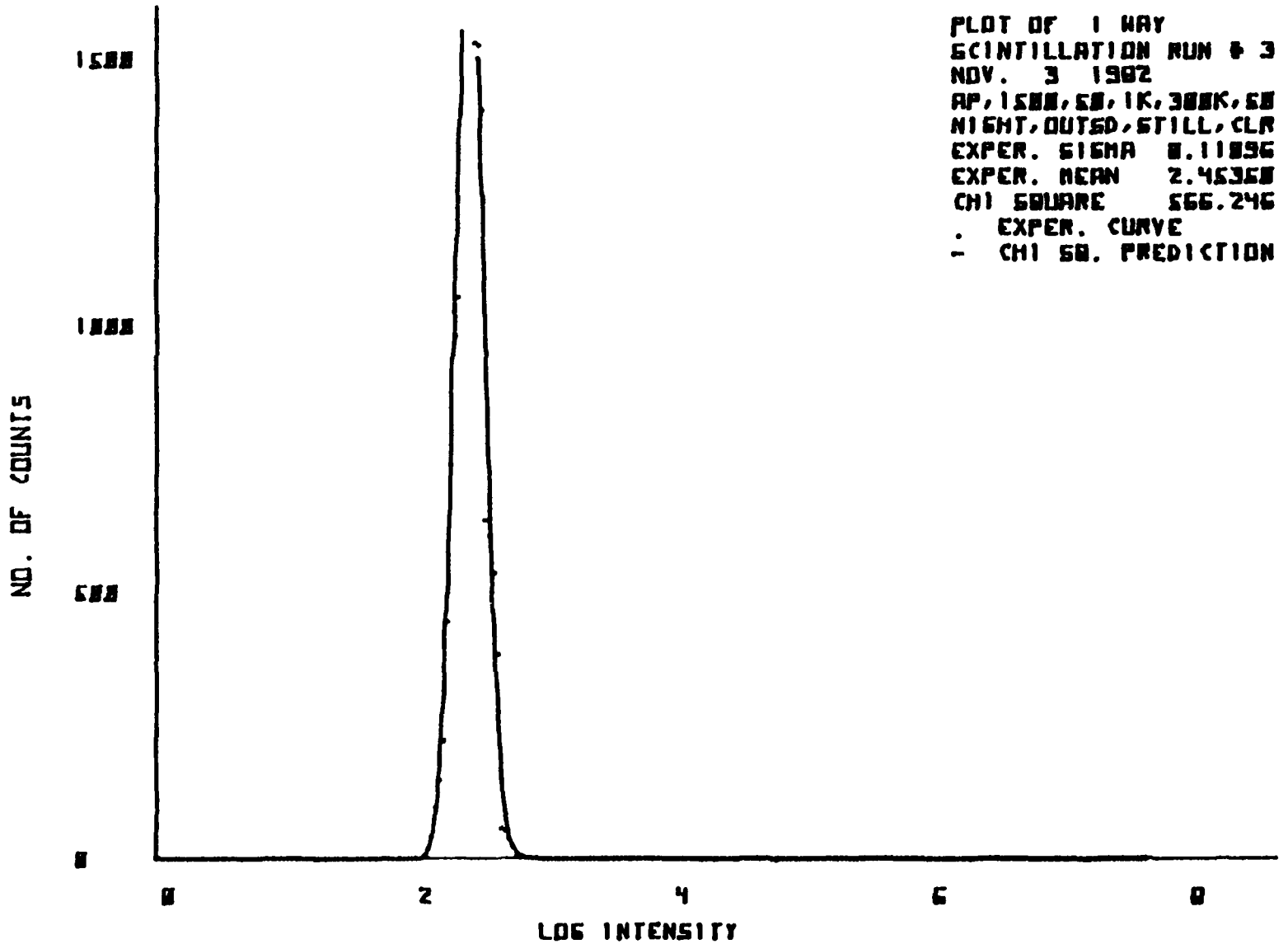

Figure 35. Scintillation Data and Theoretical Curve

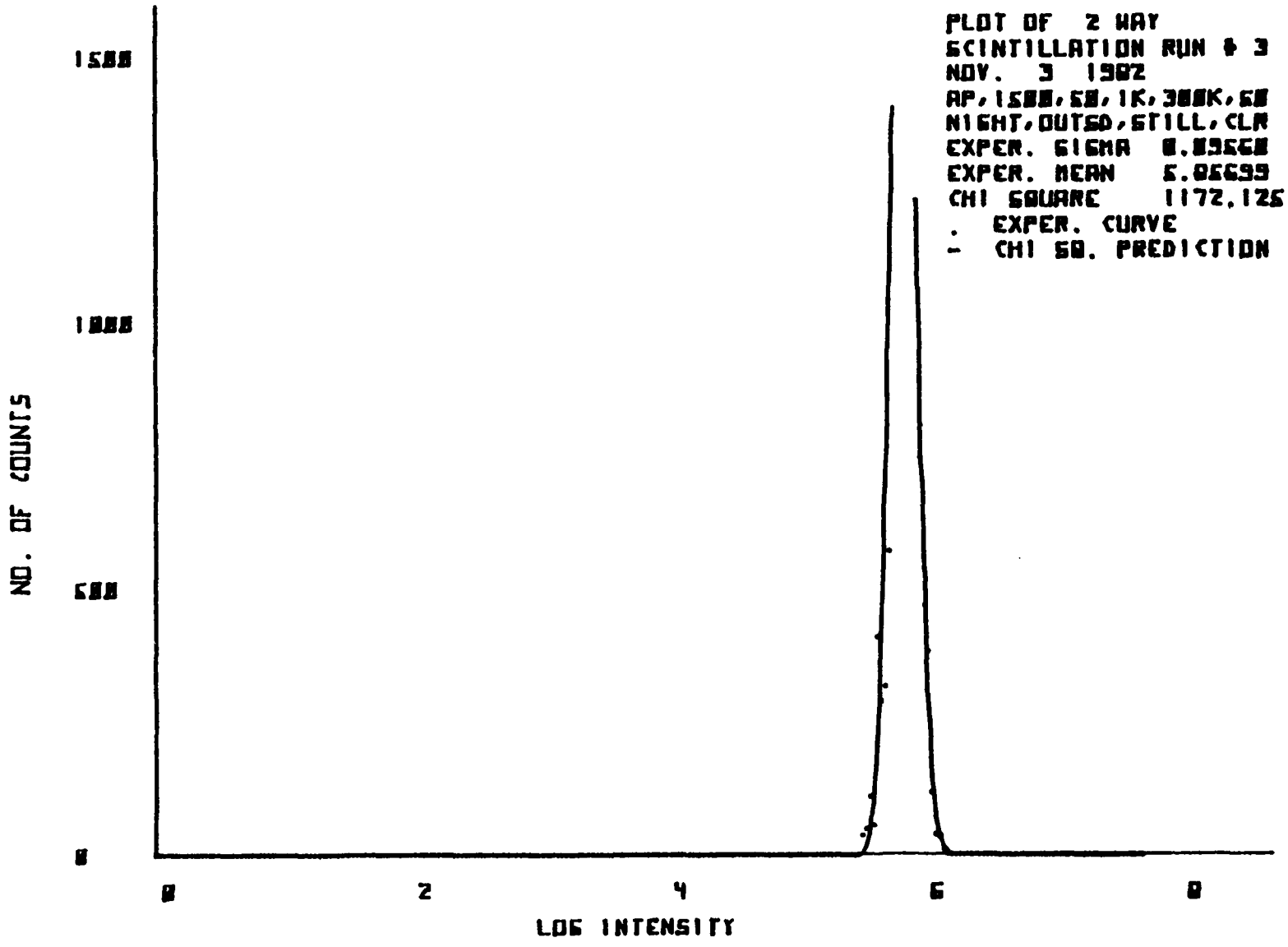

Figure 36. Scintillation Data and Theoretical Curve

NOV. 3 1982
Ap,1500,200,1k,300k,60
Night,clr,outsd
Wavelength= 6.33E-07 meters

Scintillation measurements of Sigma
16384 samples for each measurement
Fixed range= 100 meters

# pts	Sigma	Chi Square
1:16383	0.1034	4.96E 02**
1:16385	0.1007	7.61E 02**
2:16383	0.1177	5.42E 02**
2:16385	0.1146	9.26E 02**
3:16383	0.1169	4.47E 02**
3:16385	0.1174	7.08E 02**
4:16382	0.1453	4.47E 02**
4:16385	0.1434	7.05E 02**
5:16383	0.1411	4.67E 02**
5:16385	0.1369	7.50E 02**
6:16383	0.1266	4.11E 02**
6:16385	0.1287	6.57E 02**
7:16383	0.1215	4.64E 02**
7:16385	0.1140	8.08E 02**
8:16383	0.1221	6.55E 02**
8:16385	0.1188	7.88E 02**
9:16383	0.1198	5.09E 02**
9:16385	0.1119	7.79E 02**
10:16383	0.1337	4.95E 02**
10:16385	0.1291	6.29E 02**
11:16383	0.1282	5.11E 02**
11:16385	0.1251	7.84E 02**
12:16383	0.1296	4.71E 02**
12:16385	0.1222	1.03E 03**
13:16383	0.1276	5.47E 02**
13:16385	0.1121	8.39E 02**
14:16383	0.1027	5.28E 02**
14:16385	0.0988	9.65E 02**
15:16383	0.1085	4.78E 02**
15:16385	0.0994	1.00E 03**
16:16383	0.1236	8.58E 02**
16:16385	0.1038	1.03E 03**

Figure 37. Scintillation Statistics

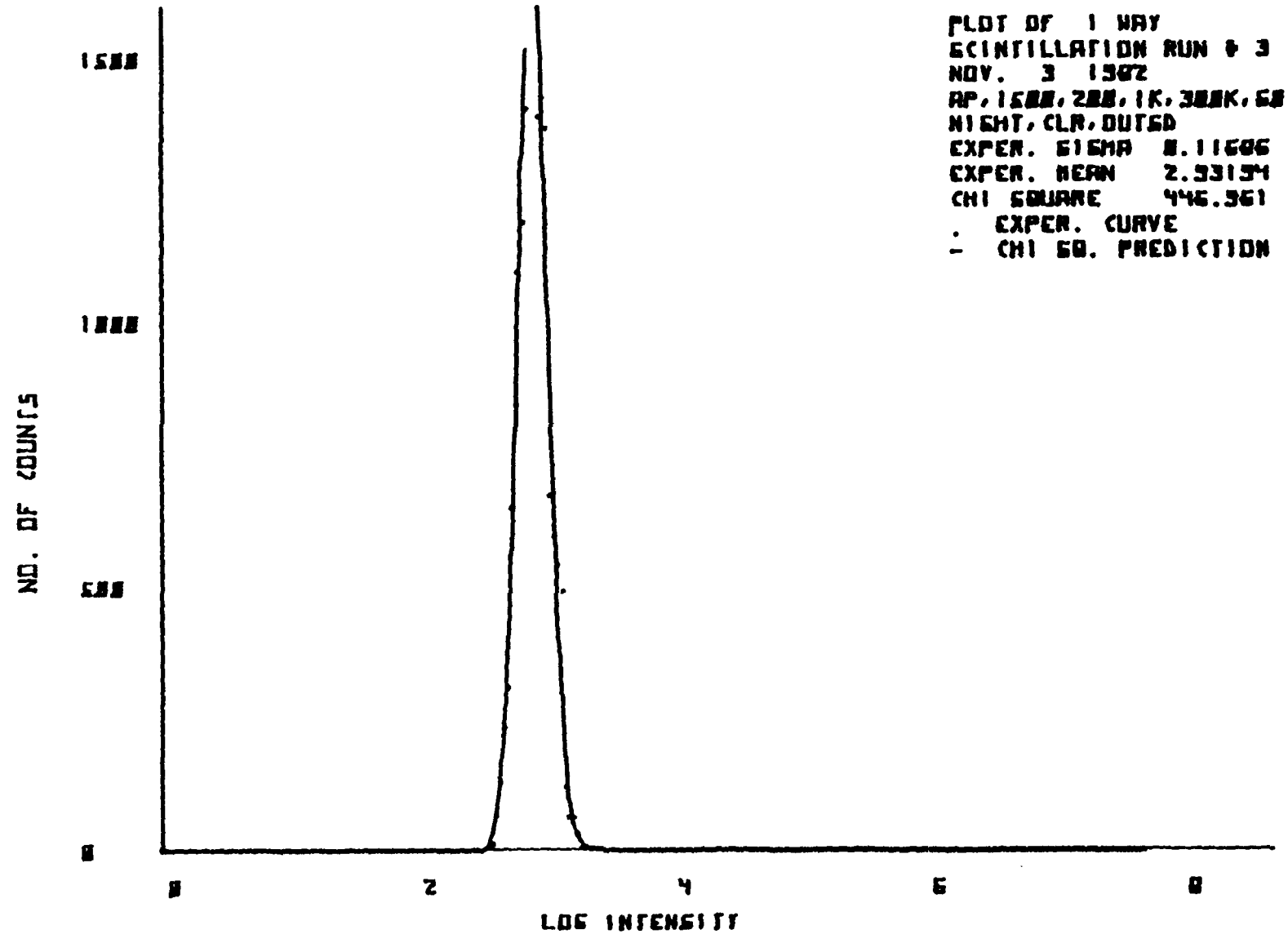

Figure 38. Scintillation Data and Theoretical Curve

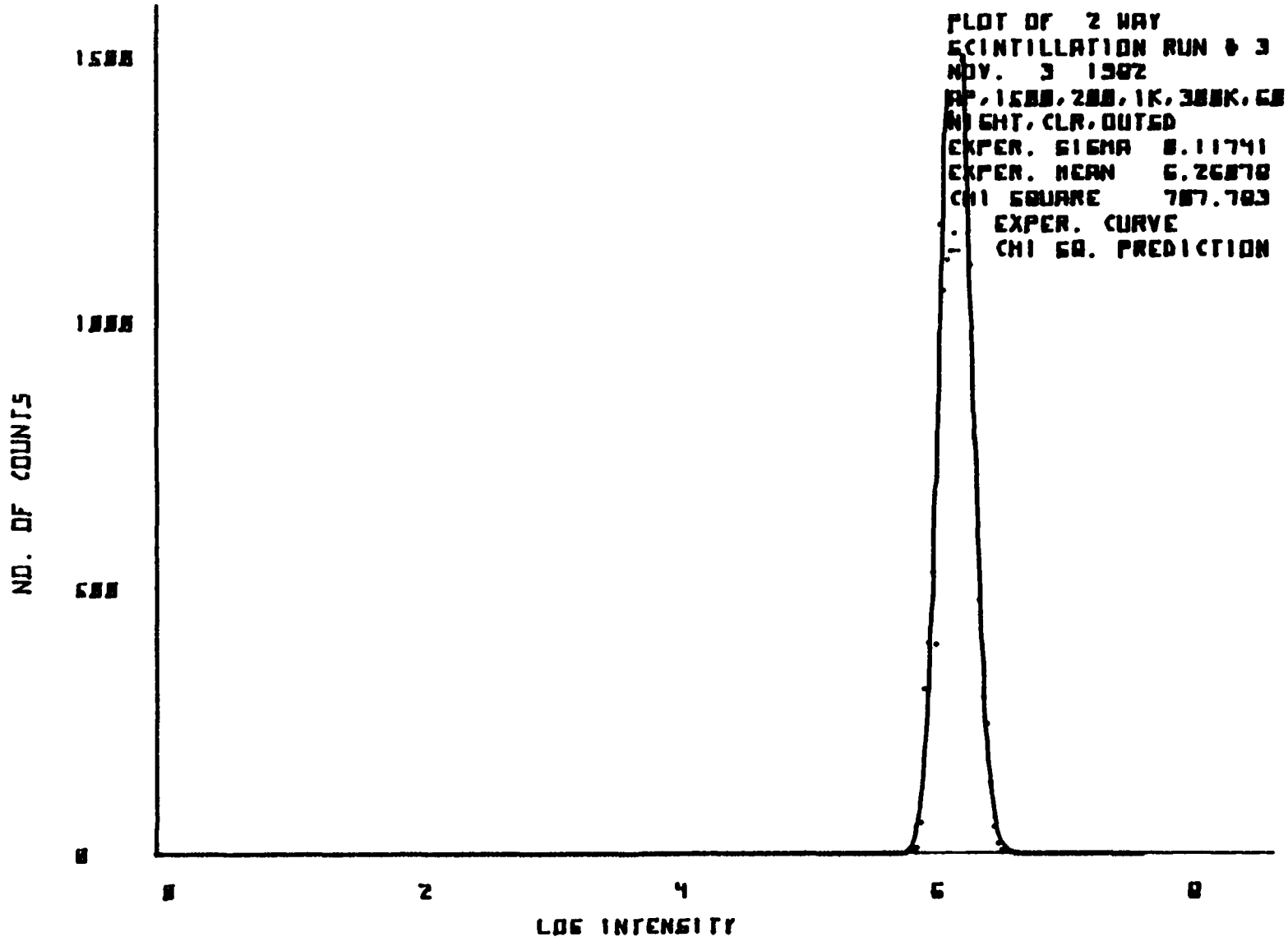

Figure 39. Scintillation Data and Theoretical Curve

NOV. 3 1982
Ap,1400,100,1k,300k,70
Night,clr,outsd,slwd
Wavelength= 6.33E-07 meters

Scintillation measurements of Sigma
16384 samples for each measurement
Fixed range= 100 meters

# pts	Sigma	Chi Square
1:16384	0.1069	6.42E 02**
1:16384	0.0729	1.80E 03**
2:16385	0.1250	6.46E 02**
2:16383	0.0816	1.60E 03**
3:16385	0.1275	6.70E 02**
3:16383	0.0857	2.19E 03**
4:16385	0.1630	6.86E 02**
4:16383	0.0921	1.28E 03**
5:16385	0.1406	5.83E 02**
5:16383	0.0895	1.12E 03**
6:16385	0.1154	7.45E 02**
6:16383	0.0822	2.40E 03**
7:16385	0.1105	6.87E 02**
7:16383	0.0742	5.07E 03**
8:16385	0.1087	6.10E 02**
8:16383	0.0743	4.18E 03**
9:16385	0.1201	5.80E 02**
9:16383	0.0860	2.14E 03**
10:16385	0.1592	6.68E 02**
10:16383	0.1051	9.76E 02**
11:16385	0.1457	4.75E 02**
11:16383	0.1077	8.63E 02**
12:16385	0.1396	5.06E 02**
12:16383	0.1174	7.79E 02**
13:16385	0.1435	1.06E 03**
13:16383	0.0934	1.45E 03**
14:16385	0.1238	6.63E 02**
14:16383	0.0899	1.48E 03**
15:16385	0.1200	6.88E 02**
15:16383	0.0791	2.64E 03**
16:16385	0.1147	6.39E 02**
16:16383	0.0746	3.99E 03**

Figure 40. Scintillation Statistics

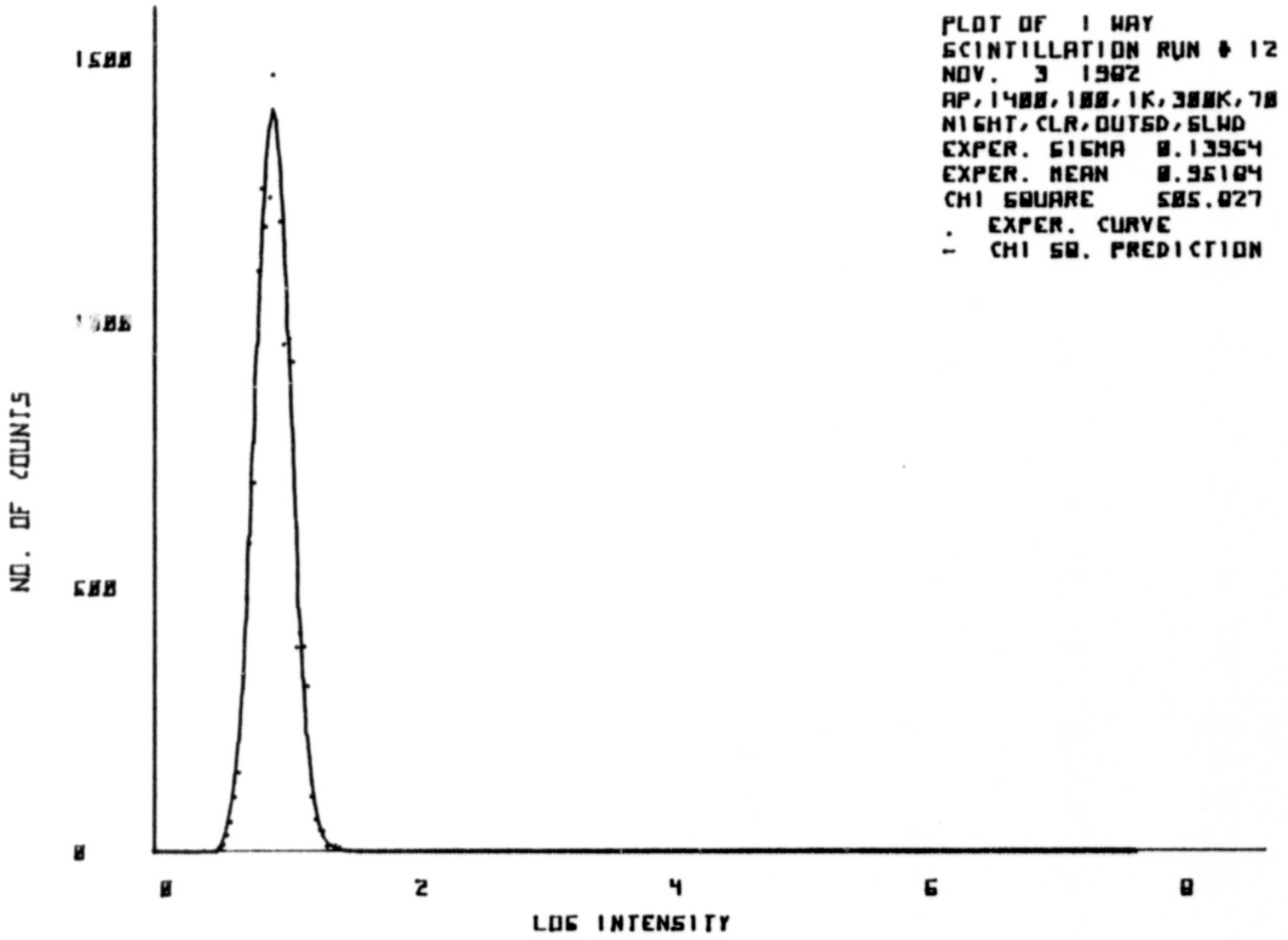

Figure 41. Scintillation Data and Theoretical Curve

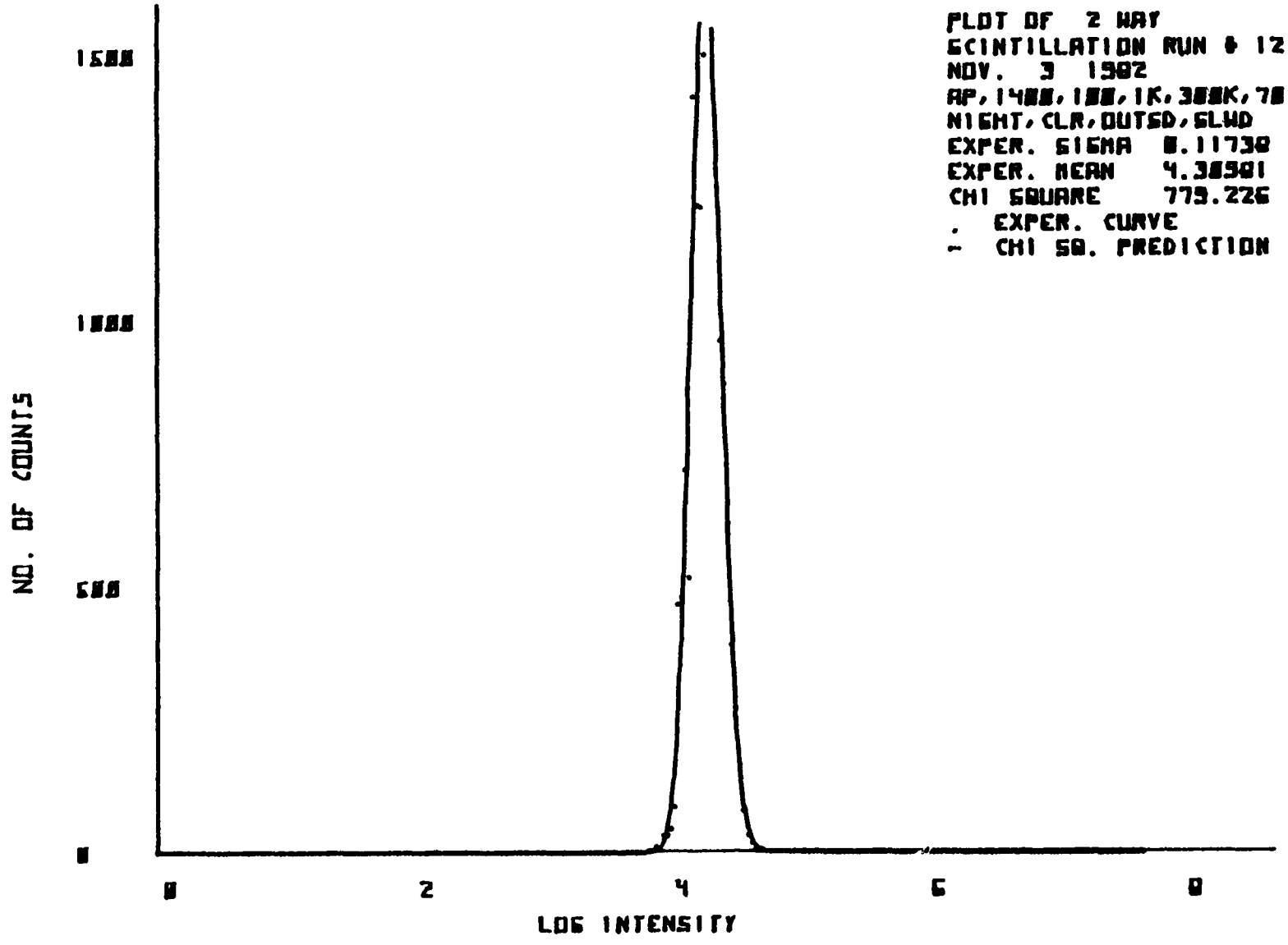

Figure 42. Sctintillation Data and Theoretical Curve

NOV. 3 1982
Ap,1500,200,1k,300k,80
Night,outsd,clr,slwd
Wavelength= 6.33E-97 meteres

Scintillation measurements of Sigma
16384 samples for each measurement
Fixed range= 100 meters

# pts	Sigma	Chi Square
1:16384	0.1045	9.78E 02**
1:16384	0.0849	1.42E 03**
2:16383	0.1175	7.21E 02**
2:16385	0.0952	1.42E 03**
3:16383	0.1011	7.96E 02**
3:16385	0.0914	1.52E 03**
4:16384	0.1170	7.72E 02**
4:16384	0.1049	1.08E 03**
5:16385	0.1206	6.14E 02**
5:16383	0.0942	1.16E 03**
6:16385	0.2736	4.72E 03**
6:16383	0.0920	1.24E 03**
7:16385	0.1003	9.70E 02**
7:16383	0.0828	1.64E 03**
8:16385	0.0931	6.69E 02**
8:16383	0.0762	1.07E 03**
9:16385	0.0735	8.25E 02**
9:16383	0.0651	1.73E 03**
10:16385	0.0745	9.36E 02**
10:16383	0.0695	1.55E 03**
11:16385	0.0830	5.55E 02**
11:16383	0.0704	1.76E 03**
12:16385	0.0977	1.41E 03**
12:16383	0.0688	1.29E 03**
13:16383	0.0818	2.44E 03**
13:16385	0.0838	2.64E 03**
14:16383	0.0740	4.85E 02**
14:16385	0.0731	1.37E 03**
15:16383	0.0761	5.42E 02**
15:16385	0.0772	1.27E 03**
16:16383	0.0861	4.89E 02**
16:16385	0.0794	1.60E 03**

Figure 43. Scintillation Statistics

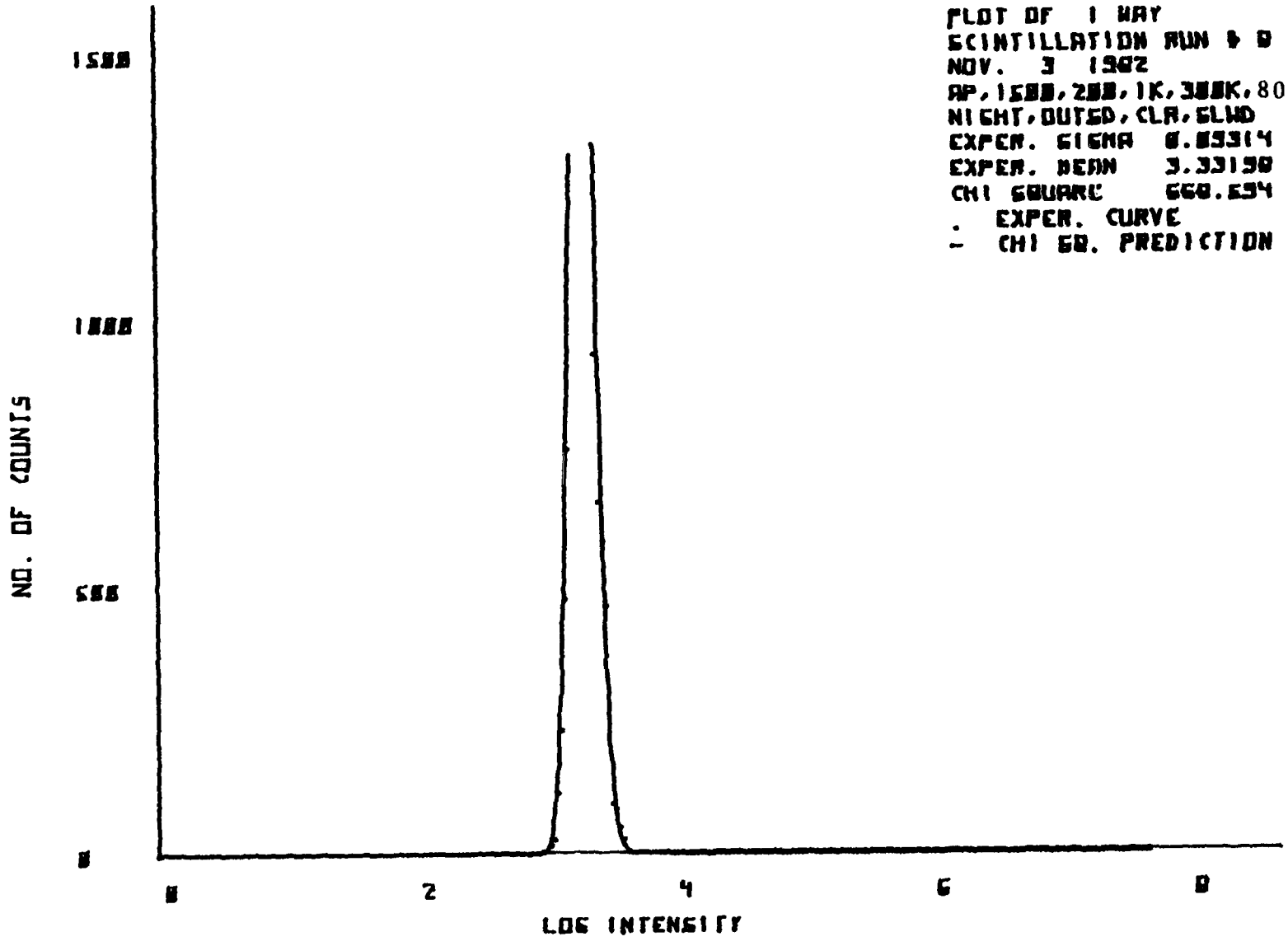

Figure 44. Scintillation Data and Theoretical Curve

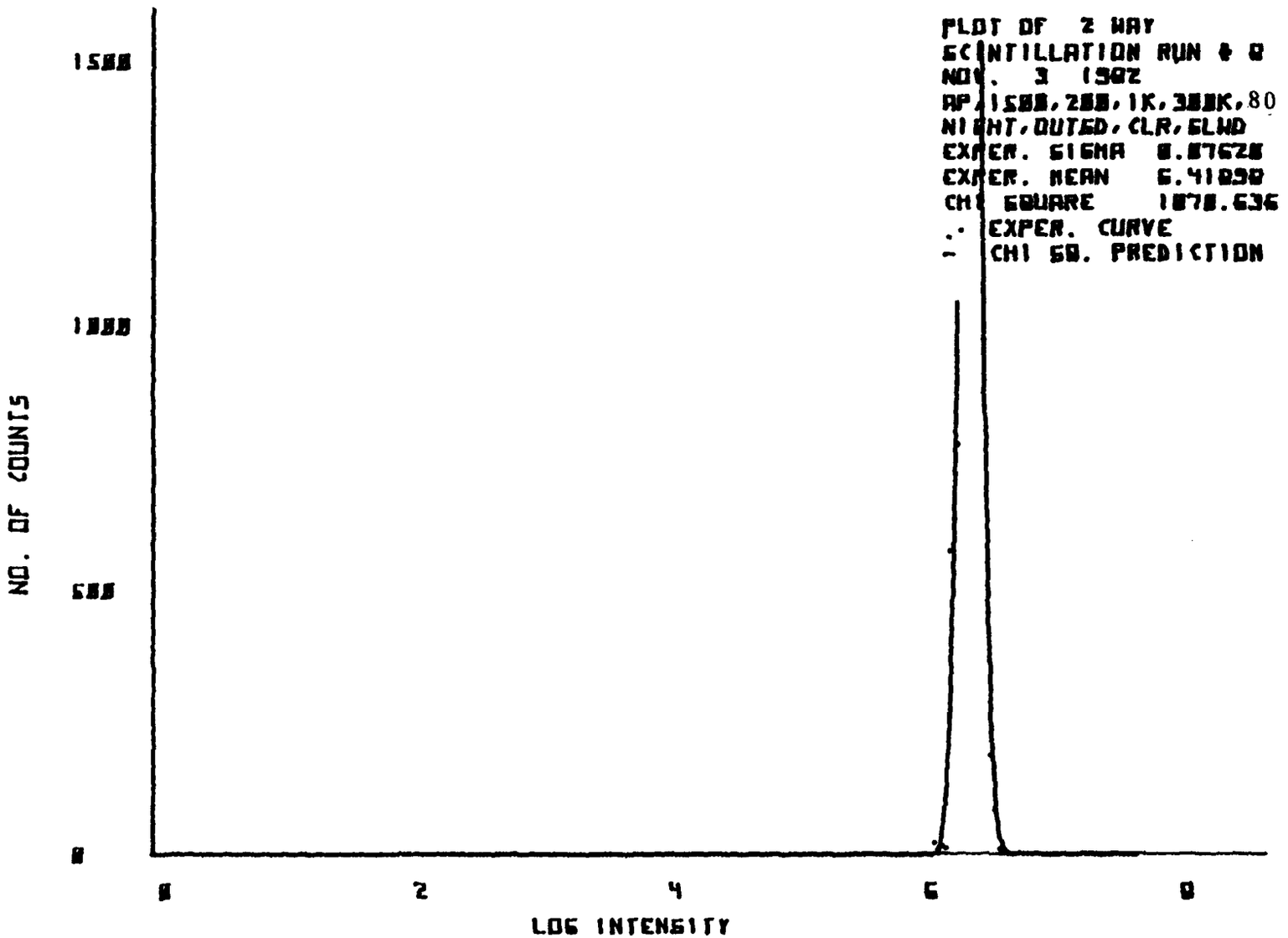

Figure 45. Scintillation Data and Theoretical Curve

NOV. 3 1982
A,1500,200,30k,300k,90
Night,outsd,clr,slwd
Wavelength= 6.33E-07 meters

Scintillation measurements of Sigma
16384 samples for each measurement
Fixed range= 100 meters

# pts	Sigma	Chi Square
1:16385	0.1390	5.99E 02**
1:16383	0.1222	6.37E 02**
2:16385	0.1186	8.47E 02**
2:16383	0.1196	6.72E 02**
3:16385	0.0857	8.55E 02**
3:16383	0.0835	1.02E 03**
4:16385	0.0901	7.97E 02**
4:16383	0.0829	1.22E 03**
5:16385	0.0845	6.44E 02**
5:16383	0.0808	1.37E 03**
6:16385	0.0863	1.09E 03**
6:16383	0.0860	1.11E 03**
7:16385	0.0900	8.47E 02**
7:16383	0.0861	1.47E 03**
8:16385	0.1117	6.43E 02**
8:16383	0.0808	1.48E 03**
9:16385	0.0938	7.94E 02**
9:16383	0.0800	1.40E 03**
10:16385	0.0961	8.37E 02**
10:16383	0.0841	1.59E 03**
11:16385	0.1094	8.96E 02**
11:16383	0.0987	1.15E 03**
12:16385	0.1046	6.64E 02**
12:16383	0.0966	1.07E 03**
13:16385	0.0983	7.01E 02**
13:16383	0.0897	1.38E 03**
14:16385	0.0978	8.04E 02**
14:16383	0.0814	1.42E 03**
15:16385	0.0959	7.48E 02**
15:16383	0.0869	1.53E 03**
16:16385	0.1098	6.80E 02**
16:16383	0.0984	8.24E 02**

Figure 46. Scintillation Statistics

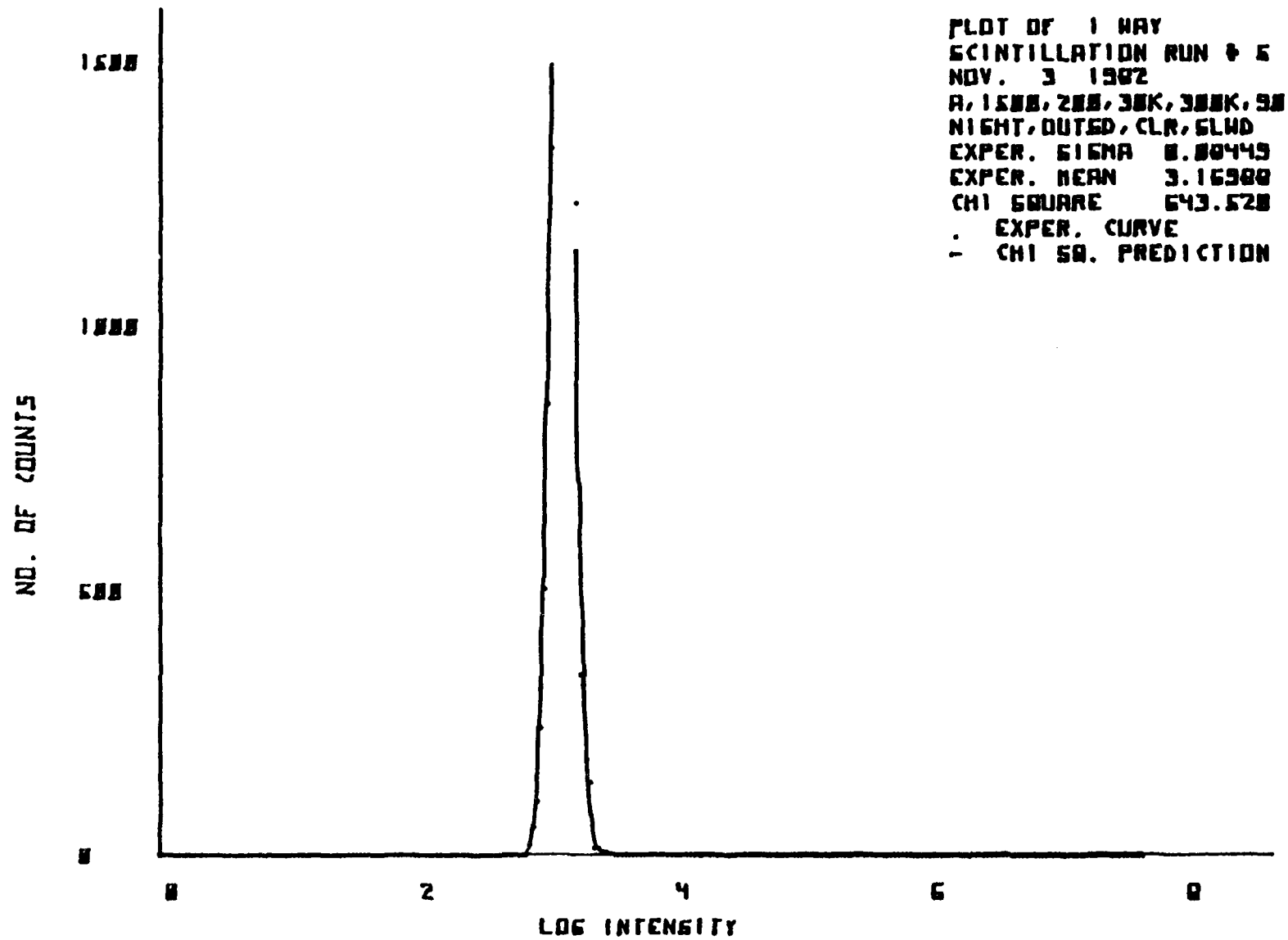

Figure 47. Scintillation Data and Theoretical Curve

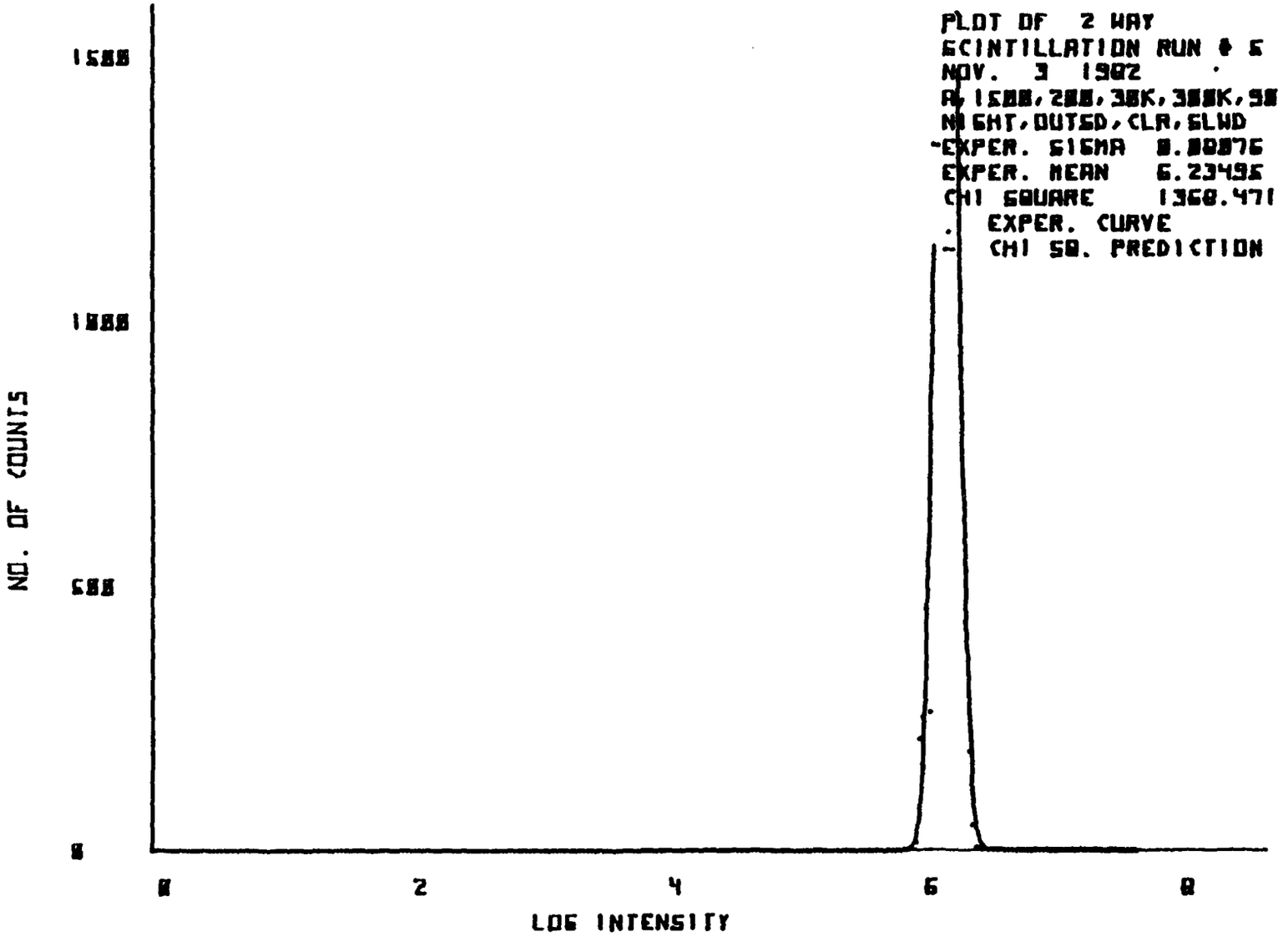

Figure 48. Scintillation Data and Theoretical Curve

NOV. 3 1982
Ap,1500,100,1k,300k,100
Night,clr,outsd,slwd
Wavelength= 6.33E-07 meters

Scintillation measurements of Sigma
16384 samples for each measurement
Fixed range= 100 meters

# pts	Sigma	Chi Square
1:16384	0.0985	9.13E 02**
1:16384	0.1025	2.76E 03**
2:16385	0.1019	7.58E 02**
2:16383	0.1031	2.04E 03**
3:16385	0.1058	9.34E 02**
3:16383	0.1060	1.94E 03**
4:16385	0.1035	9.79E 02**
4:16383	0.1072	2.20E 03**
5:16385	0.1004	1.05E 03**
5:16383	0.1076	2.91E 03**
6:16385	0.0966	9.66E 02**
6:16383	0.1043	2.46E 03**
7:16385	0.1103	6.99E 02**
7:16383	0.1158	1.61E 03**
8:16385	0.1083	8.17E 02**
8:16383	0.1126	1.81E 03**
9:16385	0.1001	1.05E 03**
9:16383	0.1118	2.30E 03**
10:16385	0.0949	7.95E 02**
10:16383	0.1115	2.35E 03**
11:16385	0.0978	8.12E 02**
11:16383	0.1136	1.98E 03**
12:16385	0.1198	8.18E 02**
12:16383	0.1276	1.18E 03**
13:16385	0.1181	6.48E 02**
13:16383	0.1263	1.36E 03**
14:16385	0.1309	6.81E 02**
14:16383	0.1397	6.57E 02**
15:16385	0.1517	4.01E 02**
15:16383	0.1529	6.75E 02**
16:16385	0.1537	5.40E 02**
16:16383	0.1441	7.99E 02**

Figure 49. Scintillation Statistics

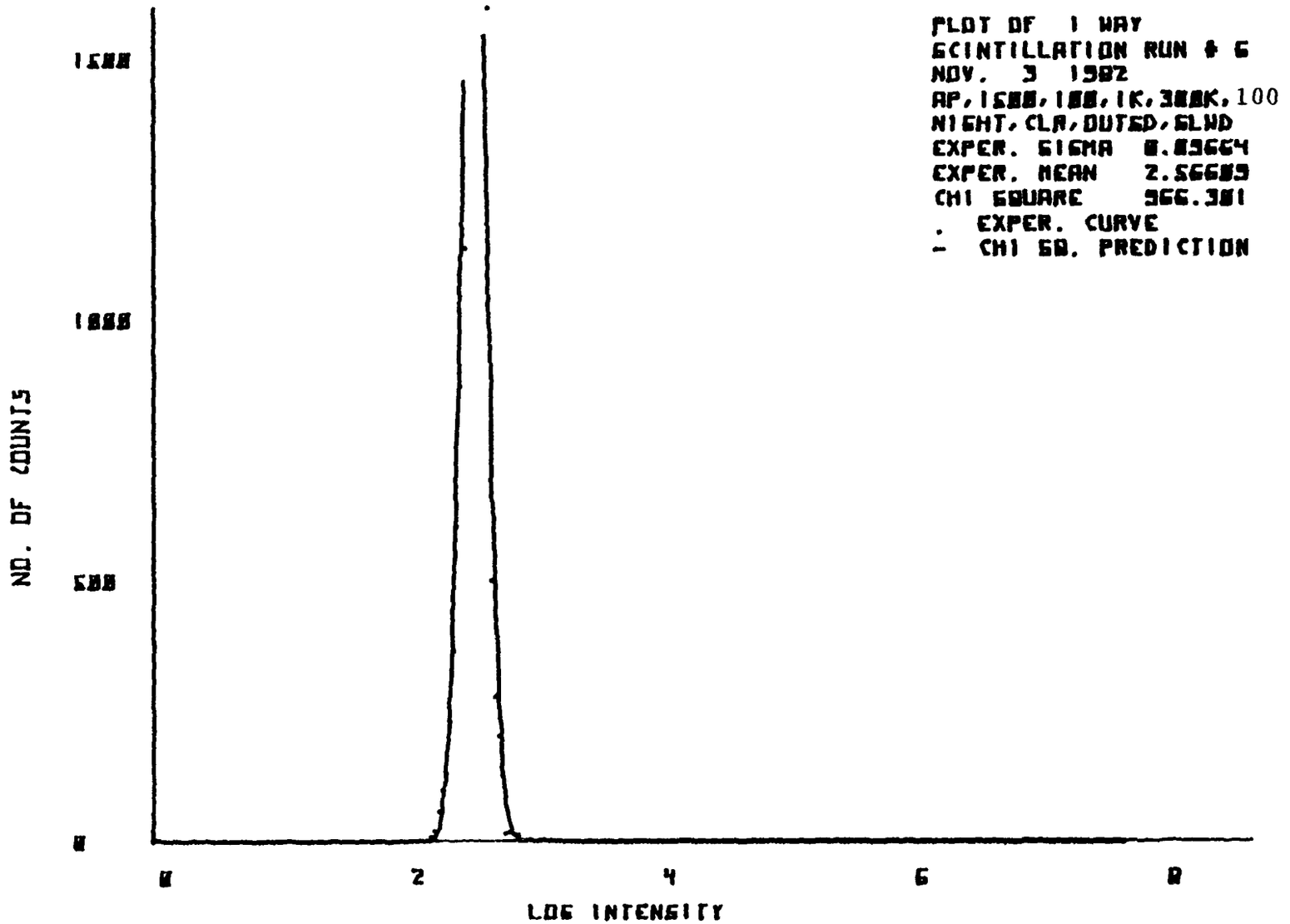

Figure 50. Scintillation Data and Theoretical Curve

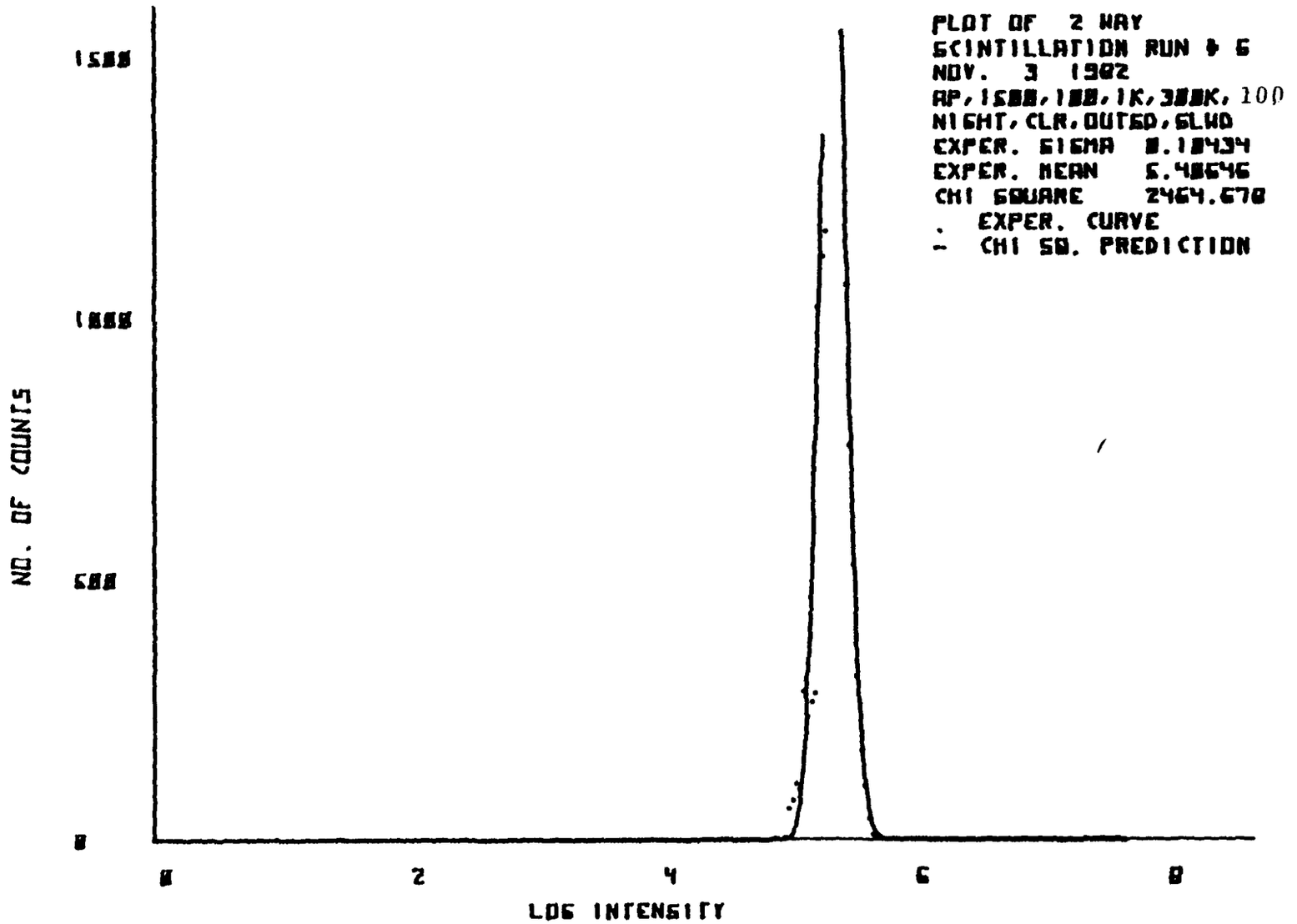

Figure 51. Scintillation Data and Theoretical Curve

APPENDIX E

DATA FROM THE SECOND EXPERIMENT

D(cm)	$\langle R \rangle \left(\left\langle \frac{\sigma F^2}{\sigma_S^2} \right\rangle\right)$	Error $\left(\pm \frac{\sigma}{N}\right)$	Runs Utilized	Comments
5	6.25	.126	All sixteen	
10	4.56	.165	excl. #16	
20	3.54	.473	All	Consistently decreasing ratios
30	1.90	.098	excl. #8, 9, 12, 13	Four pairs inverted data
40	4.32	.096	All	
50	1.93	.056	excl. #13, 14 15, 16	Setup mis-aligned midrun
60	5.16	.167	All	
70	2.55	.052	All	
80	5.87	.144	excl. 7	
90	1.40	.039	All	
100	4.98	.088	All	
110	1.96	.013	All	
150	6.01	.121	All	

NOV. 13 1982
Ap,1200G500,100,5
Night,clr,roof
wavelength= 6.33E-07 meters

Scintillation measurements of Sigma
16384 samples for each measurement
Fixed range= 40 meters

# pts	Sigma	Cni Square
1:16384	0.0962	3.24E 02**
1:16384	0.2507	2.71E 02
2:16385	0.0961	4.48E 02**
2:16383	0.2356	4.40E 02**
3:16383	0.0946	2.67E 02
3:16378	0.2497	3.86E 02**
4:16383	0.0983	1.55E 02
4:16385	0.2469	1.70E 02
5:16382	0.1021	3.17E 02**
5:16379	0.2675	4.85E 02**
6:16383	0.0885	2.26E 02
6:16385	0.2196	2.60E 02
7:16383	0.0931	5.61E 02**
7:16385	0.2359	3.75E 02**
8:16383	0.0988	3.72E 02**
8:16385	0.2432	4.14E 02**
9:16383	0.1119	4.92E 02**
9:16385	0.2661	2.91E 02**
10:16382	0.0981	4.08E 02**
10:16382	0.2470	5.76E 02**
11:16383	0.1107	2.35E 02
11:16385	0.2852	2.25E 02
12:16383	0.1026	3.76E 02**
12:16385	0.2558	4.98E 02**
13:16384	0.1122	2.36E 02
13:16383	0.2519	4.05E 02**
14:16385	0.0938	3.61E 02**
14:16383	0.2284	4.55E 02**
15:16384	0.1063	1.90E 02
15:16381	0.2704	5.35E 02**
16:16382	0.1206	3.10E 02**
16:16380	0.2996	3.65E 02**

Figure 52. Scintillation Statistics

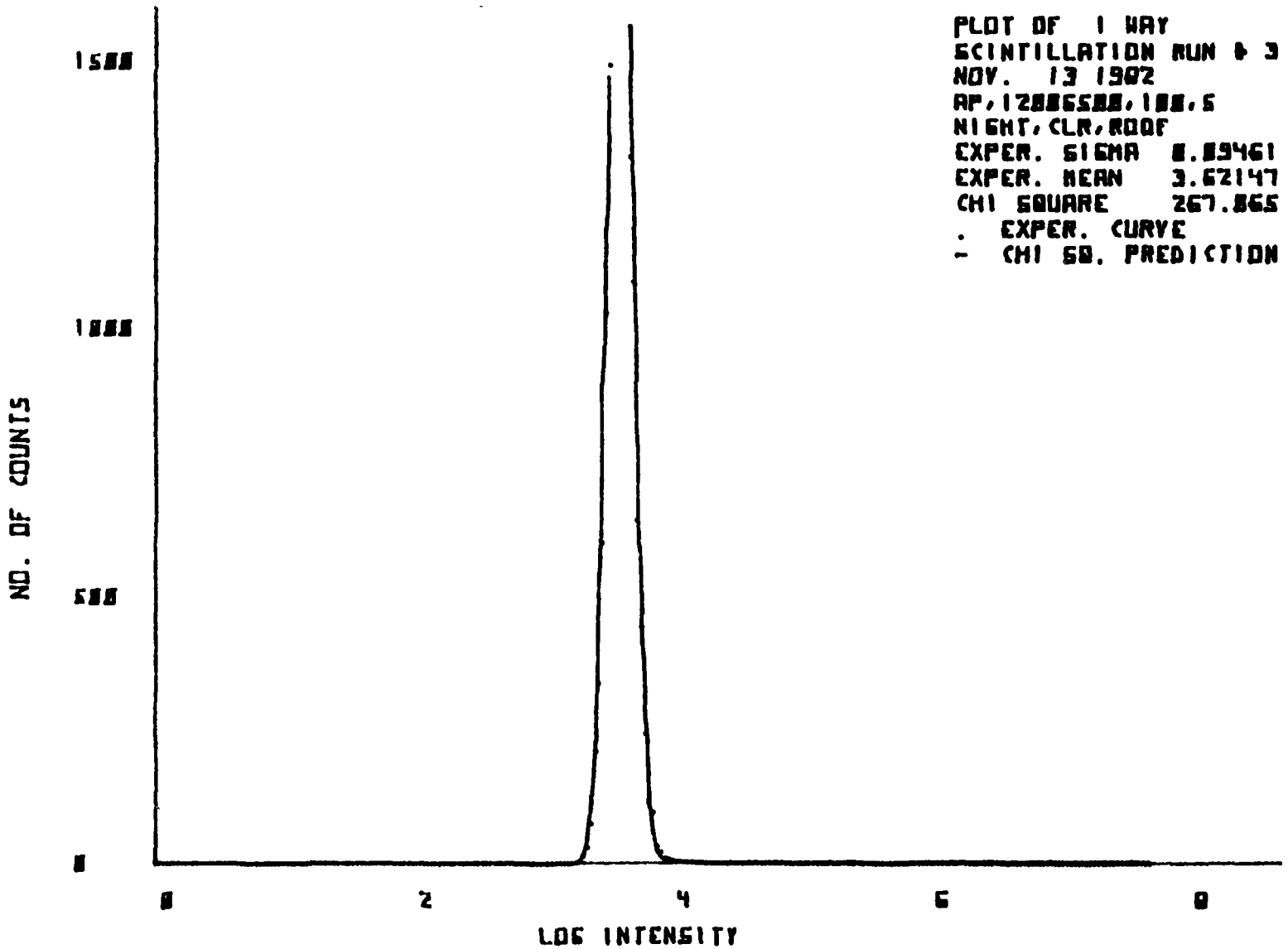

Figure 53. Scintillation Data and Theoretical Curve

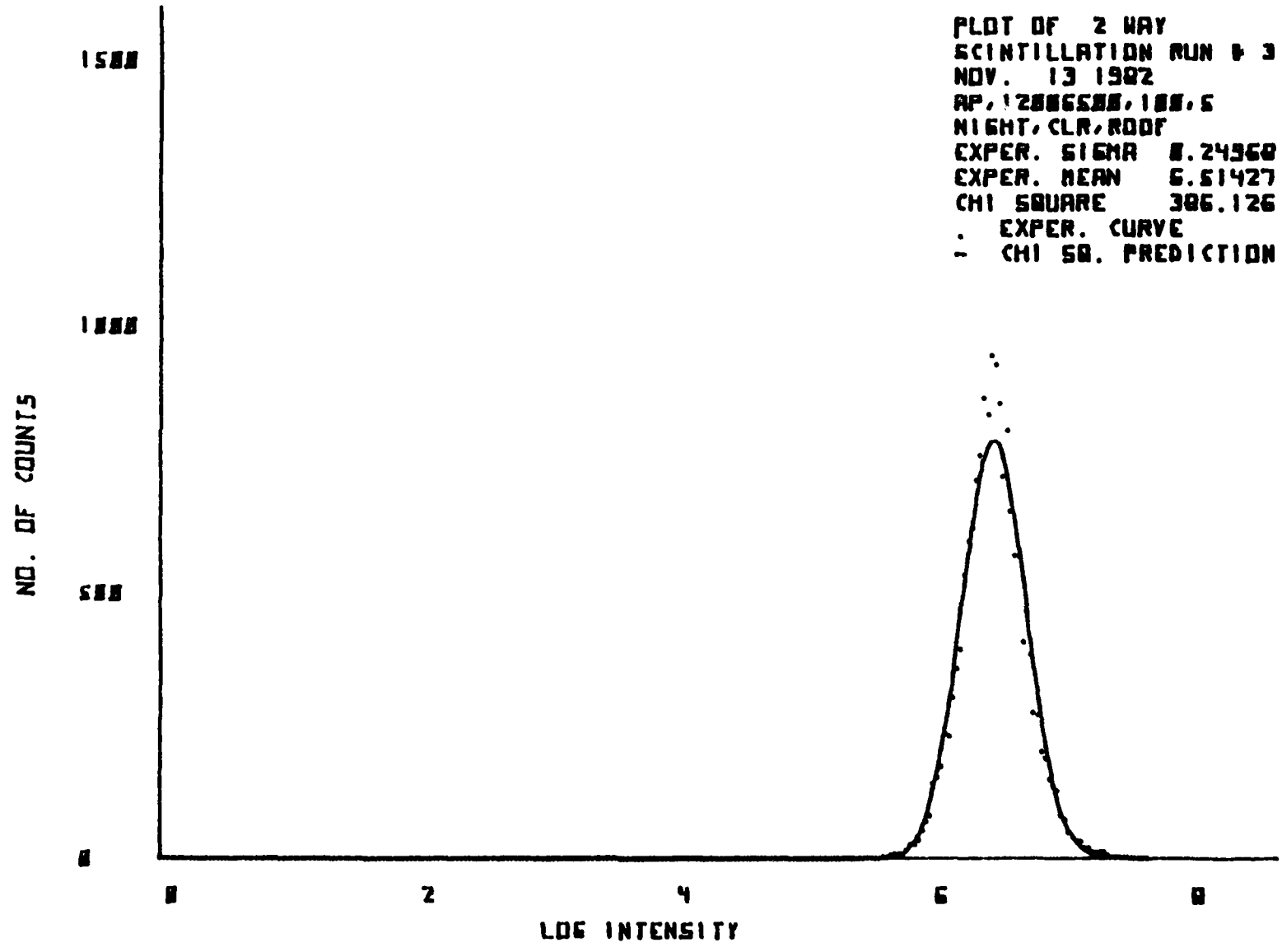

Figure 54. Scintillation Data and Theoretical Curve

NOV 13 1982
Ap,1200G200,100,10
Night,roof,clr
Wavelength= 6.33E-07 meters

Scintillation measurements of Sigma
16384 samples for each measurement
Fixed range= 40 meters

# pts	Sigma	Chi Square
1:16310	0.1401	3.73E 02**
1:16090	0.3073	1.87E 02
2:16333	0.1348	6.43E 02**
2:16160	0.2802	2.67E 02
3:16328	0.1191	4.62E 02**
3:16165	0.2694	3.16E 02**
4:16331	0.1199	8.37E 02**
4:16189	0.2475	3.29E 02**
5:16375	0.0962	3.26E 02**
5:16350	0.2075	1.47E 02
6:16291	0.1410	6.59E 02**
6:16016	0.2900	3.44E 02**
7:16313	0.1424	1.20E 03**
7:16073	0.2718	2.34E 02
8:16275	0.1539	1.82E 03**
8:15937	0.2809	3.31E 02**
9:16257	0.1418	1.02E 03**
9:15900	0.2771	4.63E 02**
10:16300	0.1194	4.16E 02**
10:16080	0.2564	2.41E 02
11:16316	0.1256	1.33E 03**
11:16101	0.2525	4.58E 02**
12:16315	0.1146	8.99E 02**
12:16110	0.2602	5.13E 02**
13:16361	0.0802	4.63E 02**
13:16294	0.1892	3.81E 02**
14:16367	0.0839	7.33E 02**
14:16315	0.1944	3.71E 02**
15:16374	0.0740	3.58E 02**
15:16344	0.1716	3.81E 02**
16:16368	0.1584	1.17E 04**
16:16322	0.1600	3.80E 02**

Figure 55. Scintillation Statistics

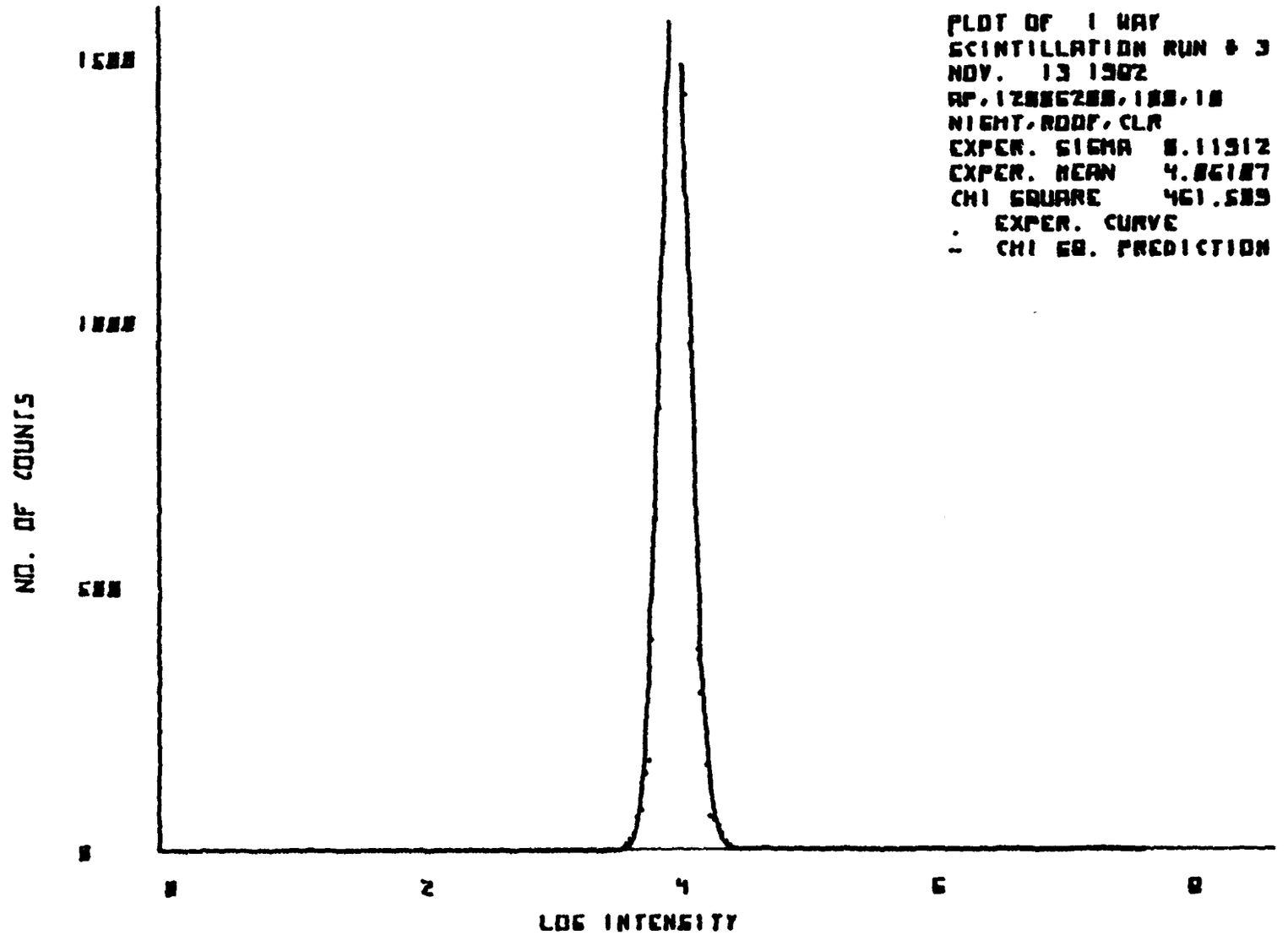

Figure 56. Scintillation Data and Theoretical Curve

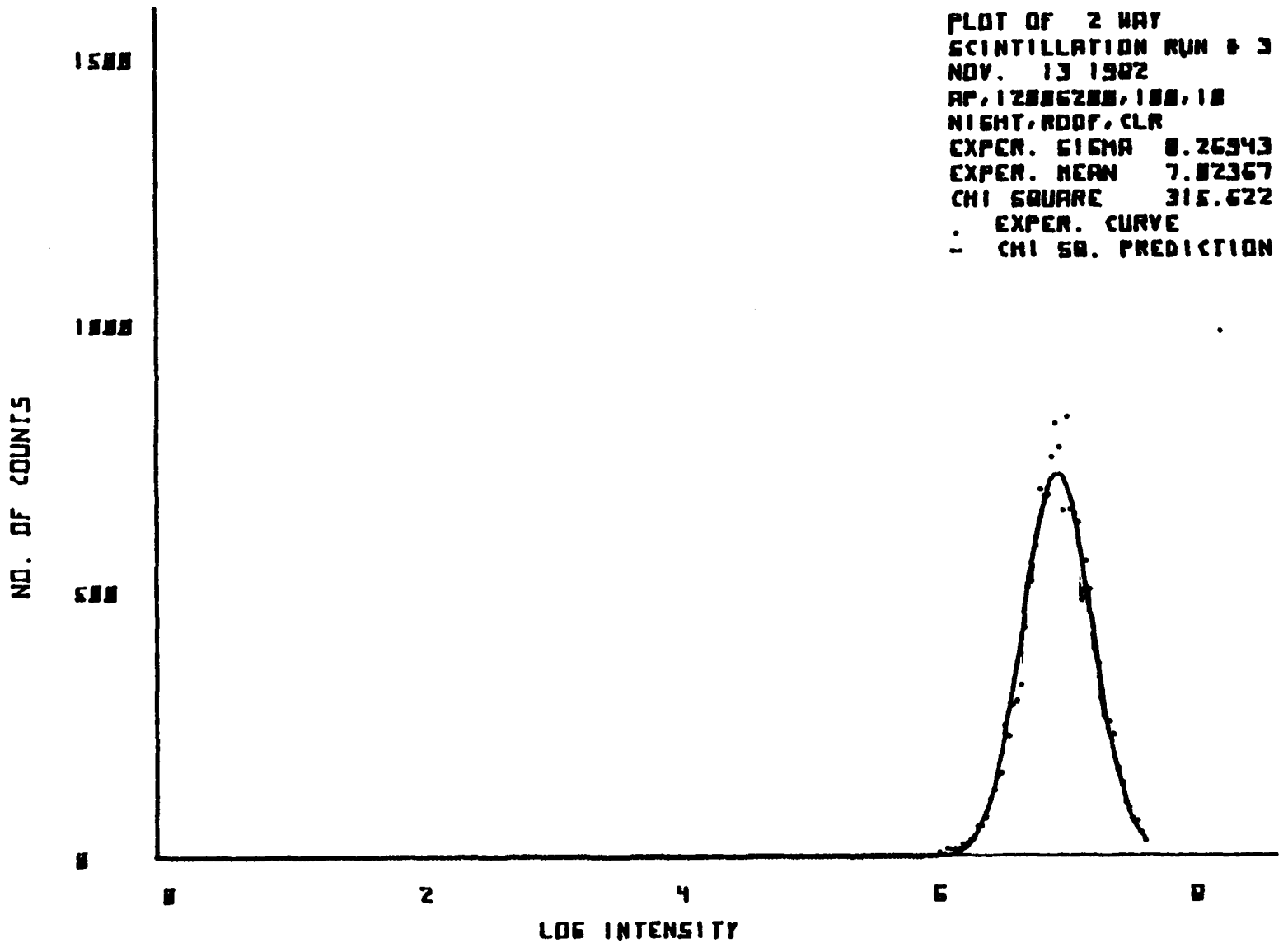

Figure 57. Scintillation Data and Theoretical Curve

NOV. 13 1982
Ap,1200,G500,100,20
Night,roof,clr
Wavelength= 6.33E-07 meters

Scintillation measurements of Sigma
16384 samples for each measurement
Fixed range= 40 meters

# pts	Sigma	Chi Square
1:16323	0.1101	4.88E 02**
1:16200	0.2694	3.30E 02**
2:16353	0.0790	9.02E 02**
2:16319	0.1996	5.29E 02**
3:16330	0.0840	8.96E 02**
3:16263	0.2186	1.63E 02
4:16310	0.0814	1.03E 03**
4:16238	0.2095	3.74E 02**
5:16153	0.1545	1.70E 03**
5:15684	0.3343	4.28E 02**
6:16218	0.1199	3.55E 03**
6:16021	0.2426	2.66E 02
7:16127	0.1407	4.97E 03**
7:15845	0.2609	3.65E 02**
8:15894	0.1904	4.52E 03**
8:15210	0.3360	2.08E 02
9:15691	0.1997	4.59E 03**
9:14992	0.3312	3.13E 02**
10:15392	0.2296	4.14E 03**
10:14447	0.3601	2.93E 02**
11:15118	0.2508	5.35E 03**
11:14082	0.3640	3.17E 02**
12:14630	0.2961	5.98E 03**
12:13131	0.3969	5.39E 02**
13:13725	0.3362	6.34E 03**
13:11730	0.4281	1.05E 03**
14:15094	0.4231	9.62E 03**
14:13399	0.5351	2.83E 03**
15:15498	0.3319	7.39E 03**
15:14030	0.4385	1.09E 03**
16:15694	0.2967	1.16E 04**
16:14764	0.3523	5.26E 02**

Figure 58. Scintillation Statistics

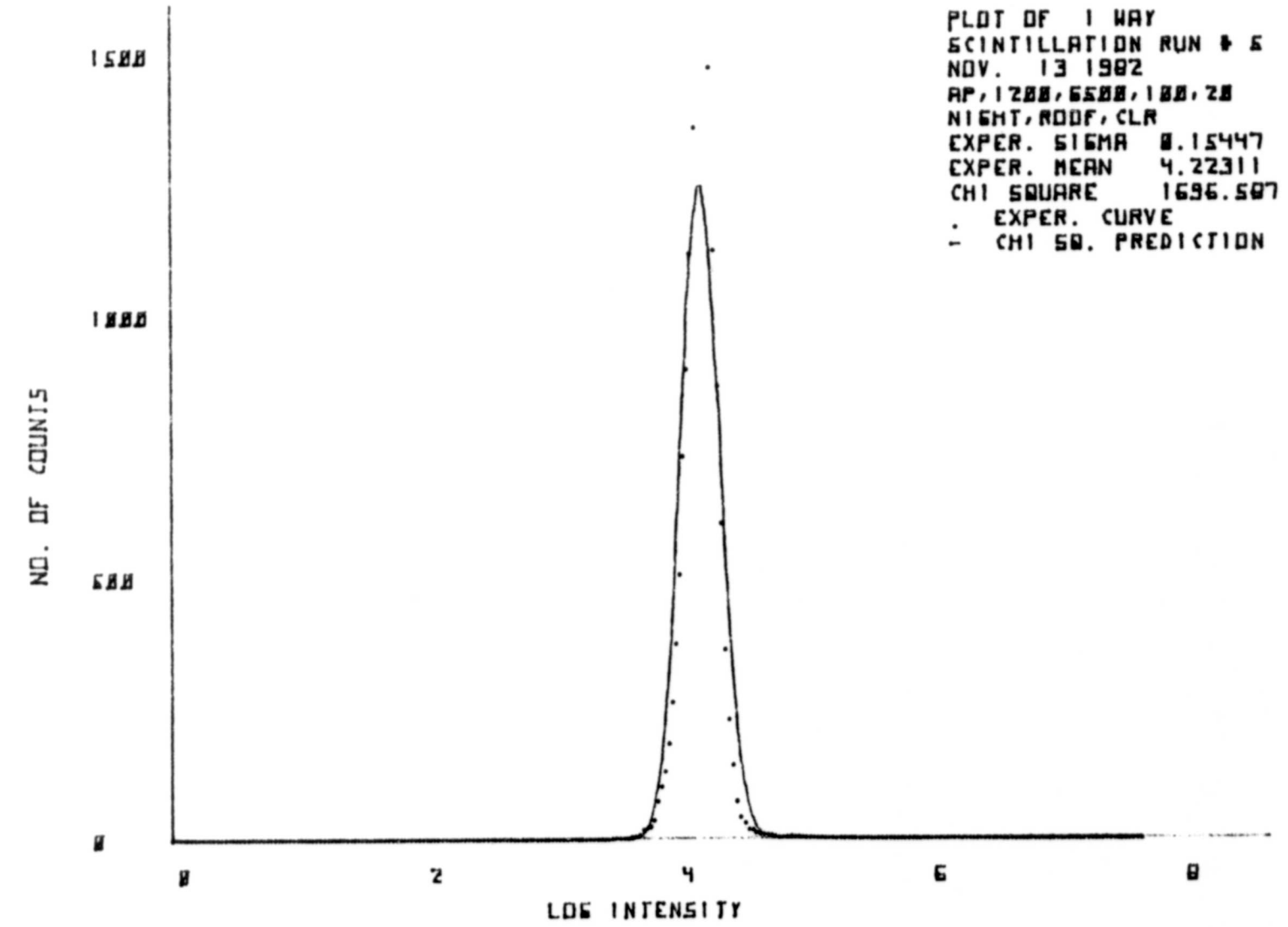

Figure 59. Scintillation Data and Theoretical Curve

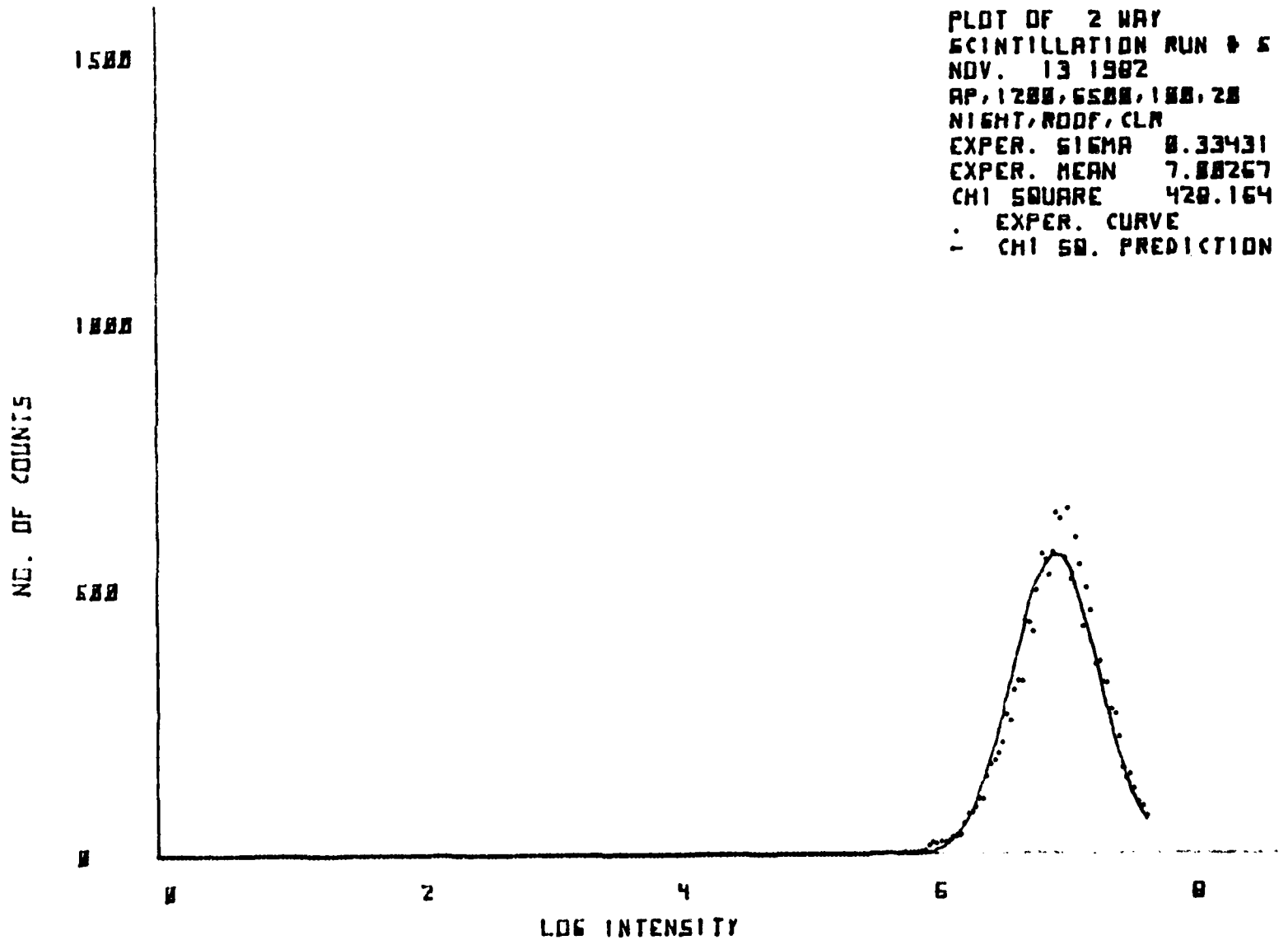

Figure 60. Scintillation Data and Theoretical Curve

NOV. 13 1982
Ap,1200G100,30
Night,roof,clr
wavelength= 6.33E-07 meters

Scintillation measurements of Sigma
16384 samples for each measurement
Fixed range= 40 meters

# pts	Sigma	Chi Square
1:16384	0.1363	5.25E 02**
1:16384	0.2128	3.47E 02**
2:16385	0.1136	5.59E 02**
2:16383	0.1507	7.69E 02**
3:16385	0.0891	1.08E 03**
3:16383	0.1070	2.69E 03**
4:16385	0.1582	1.65E 03**
4:16383	0.2368	3.71E 02**
5:16385	0.1122	6.13E 02**
5:16383	0.1612	5.24E 02**
6:16385	0.0937	3.88E 02**
6:16383	0.1067	2.35E 02
7:16385	0.1262	9.15E 02**
7:16383	0.1811	7.92E 02**
8:16385	0.0933	4.47E 02**
8:16383	0.0884	3.20E 02**
9:16385	0.1126	2.57E 03**
9:16383	0.0928	1.18E 03**
10:16385	0.1547	1.27E 03**
10:16383	0.2256	4.81E 02**
11:16385	0.1424	1.91E 03**
11:16383	0.1712	1.02E 03**
12:16385	0.1010	6.20E 02**
12:16383	0.0992	1.05E 02
13:16385	0.0980	3.45E 02**
13:16383	0.0962	3.01E 02**
14:16385	0.1145	1.14E 03**
14:16383	0.1483	1.97E 03**
15:16385	0.1461	6.05E 02**
15:16383	0.2085	1.42E 02
16:16385	0.1631	1.01E 03**
16:16383	0.2432	2.43E 02

Figure 61. Scintillation Statistics

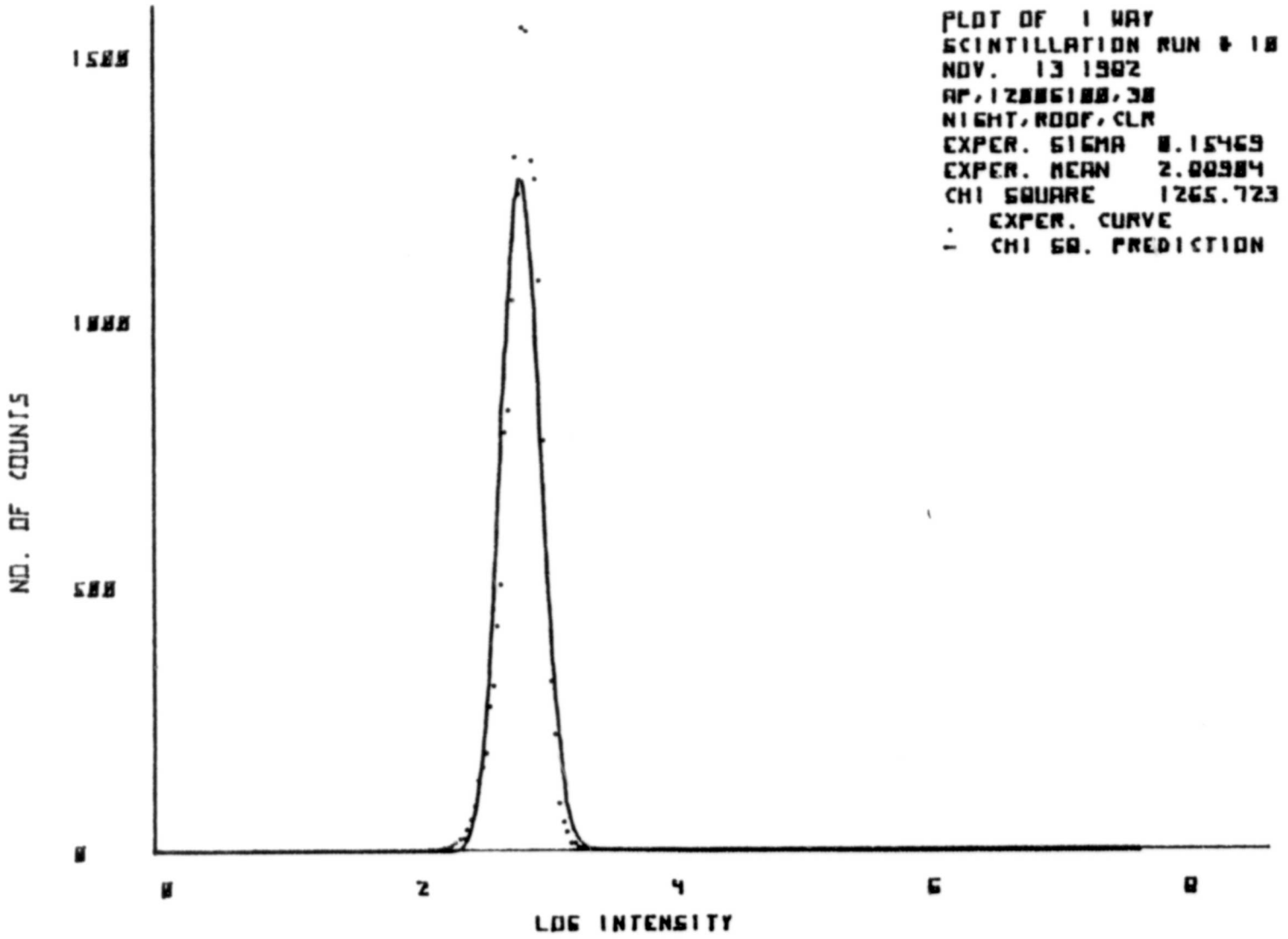

Figure 62. Scintillation Data and Theoretical Curve

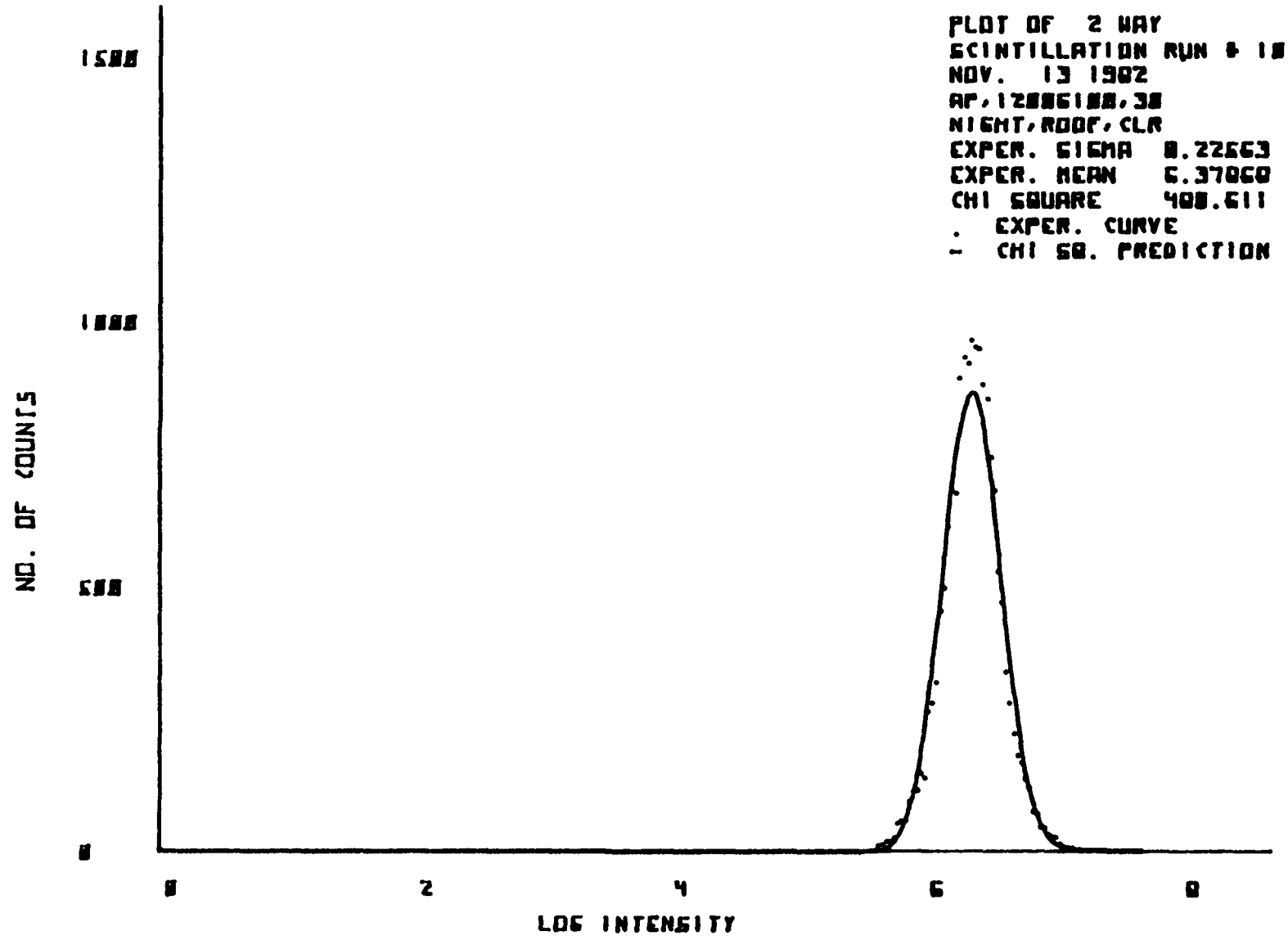

Figure 63. Scintillation Data and Theoretical Curve

NOV. 13 1982
Ap,1200G200,40
Night,roof,clr
wavelength= 6.33E-07 meters

Scintillation measurements or Sigma
16384 samples for each measurement
Fixed range= 40 meters

# pts	Sigma	Chi Square
1:16314	0.1543	2.60E 02
1:16132	0.3395	1.64E 02
2:16326	0.1470	4.93E 02**
2:16176	0.3088	1.64E 02
3:16358	0.1227	5.28E 02**
3:16279	0.2618	1.99E 02
4:16331	0.1486	3.86E 02**
4:16169	0.3157	2.33E 02
5:16323	0.1528	5.12E 02**
5:16167	0.3224	2.58E 02
6:16340	0.1372	3.40E 02**
6:16209	0.3083	1.78E 02
7:16362	0.1219	4.12E 02**
7:16292	0.2756	1.41E 02
8:16305	0.1611	2.39E 02
8:16088	0.3302	1.73E 02
9:16225	0.1934	4.24E 02**
9:15772	0.3759	2.93E 02**
10:16323	0.1390	8.98E 02**
10:16154	0.2833	5.25E 02**
11:16249	0.1857	5.54E 02**
11:15860	0.3590	2.12E 02
12:16275	0.1709	7.85E 02**
12:15971	0.3374	1.75E 02
13:16310	0.1659	6.59E 02**
13:16080	0.3384	1.82E 02
14:16258	0.1795	5.94E 02**
14:15904	0.3562	2.64E 02
15:16305	0.1751	5.76E 02**
15:16076	0.3410	2.01E 02
16:16371	0.1137	6.68E 02**
16:16333	0.2407	4.25E 02**

Figure 64. Scintillation Statistics.

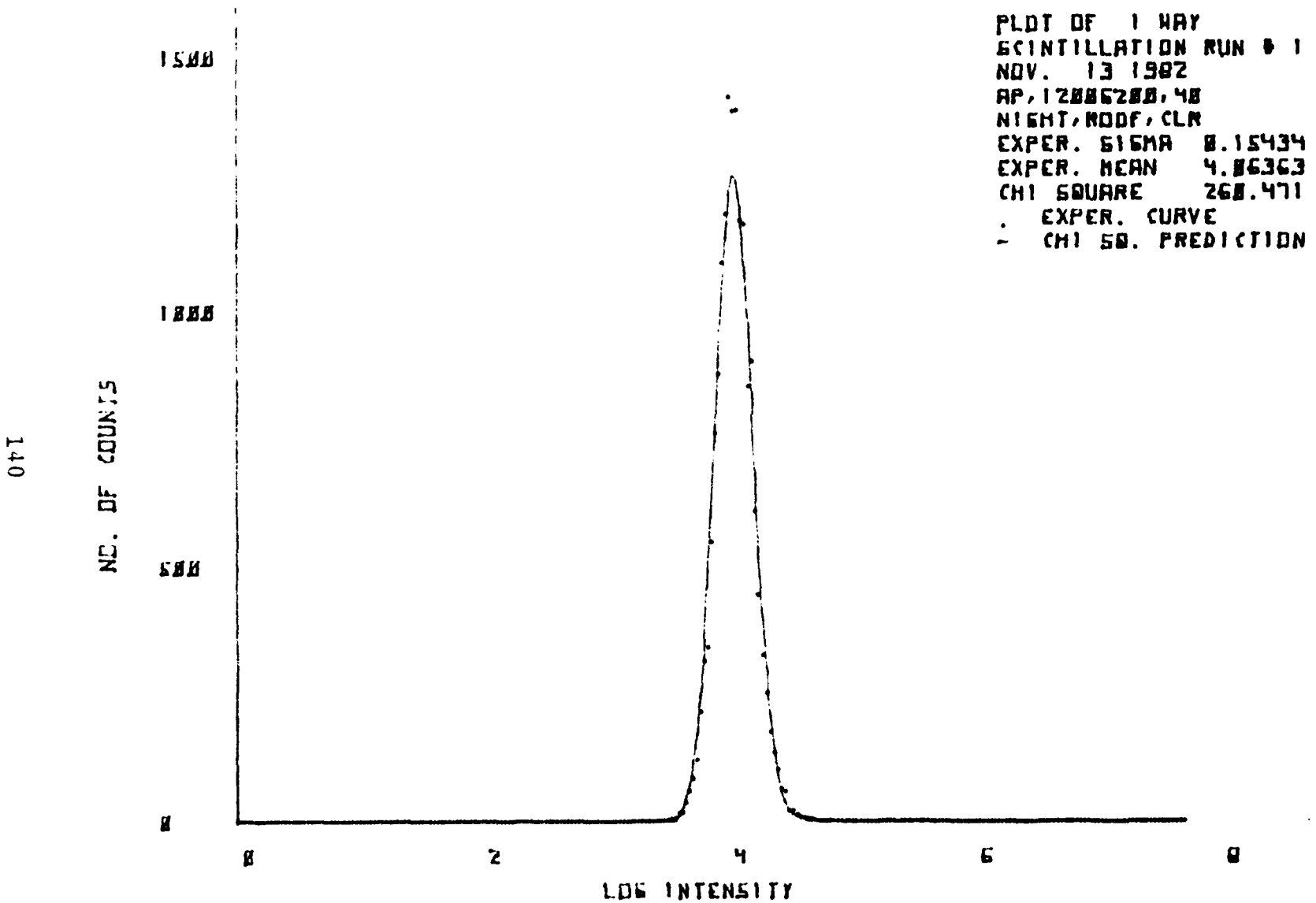

Figure 65. Scintillation Data and Theoretical Curve

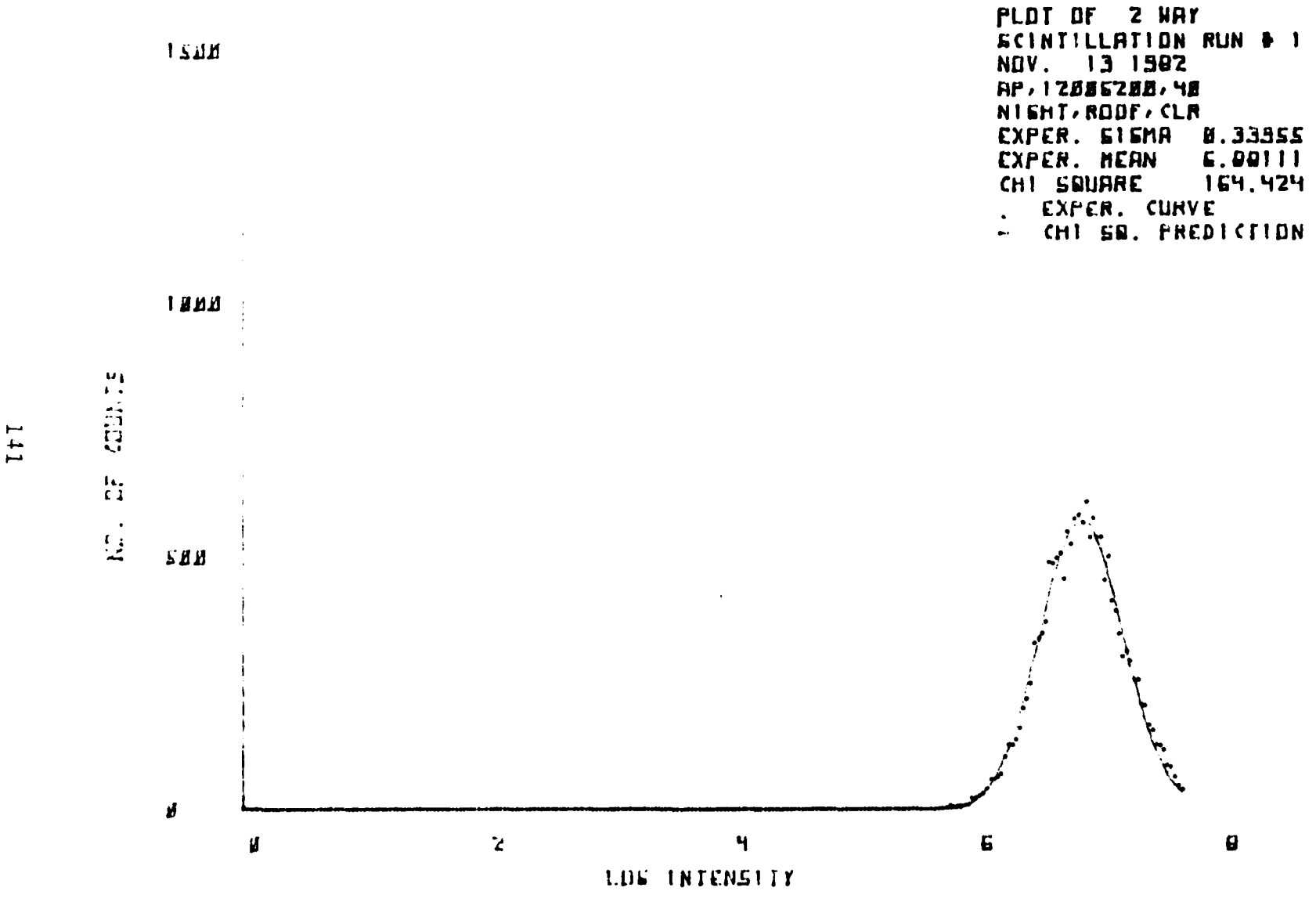

Figure 66. Scintillation Data and Theoretical Curve

```
NOV, 13 1982
Ap,1200G100,50
Night,clr,roof
Wavelength=   6.33E-07 meters


Scintillation measurements of Sigma
16384 samples for each measurement
Fixed range=    40 meters

    # pts        Sigma     Chi Square

   1:16278      0.2057    8.56E 02**
   1:16006      0.2936    3.49E 02**
   2:16274      0.2221    7.15E 02**
   2:15978      0.3100    1.61E 02
   3:16224      0.2467    8.58E 02**
   3:15776      0.3309    2.34E 02
   4:16293      0.2219    5.41E 02**
   4:16032      0.3085    2.01E 02
   5:16282      0.2217    5.95E 02**
   5:16031      0.3243    2.14E 02
   6:16315      0.1910    7.92E 02**
   6:16135      0.2893    5.59E 02**
   7:16337      0.1988    4.40E 02**
   7:16194      0.2907    1.86E 02
   8:16270      0.2572    1.43E 03**
   8:15963      0.3497    4.39E 02**
   9:16272      0.2684    1.45E 03**
   9:15953      0.3498    2.23E 02
  10:16214      0.2790    1.30E 03**
  10:15814      0.3734    2.54E 02
  11:16082      0.3507    1.86E 03**
  11:15534      0.4696    3.56E 02**
  12:16274      0.2541    1.31E 03**
  12:15989      0.3367    1.66E 02
  13: 3851      0.2811    6.27E 02**
  13:12171      1.7187    6.88E 04**
Division by zero occured in line                    56
```

Figure 67. Scintillation Statistics.

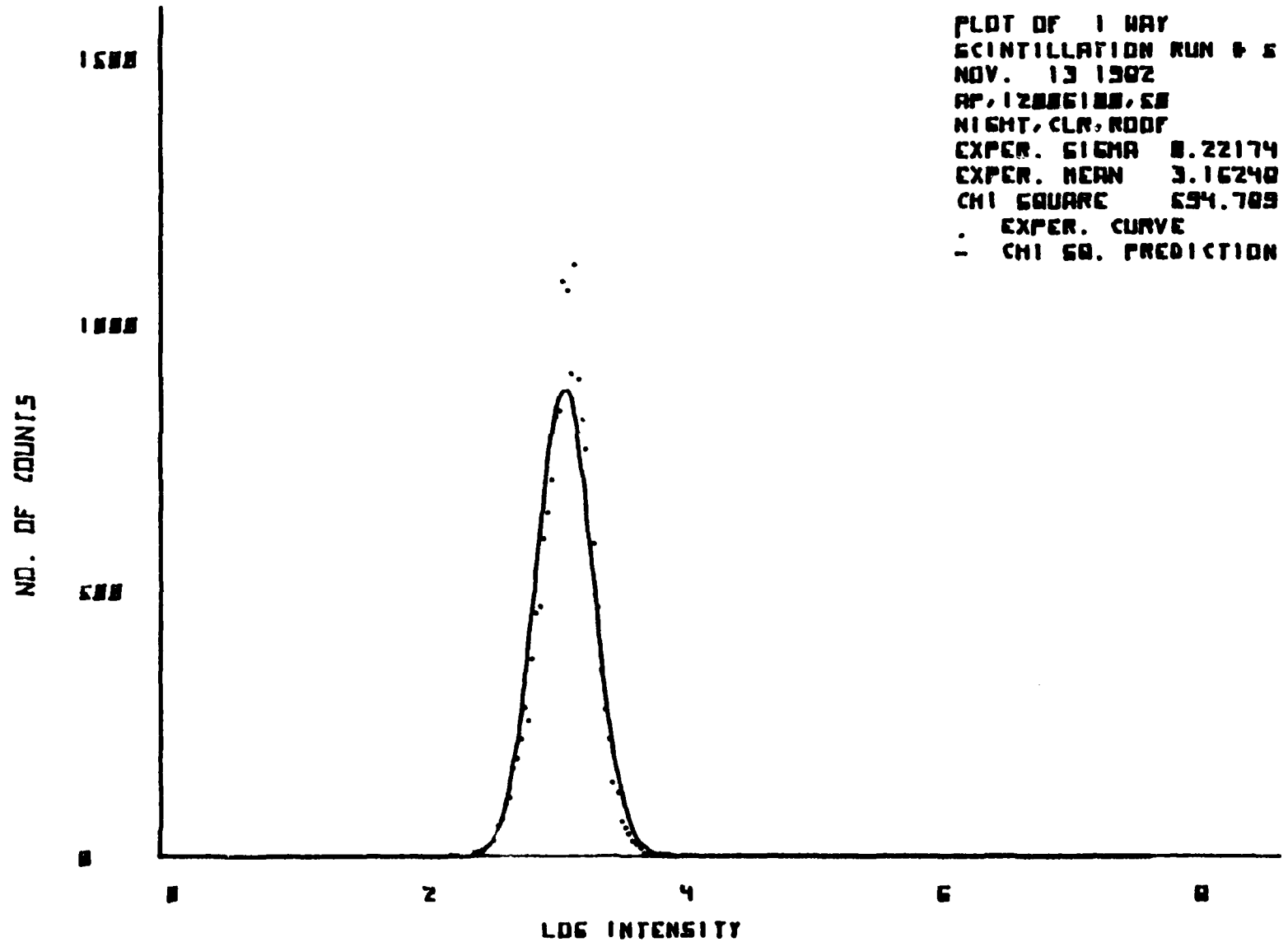

Figure 68. Scintillation Data and Theoretical Curve

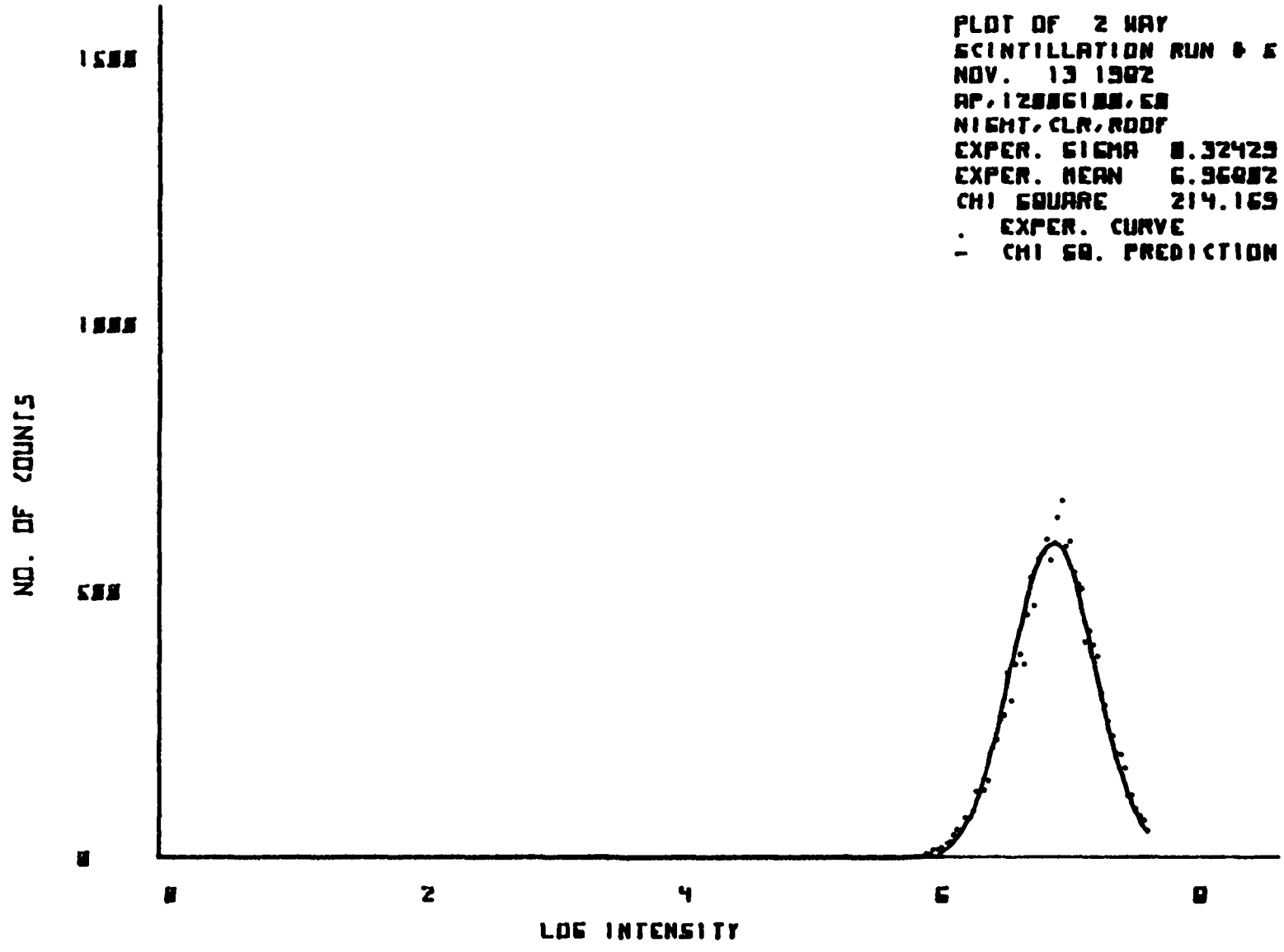

Figure 69. Scintillation Data and Theoretical Curve

NOV. 13 1982
Ap,1200,G100,60
Night,root,clr
wavelength= 6.33E-07 meters

Scintillation measurements of Sigma
16384 samples for each measurement
Fixed range= 40 meters

# pts	Sigma	Chi Square
1:16384	0.1244	3.80E 02**
1:16381	0.2827	4.82E 02**
2:16385	0.0984	4.69E 02**
2:16383	0.2254	1.91E 02
3:16385	0.0906	5.94E 02**
3:16383	0.1967	3.23E 02**
4:16385	0.0626	4.36E 02**
4:16383	0.1222	2.85E 02
5:16385	0.0712	7.29E 02**
5:16383	0.1472	3.74E 02**
6:16385	0.0941	5.10E 02**
6:16383	0.2146	6.82E 02**
7:16385	0.1025	5.12E 02**
7:16383	0.2289	2.89E 02**
8:16385	0.1091	4.96E 02**
8:16383	0.2486	1.75E 02
9:16385	0.1083	4.42E 02**
9:16382	0.2442	4.28E 02**
10:16385	0.1203	2.30E 02
10:16383	0.2789	2.29E 02
11:16385	0.1071	2.52E 02
11:16383	0.2556	1.67E 02
12:16385	0.0934	2.57E 02
12:16383	0.2388	2.61E 02
13:16385	0.0947	8.68E 02**
13:16383	0.2226	2.93E 02**
14:16385	0.0799	8.81E 02**
14:16383	0.1939	7.72E 02**
15:16385	0.0676	6.20E 02**
15:16383	0.1421	1.72E 02
16:16385	0.0789	2.55E 02
16:16383	0.1853	2.03E 02

Figure 70. Scintillation Statistics.

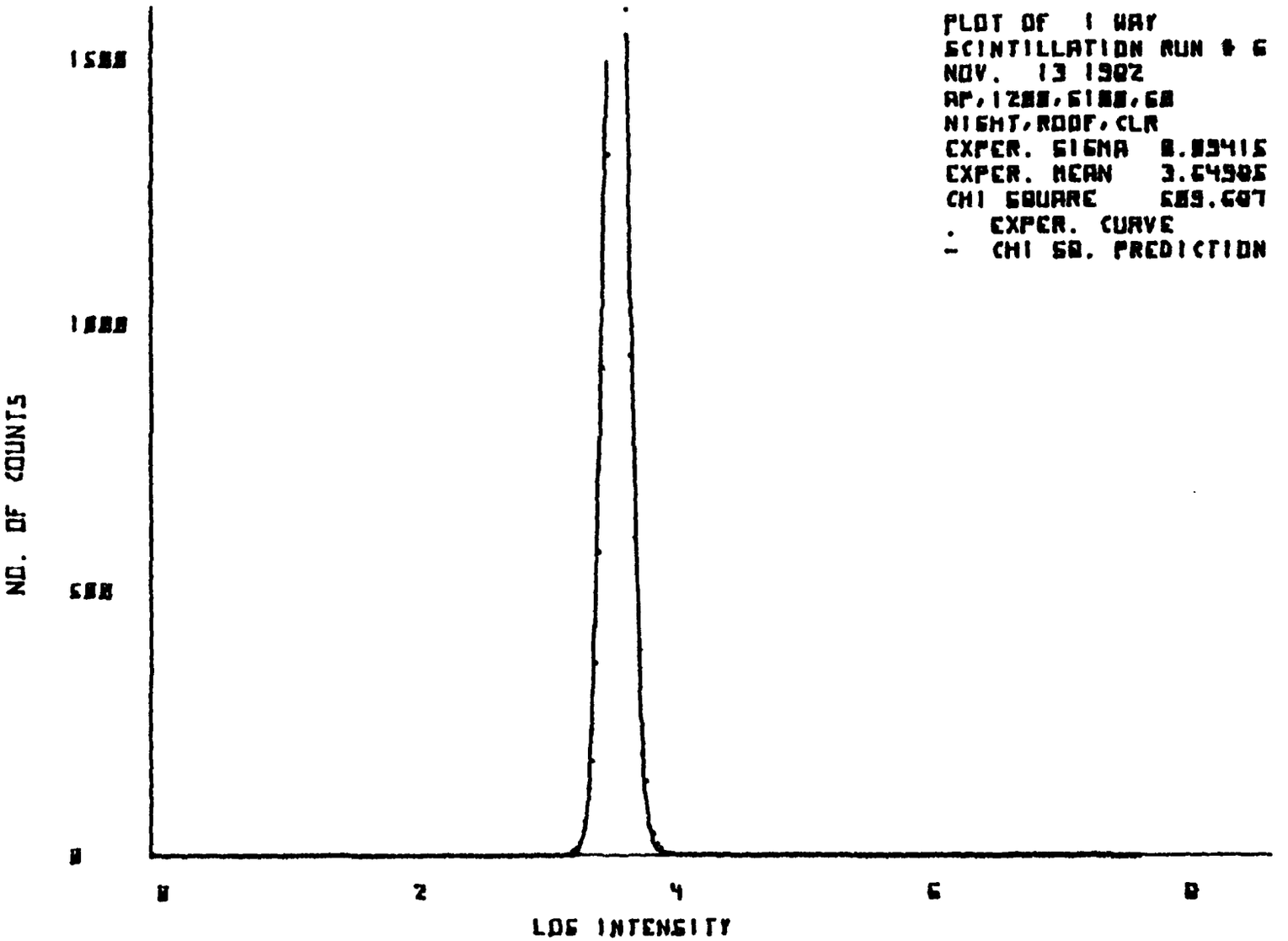

Figure 71. Scintillation Data and Theoretical Curve

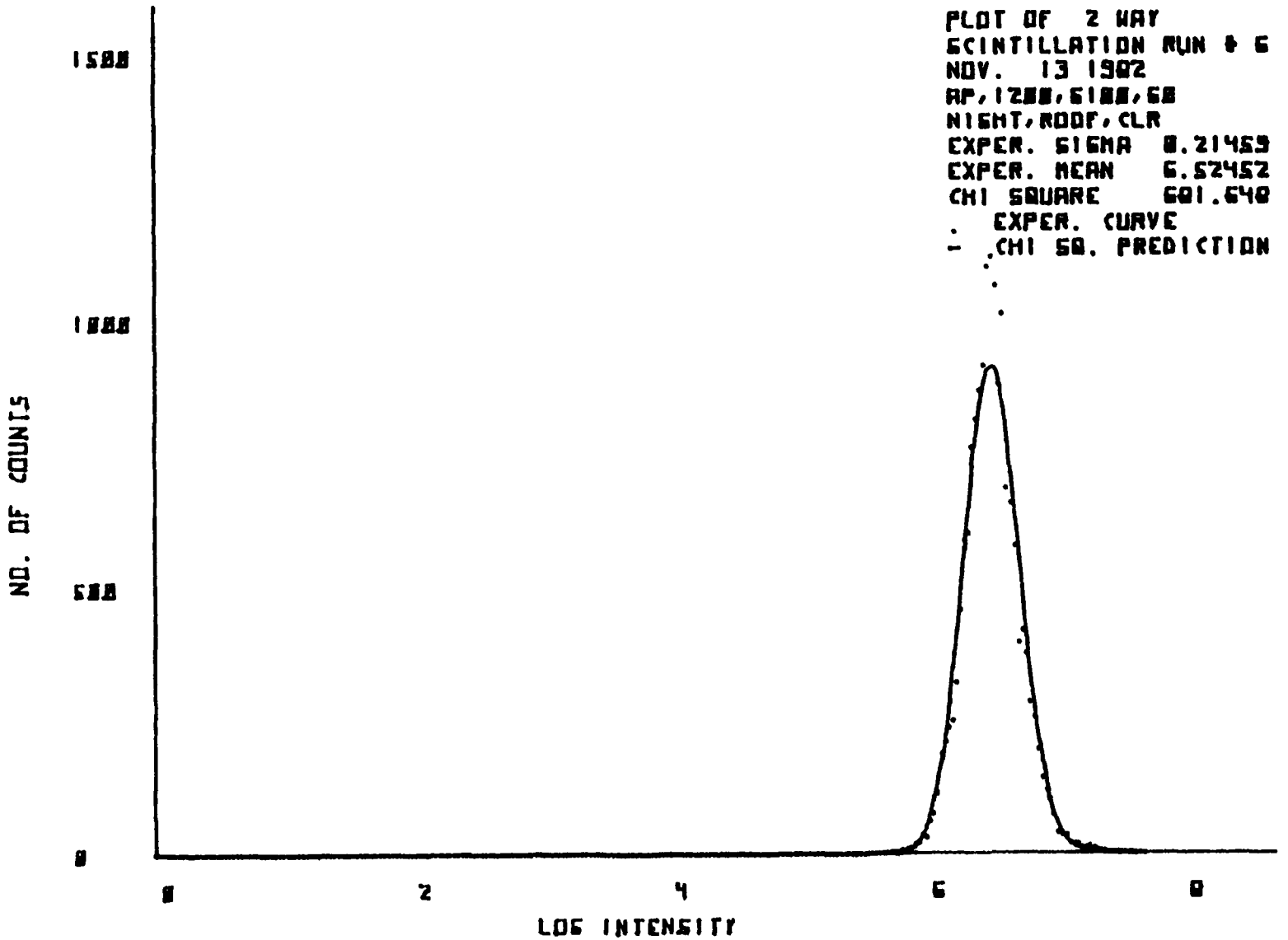

Figure 72. Scintillation Data and Theoretical Curve

NOV. 13 1982
Ap,1200Glk,100,70
Night,root,clr
Wavelength= 6.33E-07 meters

Scintillation measurements of Sigma
16384 samples for each measurement
Fixed range= 40 meters

# pts	Sigma	Cni Square
1:16384	0.1687	4.51E 02**
1:16384	0.2606	2.48E 02
2:16385	0.1517	4.49E 02**
2:16383	0.2360	3.17E 02**
3:16385	0.1266	4.73E 02**
3:16383	0.1851	5.83E 02**
4:16385	0.1169	4.80E 02**
4:16383	0.1543	5.59E 02**
5:16383	0.1972	6.35E 02**
5:16382	0.3320	1.01E 03**
6:16380	0.2272	6.86E 02**
6:16382	0.3486	4.10E 02**
7:16379	0.2727	9.05E 02**
7:16373	0.4092	2.95E 02**
8:16383	0.2343	7.17E 02**
8:16383	0.3525	2.97E 02**
9:16385	0.1706	6.84E 02**
9:16383	0.2398	6.01E 02**
10:16385	0.1601	3.53E 02**
10:16383	0.2298	2.93E 02**
11:16385	0.1698	7.18E 02**
11:16383	0.2651	4.65E 02**
12:16385	0.1421	3.76E 02**
12:16383	0.2187	6.85E 02**
13:16385	0.1215	3.36E 02**
13:16383	0.1669	3.48E 02**
14:16385	0.1549	3.59E 02**
14:16383	0.2210	4.86E 02**
15:16385	0.1519	4.32E 02**
15:16383	0.2376	2.76E 02
16:16385	0.2090	6.31E 02**
16:16383	0.3179	2.75E 02

Figure 73. Scintillation Statistics.

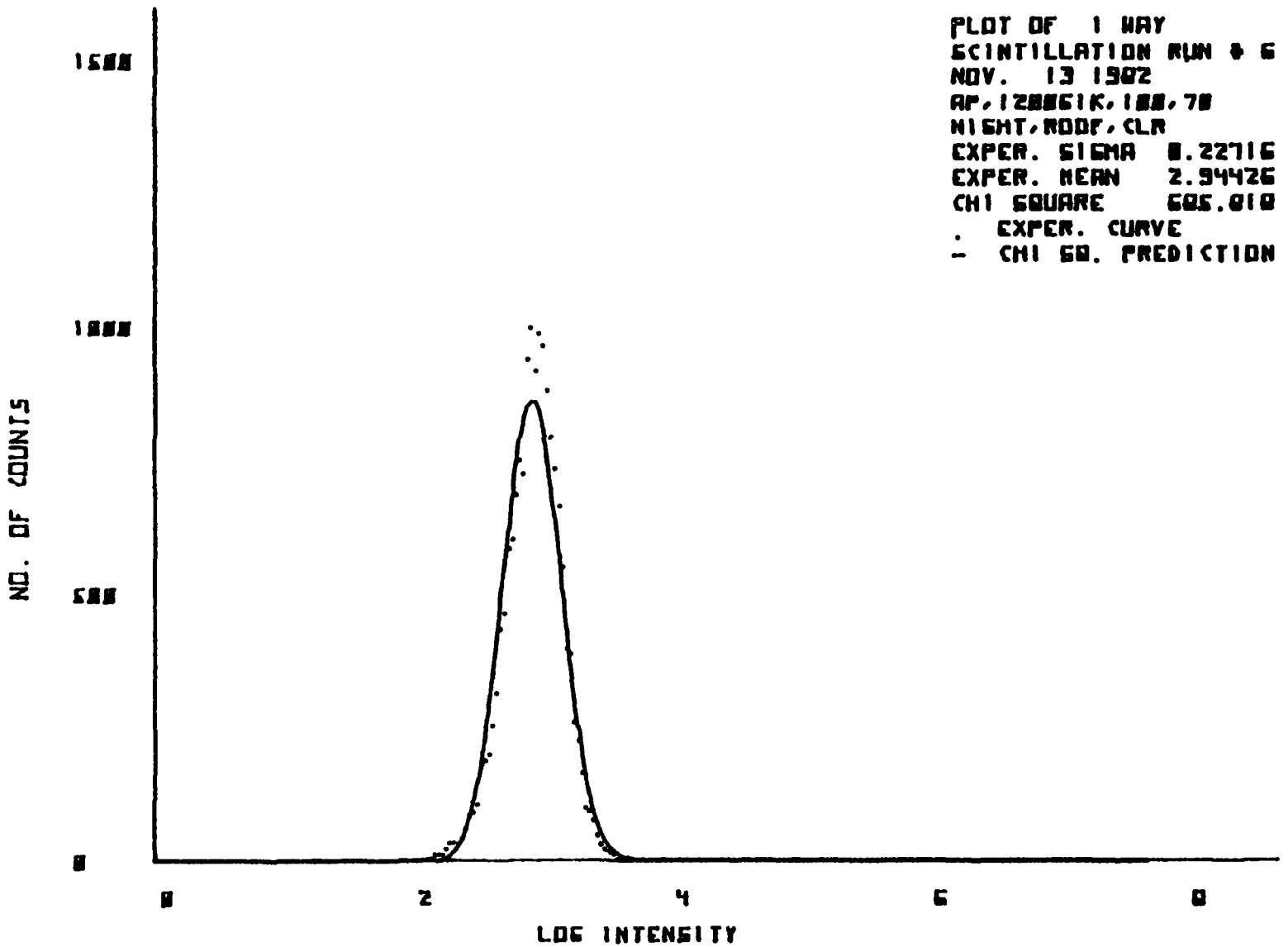

Figure 74. Scintillation Data and Theoretical Curve

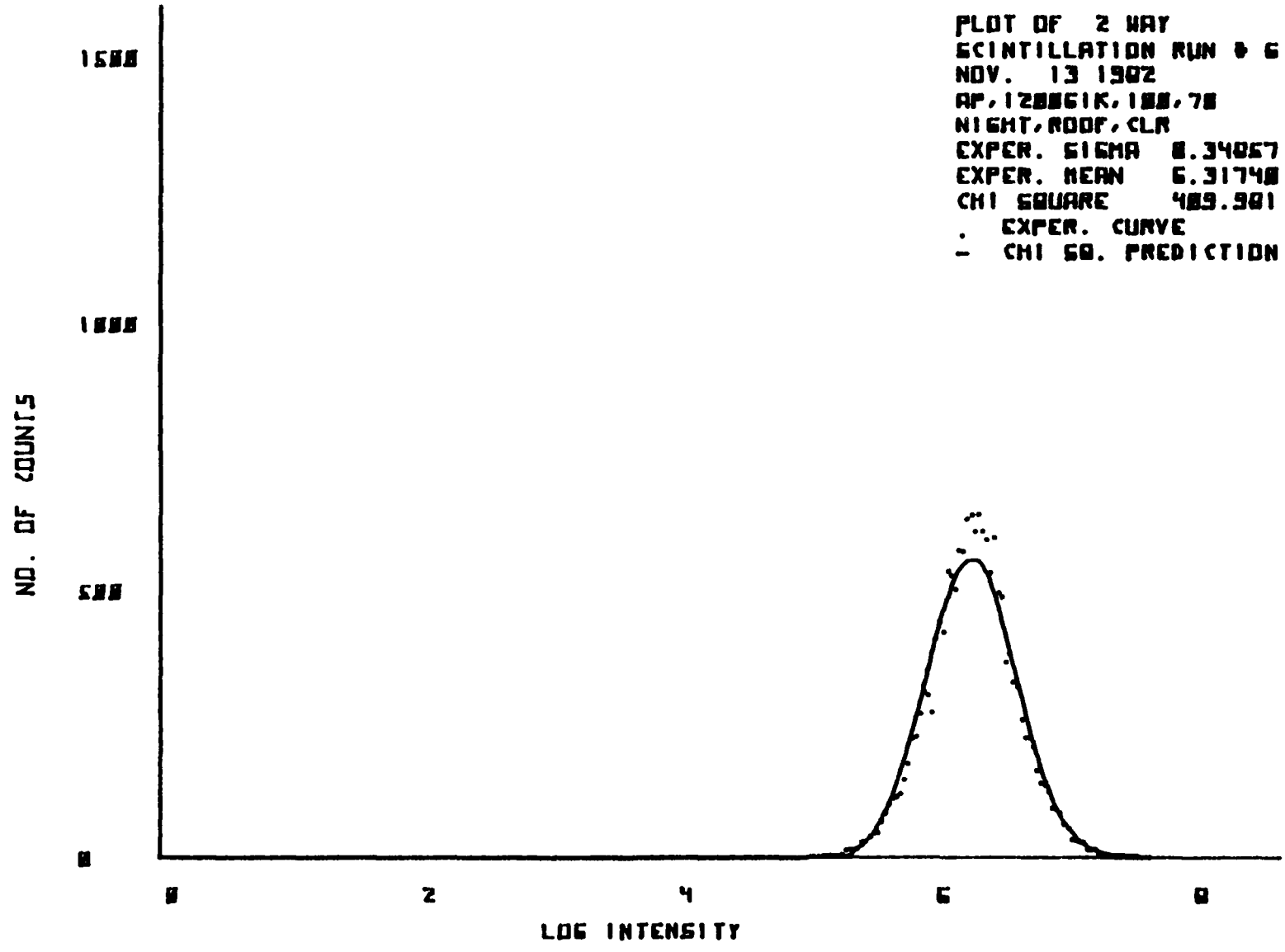

Figure 75. Scintillation Data and Theoretical Curve

NOV. 13 1982
Ap,1200,G100,80
Night,clr,roof
Wavelength= 6.33E-07 meters

Scintillation measurements of Sigma
16384 samples for each measurement
Fixed range= 40 meters

# pts	Sigma	Chi Square
1:16383	0.1202	9.41E 02**
1:16381	0.3218	5.36E 02**
2:16383	0.1262	4.50E 02**
2:16385	0.3341	2.59E 02
3:16383	0.1092	6.34E 02**
3:16385	0.2715	3.60E 02**
4:16383	0.0978	7.57E 02**
4:16385	0.2398	6.38E 02**
5:16383	0.1434	3.23E 02**
5:16385	0.3518	1.96E 02
6:16383	0.1382	3.46E 02**
6:16385	0.3391	3.01E 02**
7:16383	0.1273	1.44E 03**
7:16385	0.2316	3.86E 02**
8:16383	0.1140	2.50E 02
8:16385	0.2679	2.69E 02
9:16383	0.1080	1.55E 02
9:16385	0.2626	2.76E 02
10:16383	0.1054	3.48E 02**
10:16385	0.2528	4.02E 02**
11:16383	0.0918	6.70E 02**
11:16385	0.2176	9.67E 02**
12:16382	0.1251	1.23E 03**
12:16380	0.3046	1.30E 03**
13:16385	0.0871	1.97E 02
13:16383	0.1986	5.04E 02**
14:16385	0.0997	2.82E 02
14:16383	0.2231	2.23E 02
15:16385	0.1145	3.18E 02**
15:16383	0.2650	2.08E 02
16:16385	0.1070	2.49E 02
16:16383	0.2463	3.67E 02**

Figure 76. Scintillation Statistics.

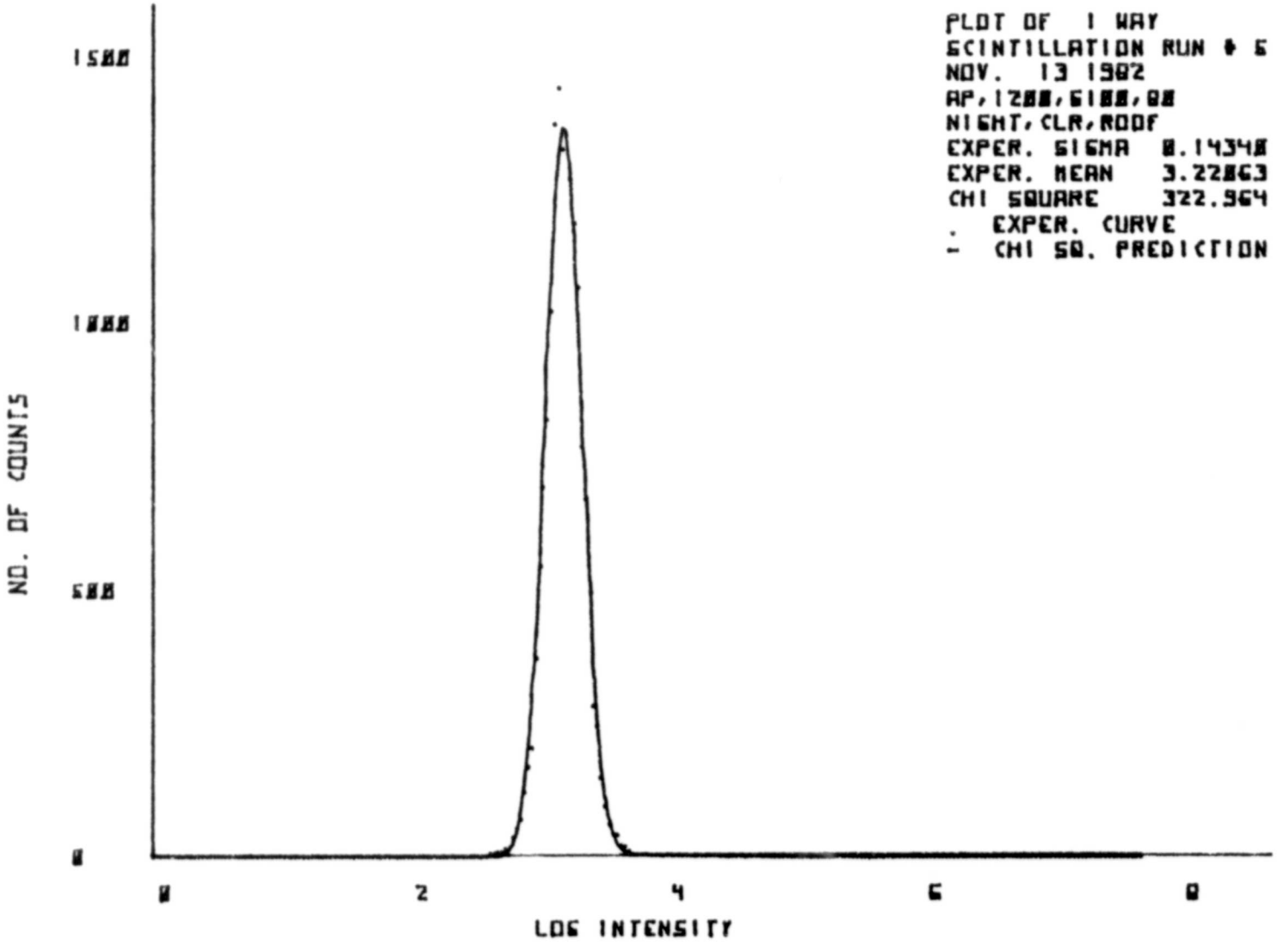

Figure 77. Scintillation Data and Theoretical Curve

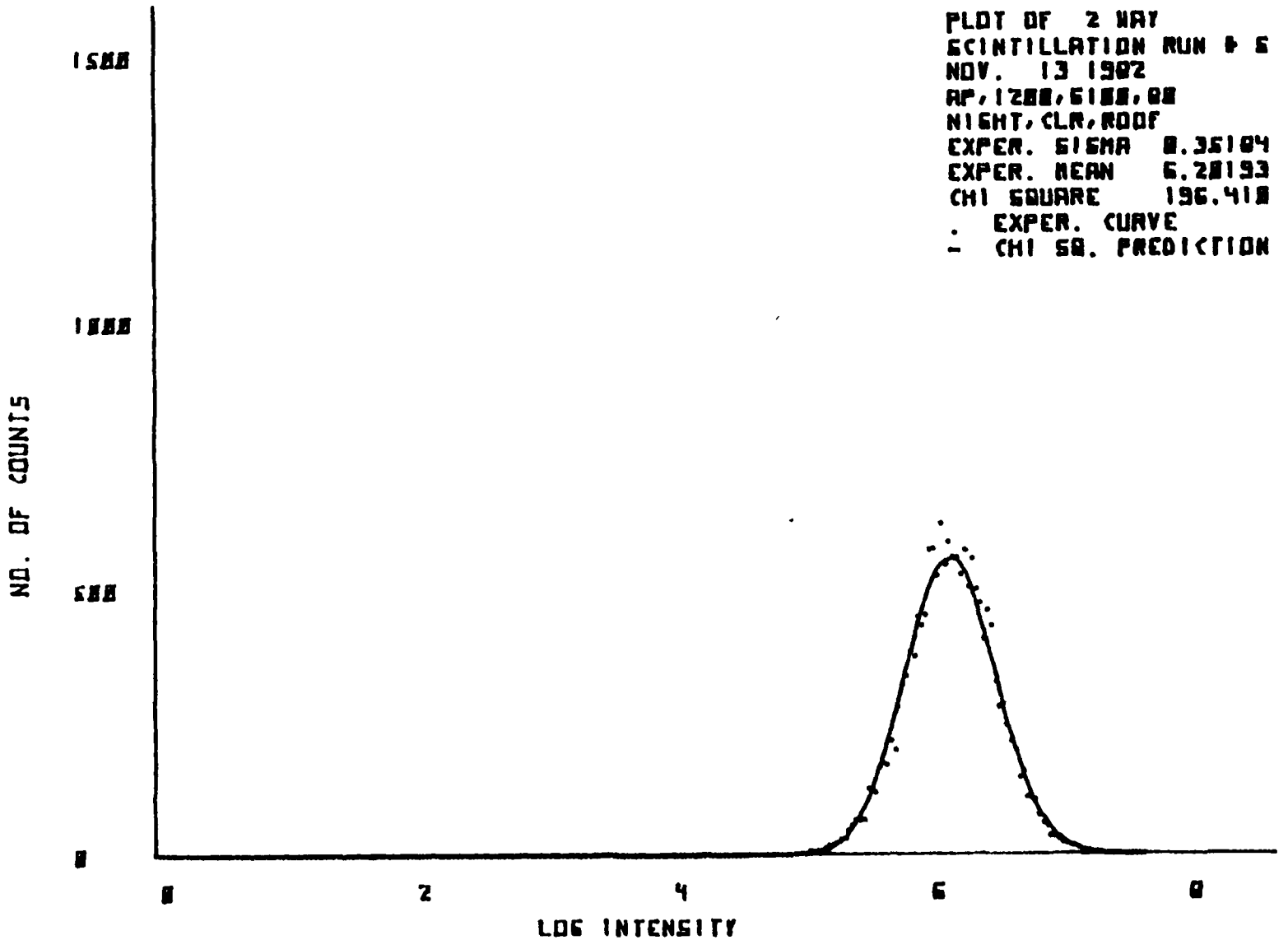

Figure 78. Scintillation Data and Theoretical Curve

NOV, 13 1982
Ap,1200G200,1k300k,90
Night,rcor,clr
wavelengtn= 6.33E-07 meters

Scintillation measurements of Sigma
16384 samples for each measurement
Fixed range= 40 meters

# pts	Sigma	Chi Square
1:16380	0.1520	4.62E 02**
1:16371	0.1830	6.69E 02**
2:16381	0.1487	5.77E 02**
2:16377	0.1698	5.34E 02**
3:16382	0.1725	5.40E 02**
3:16375	0.1922	3.90E 02**
4:16378	0.1543	3.17E 02**
4:16369	0.1758	2.46E 02
5:16378	0.1547	4.35E 02**
5:16366	0.1897	6.99E 02**
6:16365	0.1976	5.62E 02**
6:16310	0.2575	1.46E 02
7:16378	0.1725	7.88E 02**
7:16361	0.2161	3.83E 02**
8:16383	0.1547	6.35E 02**
8:16383	0.1779	2.26E 02
9:16382	0.1521	3.81E 02**
9:16373	0.1705	3.71E 02**
10:16381	0.1437	7.48E 02**
10:16370	0.1691	9.89E 02**
11:16379	0.1813	5.55E 02**
11:16354	0.2096	2.78E 02
12:16383	0.1133	3.62E 02**
12:16385	0.1289	1.56E 03**
13:16372	0.1815	1.09E 03**
13:16347	0.2243	6.38E 02**
14:16335	0.2540	1.09E 03**
14:16216	0.3055	3.57E 02**
15:16367	0.2289	5.87E 02**
15:16323	0.2673	1.45E 02
16:16373	0.1919	7.13E 02**
16:16344	0.2322	2.42E 02

Figure 79. Scintillation Statistics.

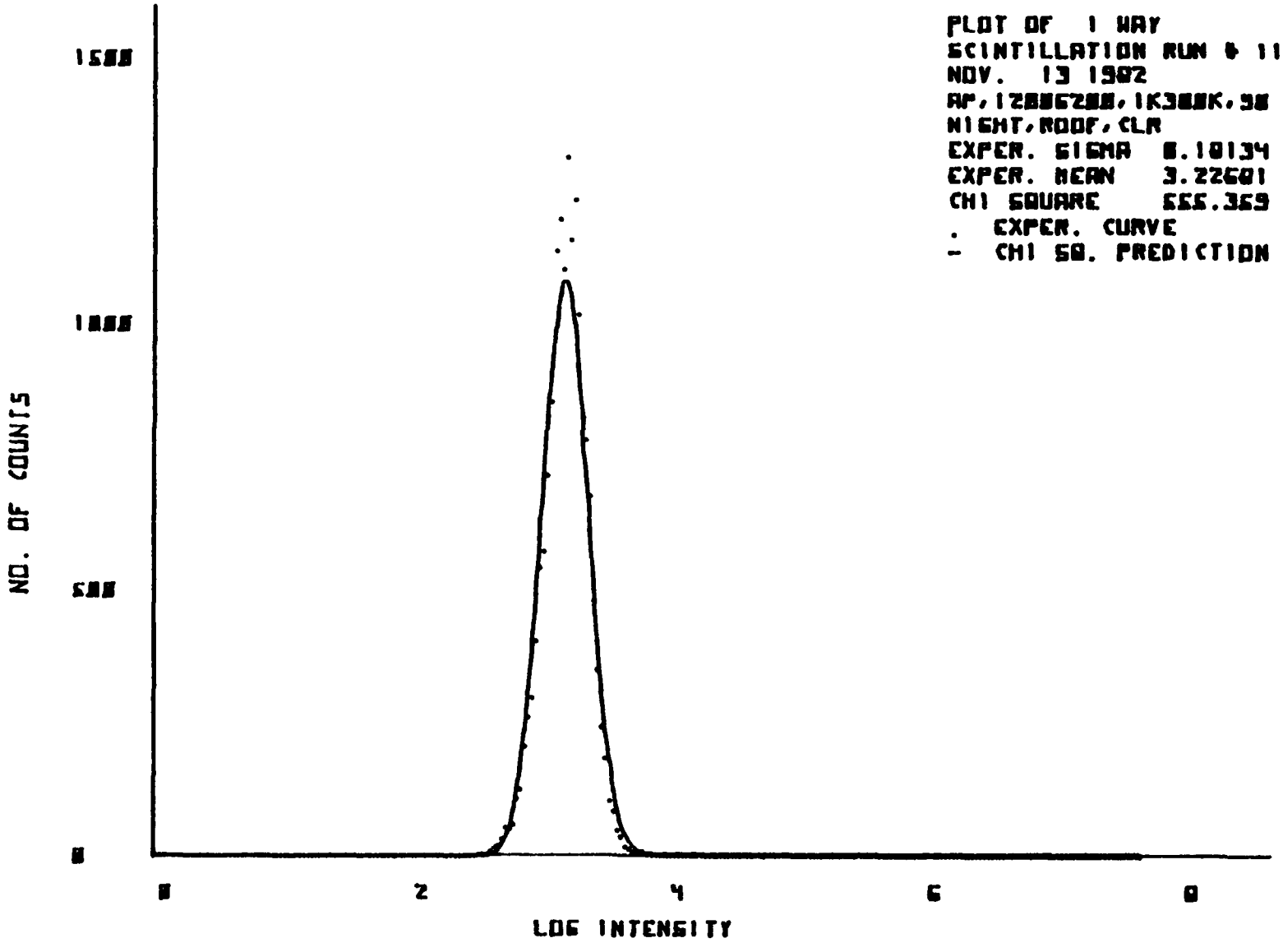

Figure 80. Scintillation Data and Theoretical Curve

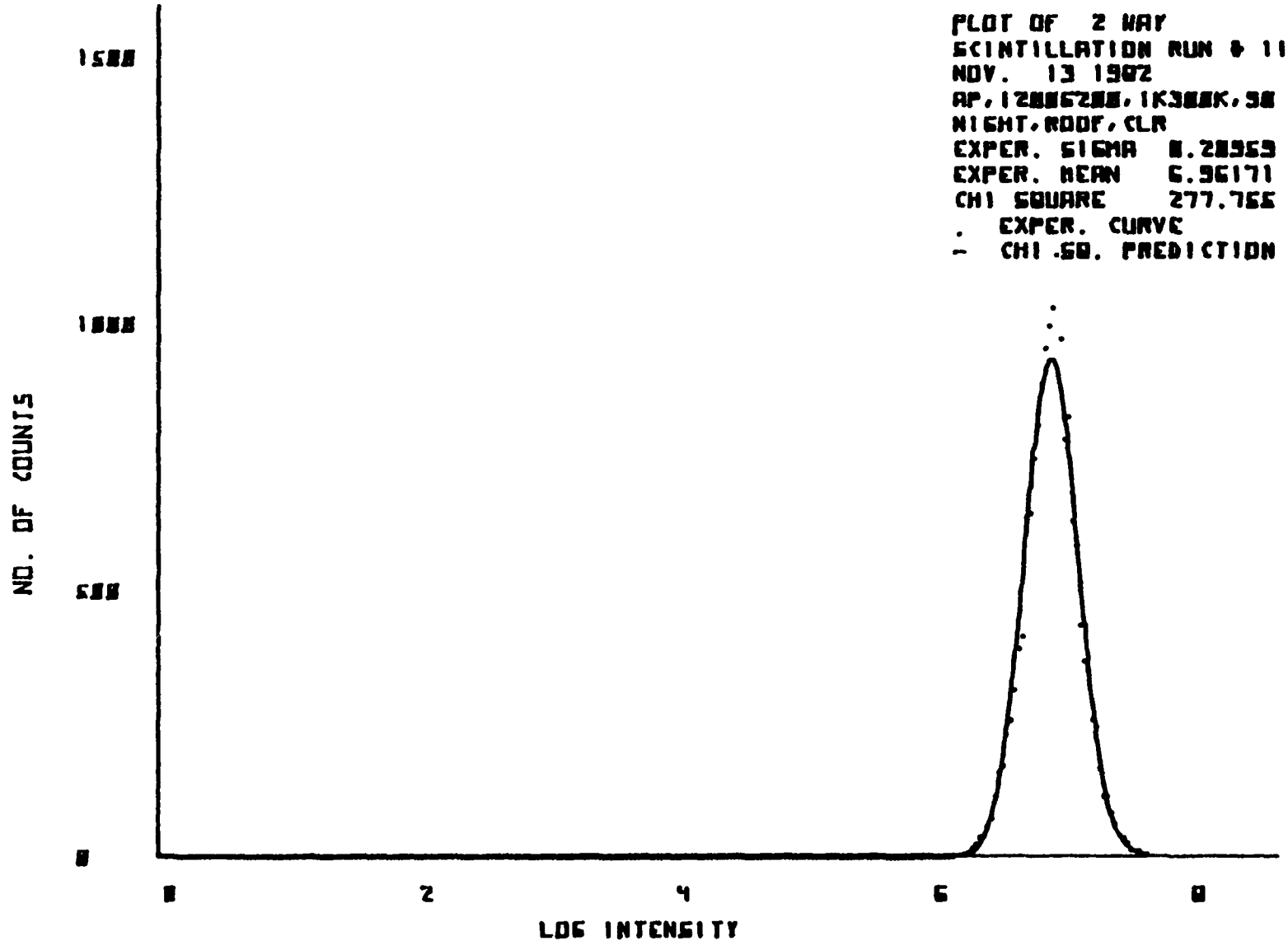

Figure 81. Scintillation Data and Theoretical Curve

NOV. 13 1982
Ap,1200G100,100
Night,root,clr
Wavelength= 6.33E-07 meters

Scintillation measurements of Sigma
16384 samples for each measurement
Fixed range= 40 meters

# pts	Sigma	Chi Square
1:16380	0.1349	3.85E 02**
1:16371	0.2994	2.68E 02
2:16384	0.1374	3.11E 02**
2:16382	0.2911	2.35E 02
3:16382	0.1484	8.26E 02**
3:16379	0.3248	3.78E 02**
4:16385	0.1521	2.64E 02
4:16383	0.3285	1.95E 02
5:16384	0.1507	5.95E 02**
5:16382	0.3289	2.33E 02
6:16381	0.1496	5.09E 02**
6:16379	0.3409	2.35E 02
7:16382	0.1194	4.91E 02**
7:16380	0.2881	2.44E 02
8:16383	0.1540	7.92E 02**
8:16376	0.3334	1.96E 02
9:16383	0.1386	4.79E 02**
9:16379	0.2955	2.22E 02
10:16383	0.1475	7.19E 02**
10:16379	0.3283	2.37E 02
11:16379	0.1354	8.66E 02**
11:16372	0.3178	5.98E 02**
12:16375	0.1743	5.39E 02**
12:16356	0.3981	2.41E 02
13:16380	0.1353	3.60E 02**
13:16375	0.3218	2.32E 02
14:16380	0.1575	3.21E 02**
14:16370	0.3484	2.28E 02
15:16369	0.1860	4.53E 02**
15:16342	0.4107	2.44E 02
16:16383	0.1409	3.52E 02**
16:16381	0.3038	1.95E 02

Figure 82. Scintillation Statistics.

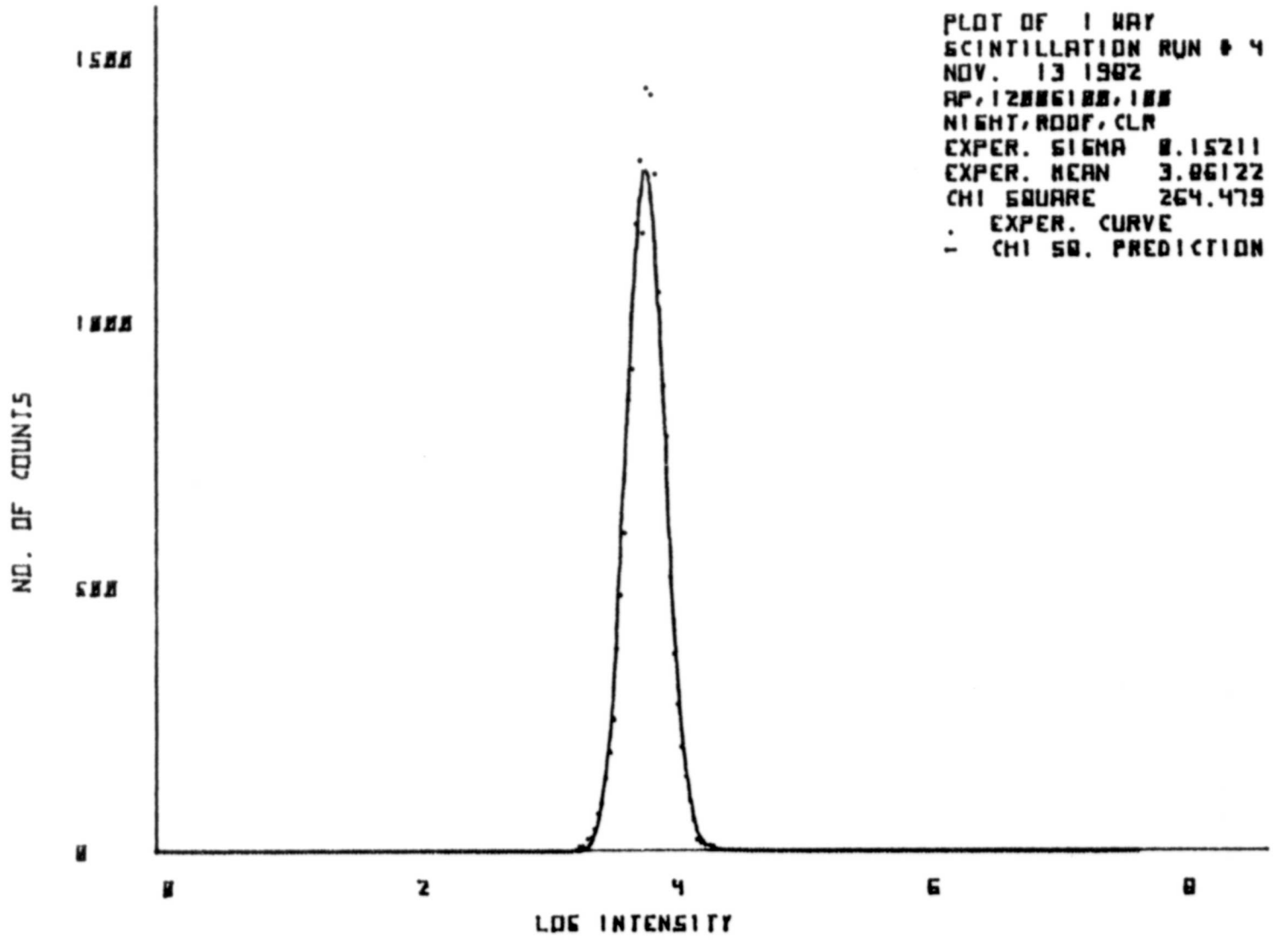

Figure 83. Scintillation Data and Theoretical Curve

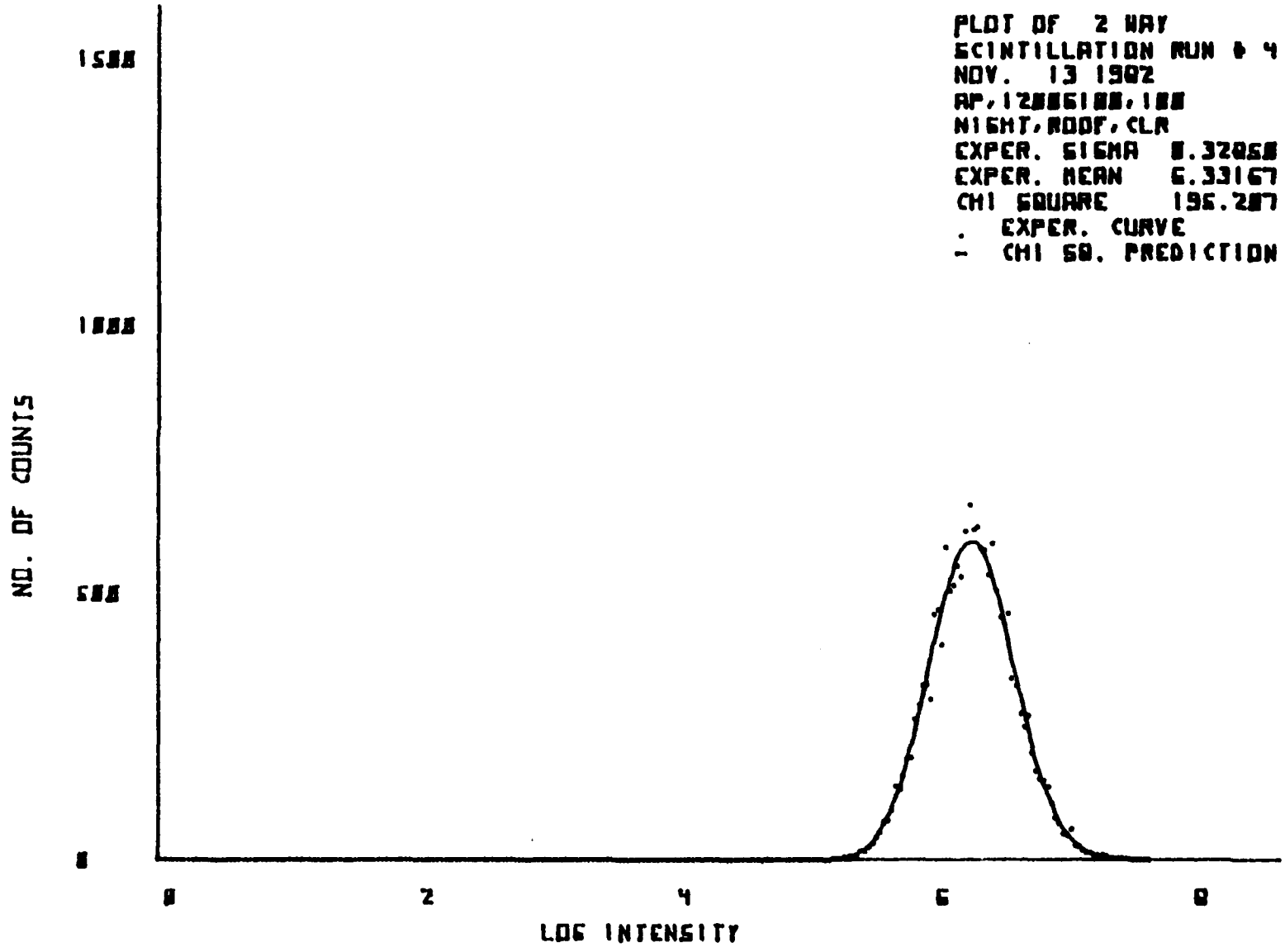

Figure 84. Scintillation Data and Theoretical Curve

NOV. 13 1982
Ap,1000,G200,1k300K,110
Night,clr,roof
wavelengtn= 6.33E-07 meters

Scintillation measurements of Sigma
16384 samples for each measurement
Fixed range= 40 meters

# pts	Sigma	Cni Square
1:16379	0.2205	6.11E 02**
1:16360	0.2979	1.41E 02
2:16384	0.1805	3.77E 02**
2:16376	0.2543	4.44E 02**
3:16360	0.2719	8.33E 02**
3:16288	0.3796	7.15E 02**
4:16347	0.2883	4.81E 02**
4:16262	0.4213	2.16E 02
5:16378	0.2063	4.33E 02**
5:16362	0.3164	3.68E 02**
6:16363	0.2332	1.08E 03**
6:16319	0.3313	7.67E 02**
7:16374	0.2104	4.55E 02**
7:16356	0.3154	1.61E 02
8:16381	0.2040	6.81E 02**
8:16375	0.2954	4.38E 02**
9:16380	0.1948	4.12E 02**
9:16372	0.2882	3.03E 02**
10:16385	0.1405	8.98E 02**
10:16383	0.1725	2.04E 03**
11:16384	0.1533	7.93E 02**
11:16382	0.1864	1.30E 03**
12:16383	0.1610	2.15E 02
12:16385	0.2053	1.75E 02
13:16377	0.2307	6.47E 02**
13:16361	0.3240	5.99E 02**
14:16382	0.2356	3.76E 02**
14:16371	0.3320	2.58E 02
15:16384	0.2204	5.75E 02**
15:16379	0.3132	4.06E 02**
16:16376	0.2471	3.58E 02**
16:16358	0.3434	1.67E 02

Figure 85. Scintillation Statistics.

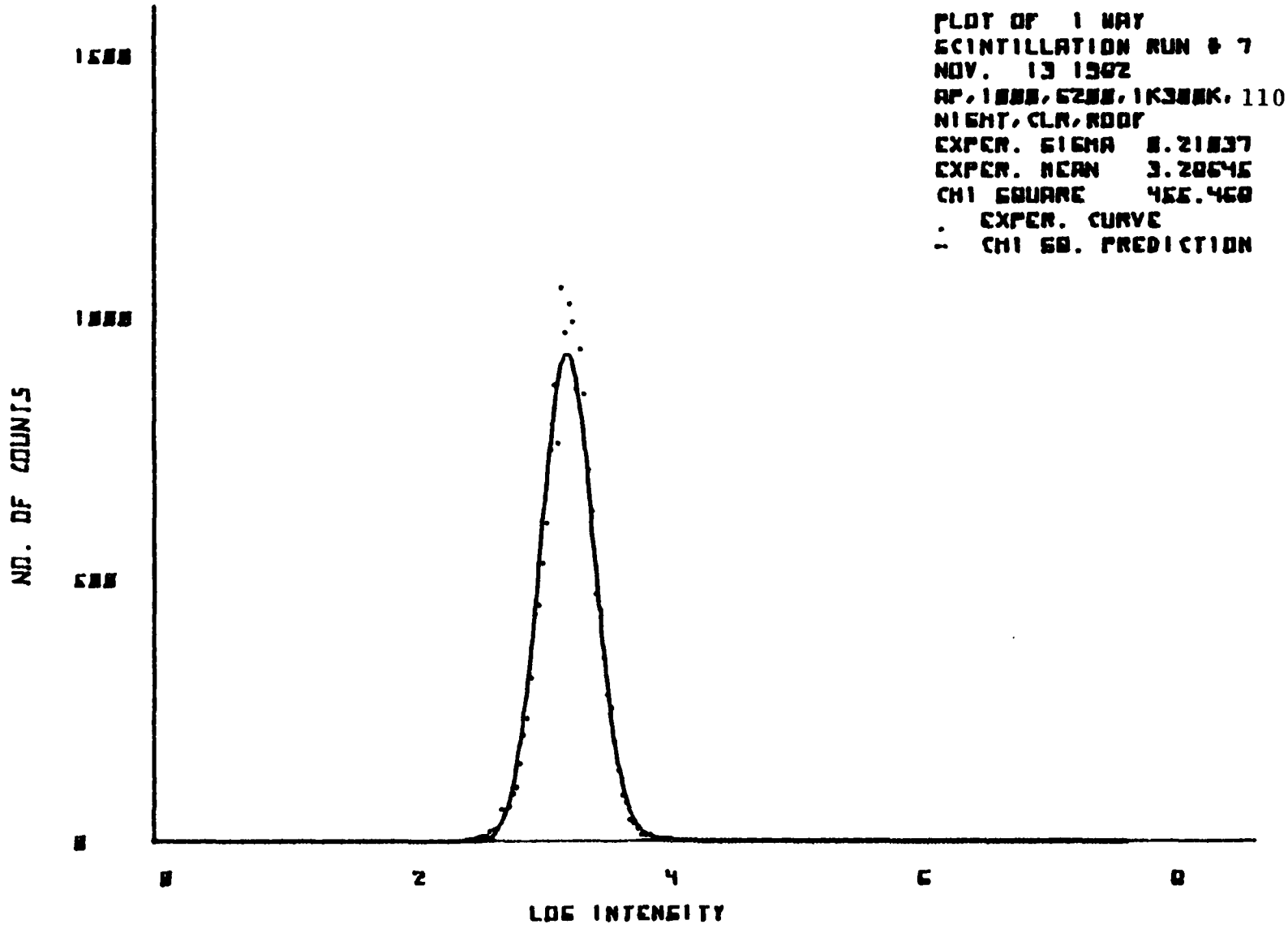

Figure 86. Scintillation Data and Theoretical Curve

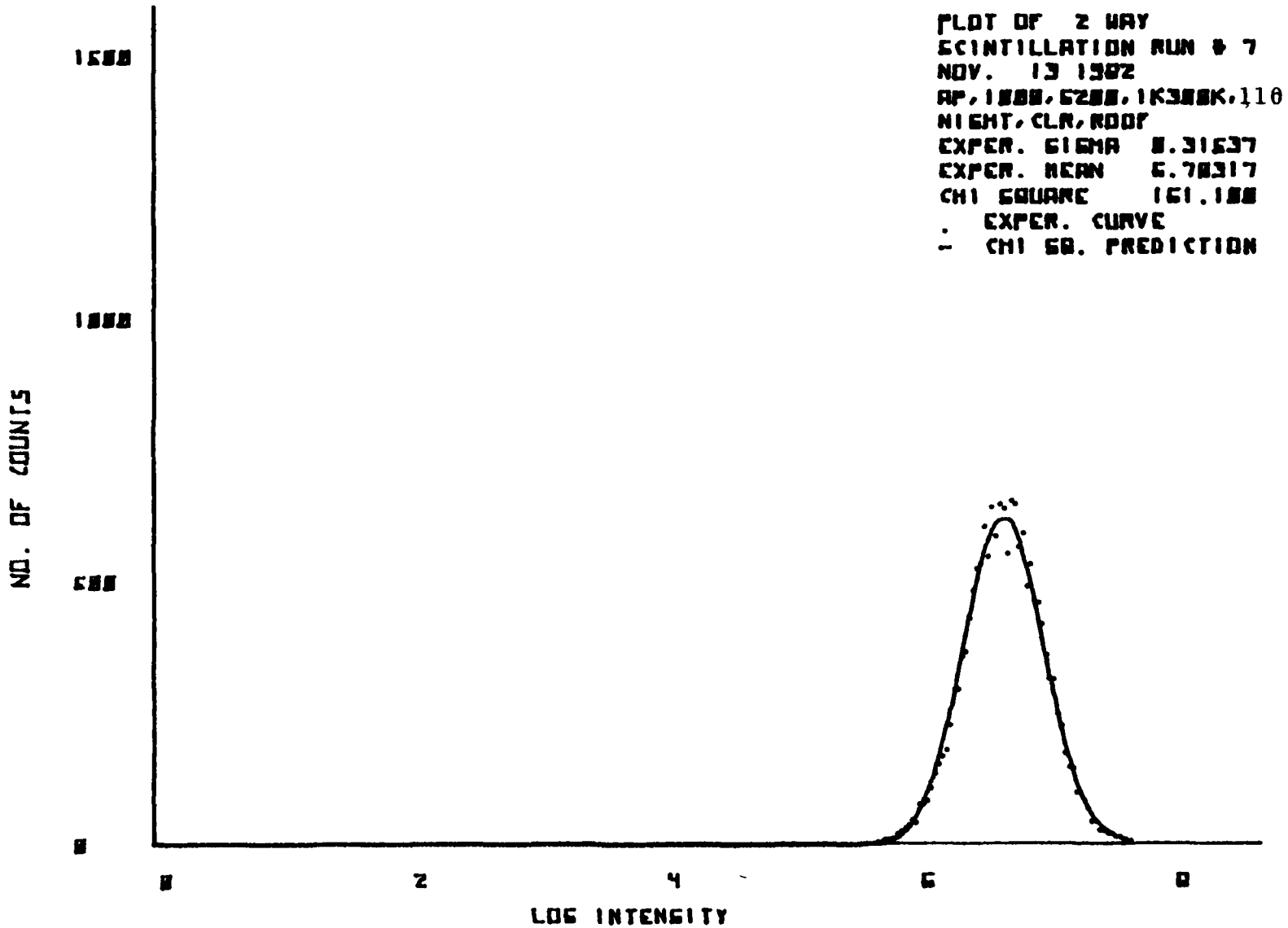

Figure 87. Scintillation Data and Theoretical Curve

NOV. 13 1982
Ap,1200G500,100,150
Night,clr,roor
Wavelength= 6.33E-07 meters

Scintillation measurements of Sigma
16384 samples for each measurement
Fixed range= 40 meters

# pts	Sigma	Chi Square
1:16384	0.1387	3.40E 02**
1:16384	0.3606	3.73E 02**
2:16385	0.1424	2.12E 02
2:16383	0.3727	3.53E 02**
3:16385	0.1220	1.48E 02
3:16383	0.3060	3.33E 02**
4:16385	0.0941	1.39E 02
4:16383	0.2423	4.11E 02**
5:16385	0.1020	1.97E 02
5:16383	0.2403	5.47E 02**
6:16385	0.1165	3.59E 02**
6:16383	0.2799	4.82E 02**
7:16385	0.1241	4.67E 02**
7:16383	0.2895	6.26E 02**
8:16384	0.1322	6.34E 02**
8:16382	0.3146	5.49E 02**
9:16383	0.1322	1.78E 02
9:16385	0.3226	4.91E 02**
10:16383	0.1277	2.45E 02
10:16385	0.3108	2.20E 02
11:16383	0.1090	1.96E 02
11:16385	0.2531	3.20E 02**
12:16383	0.1237	1.91E 02
12:16385	0.3059	3.03E 02**
13:16383	0.0993	2.21E 02
13:16385	0.2504	1.87E 02
14:16383	0.1011	2.80E 02
14:16385	0.2466	3.97E 02**
15:16383	0.0972	3.40E 02**
15:16385	0.2360	2.64E 02
16:16383	0.0991	7.94E 02**
16:16385	0.2382	4.18E 02**

Figure 88. Scintillation Statistics.

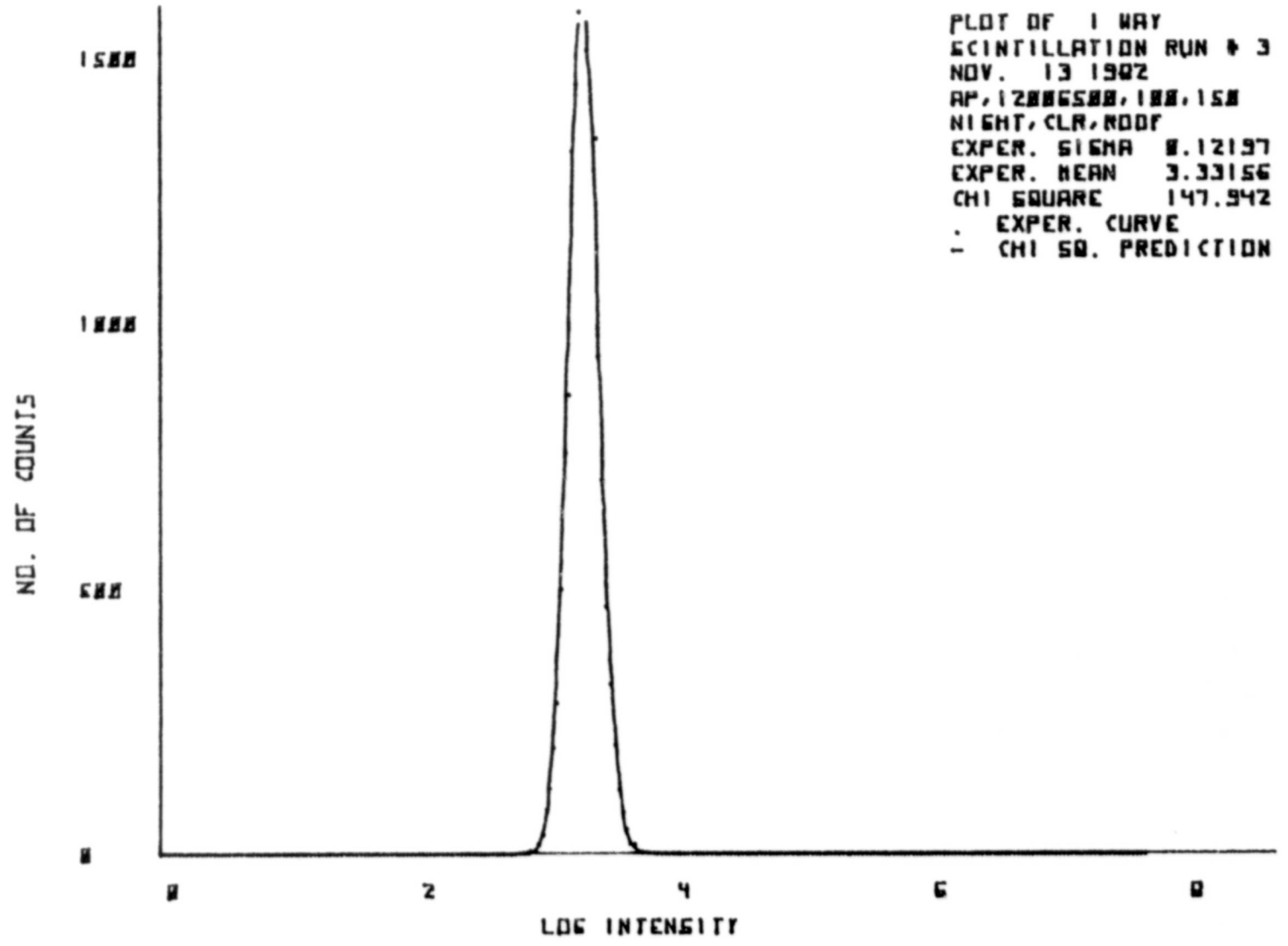

Figure 89. Scintillation Data and Theoretical Curve

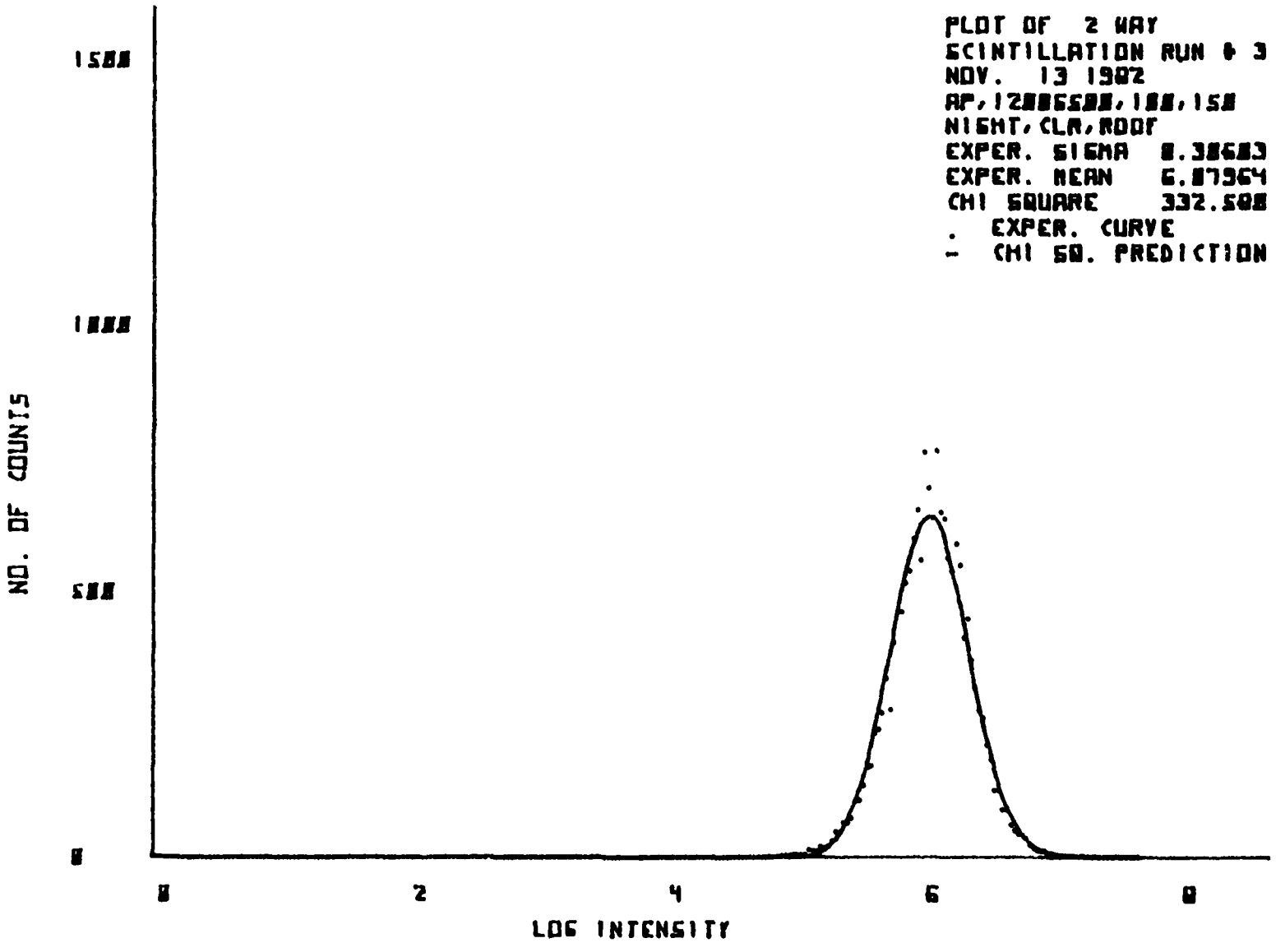

Figure 90. Scintillation Data and Theoretical Curve

APPENDIX F

DATA FROM THE THIRD EXPERIMENT

D(cm)	$\langle R \rangle \left(\left\langle \frac{\sigma F^2}{\sigma S^2} \right\rangle \right)$	Error $\left(\pm \frac{\sigma}{N} \right)$	Runs Utilized
5	2.01	.035	All four
10	2.46	.073	All
20	1.65	.018	All
30	2.24	.091	All
40	1.44	.050	All

```
NOV.  21 1982
Ap,1200,Glk,100,5
Night,ovc,root,stl
wavelength=    6.33E-07 meters


Scintillation measurements of Sigma
16384 samples for each measurement
Fixed range=     40 meters

    # pts        Sigma     Chi Square

   1:15842      0.2071    3.69E 02**
   1:15848      0.2906    2.90E 02**
   2:15799      0.2041    3.86E 02**
   2:15810      0.2979    5.45E 02**
   3:15816      0.2251    1.84E 02
   3:15830      0.3155    1.69E 02
   4:15831      0.2105    2.90E 02**
   4:15831      0.2961    1.48E 02
```

Figure 91. Scintillation Statistics

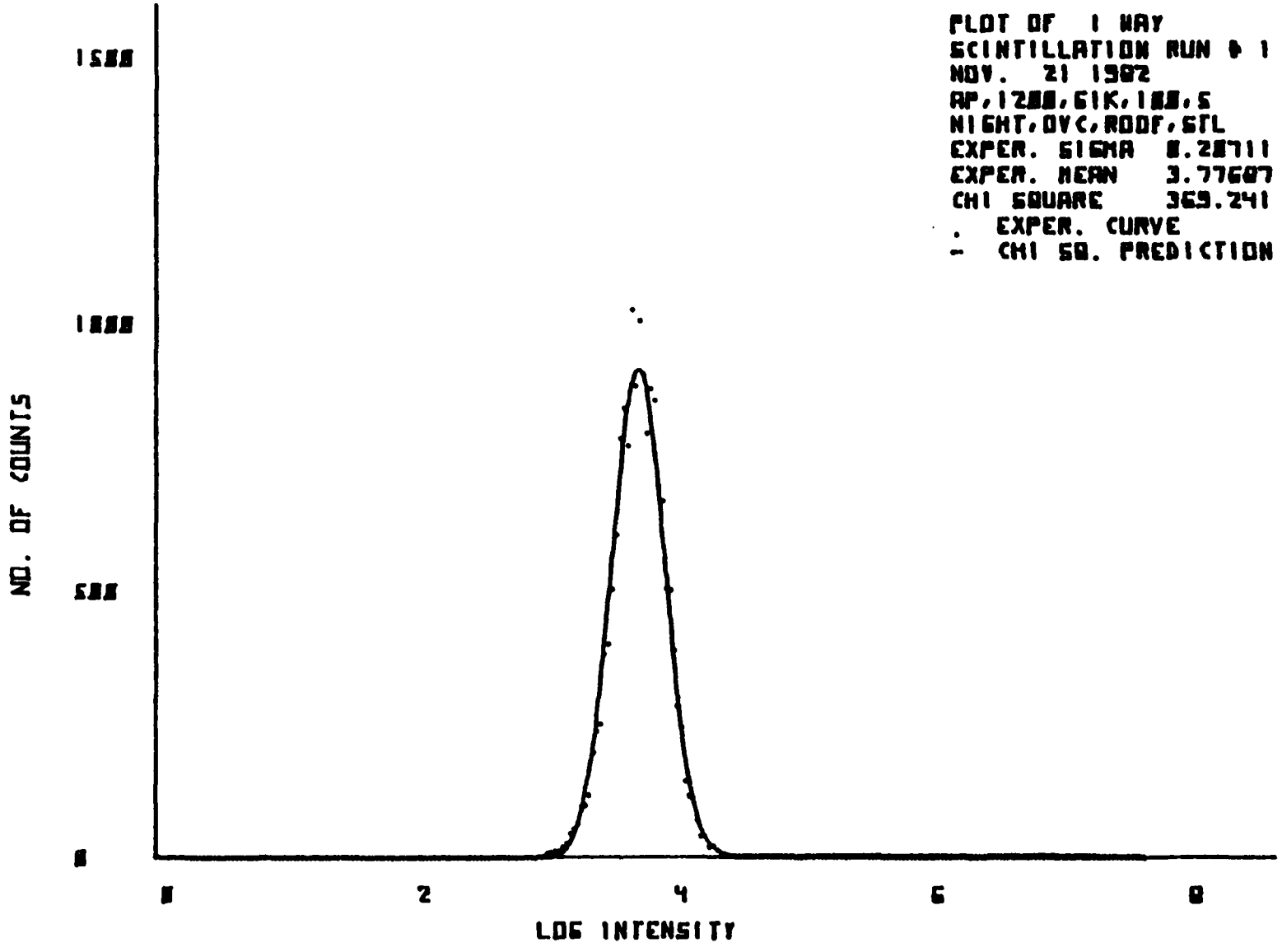

Figure 92. Scintillation Data and Theoretical Curve

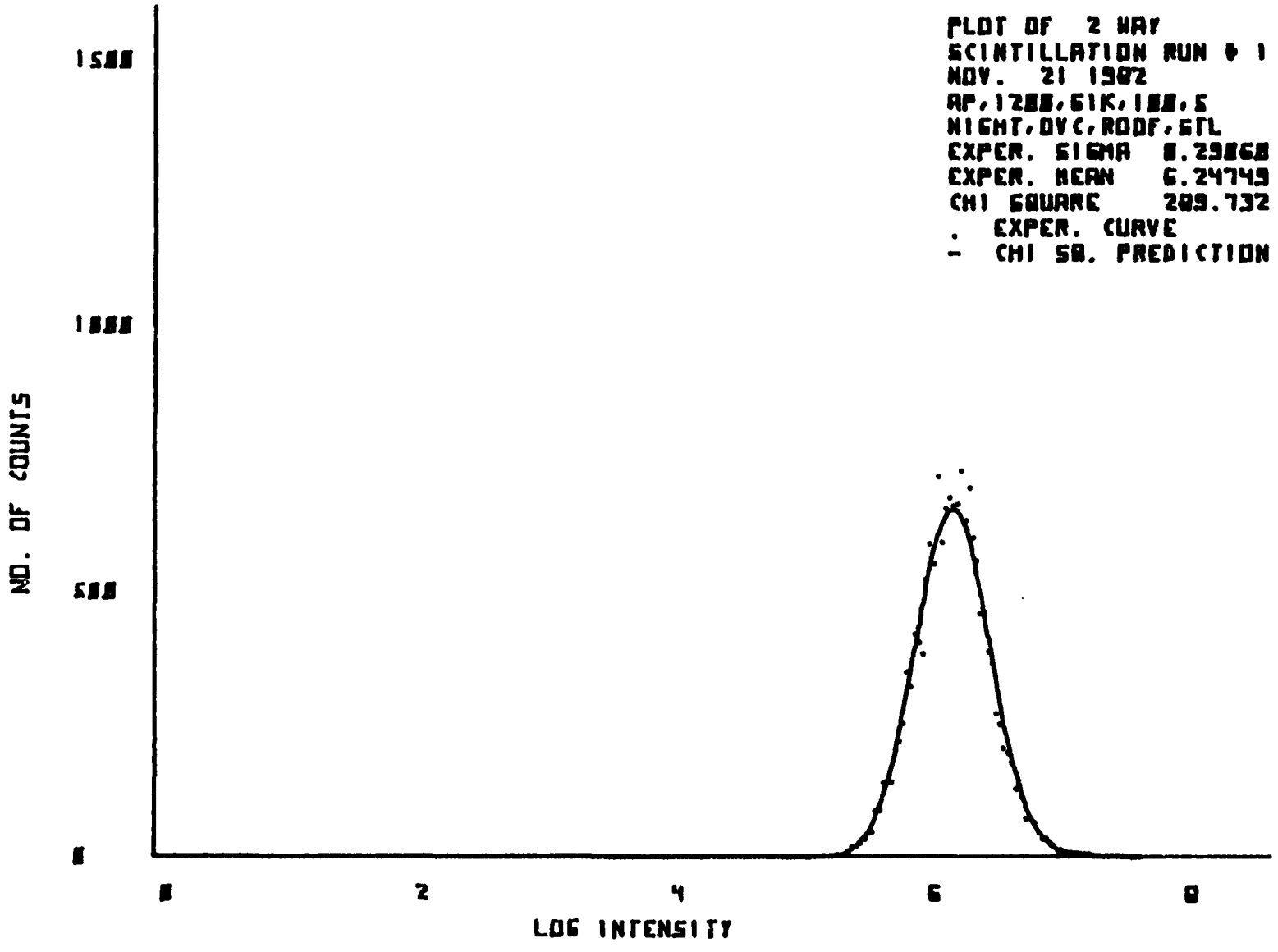

Figure 93. Scintillation Data and Theoretical Curve

NOv. 21 1982
Ap,1200,G1k,100,10
Night,cvc,root,st1
wavelength= 6.33E-07 meters

Scintillation measurements or Sigma
16384 samples ror eacn measurement
Fixed range= 40 meters

# pts	Sigma	Chi Square
1:15809	0.2038	3.71E 02**
1:15804	0.3226	2.61E 02
2:15816	0.1822	1.46E 02
2:15817	0.2865	1.78E 02
3:15844	0.2249	4.43E 02**
3:15846	0.3359	1.69E 02
4:15808	0.1927	3.08E 02**
4:15808	0.3128	2.77E 02

Figure 94. Scintillation Statistics

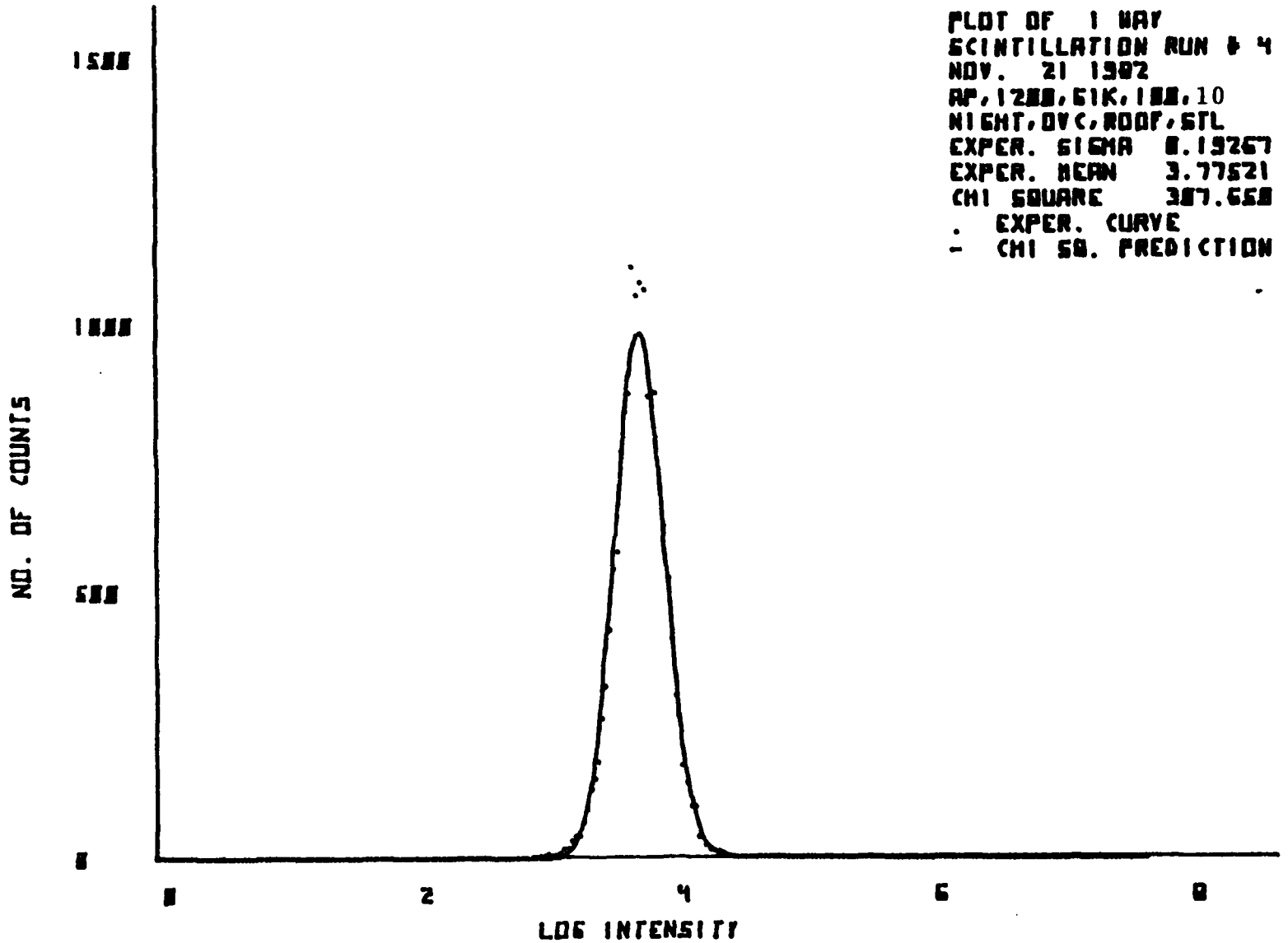

Figure 95. Scintillation Data and Theoretical Curve

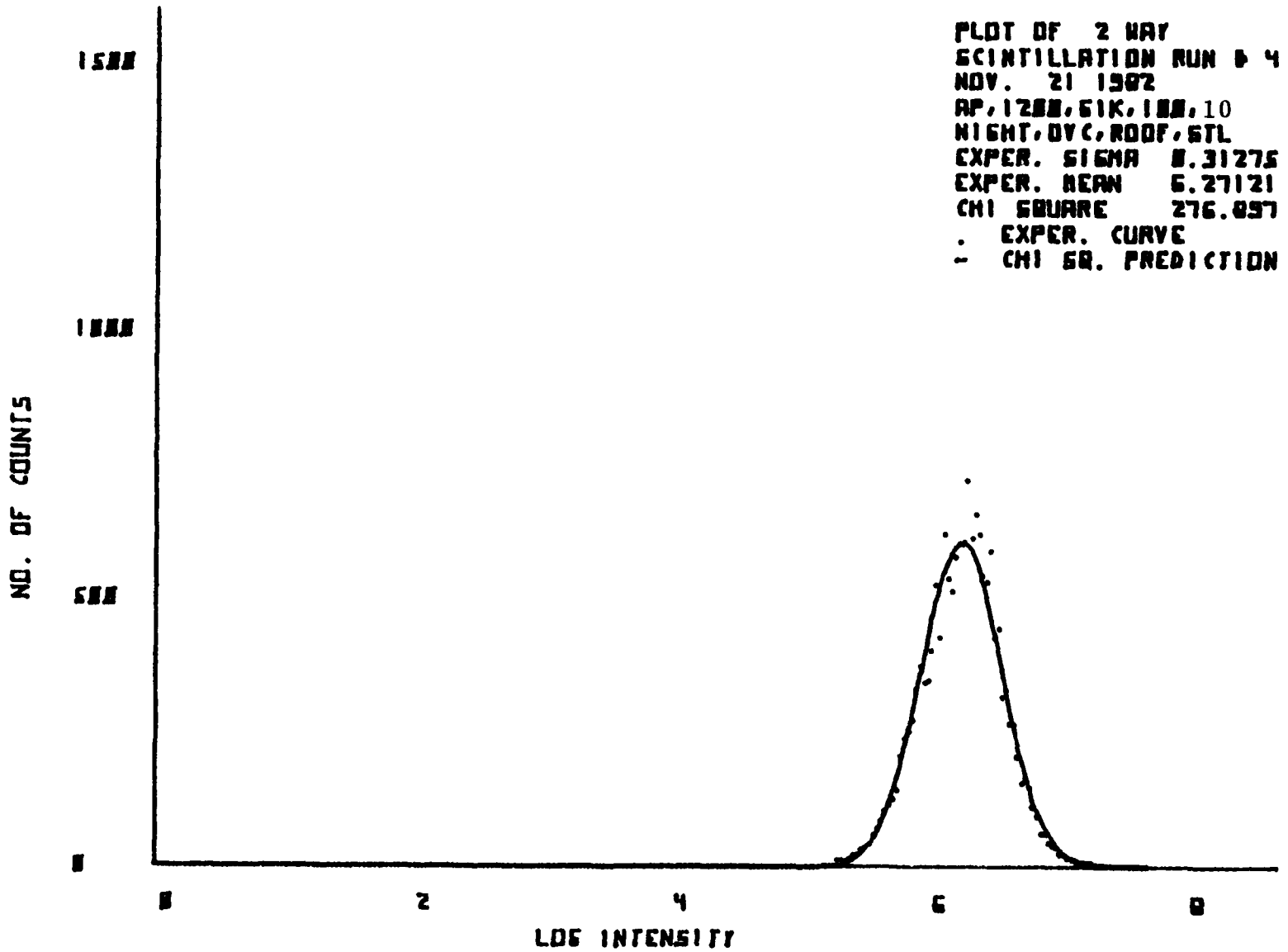

Figure 96. Scintillation Data and Theoretical Curve

NOV. 21 1982
Ap,1200,Glk,100,20
Night,ovc,root,stl
Wavelength= 6.33E-07 meters

Scintillation measurements or Sigma
16384 samples for each measurement
Fixed range= 40 meters

# pts	Sigma	Chi Square
1:15856	0.1767	3.77E 02**
1:15857	0.2250	5.65E 02**
2:15846	0.1794	2.43E 02
2:15849	0.2285	3.08E 02**
3:15854	0.1630	5.23E 02**
3:15856	0.2093	4.03E 02**
4:15843	0.1812	2.89E 02**
4:15844	0.2367	4.24E 02**

Figure 97. Scintillation Statistics

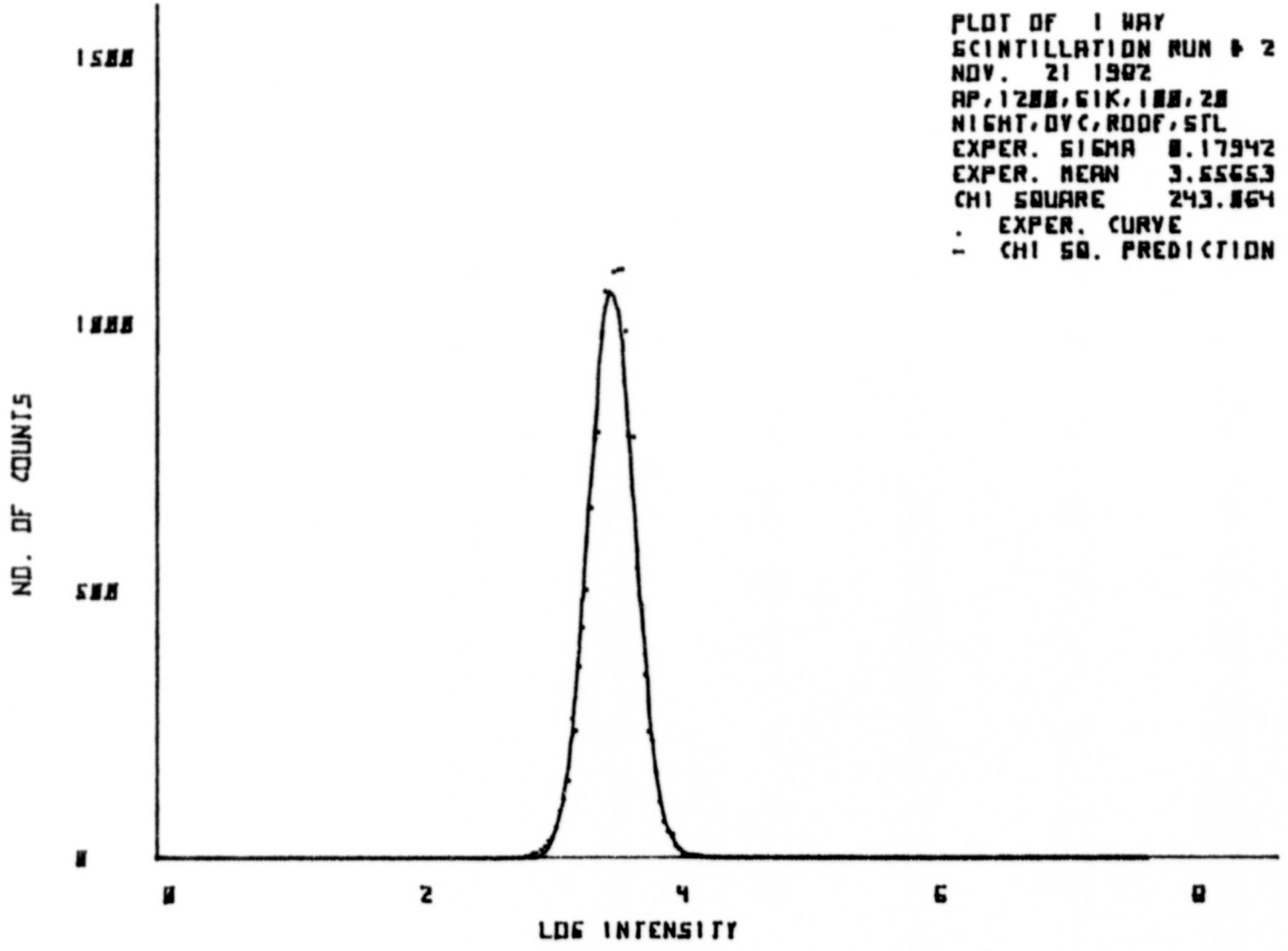

Figure 98. Scintillation Data and Theoretical Curve

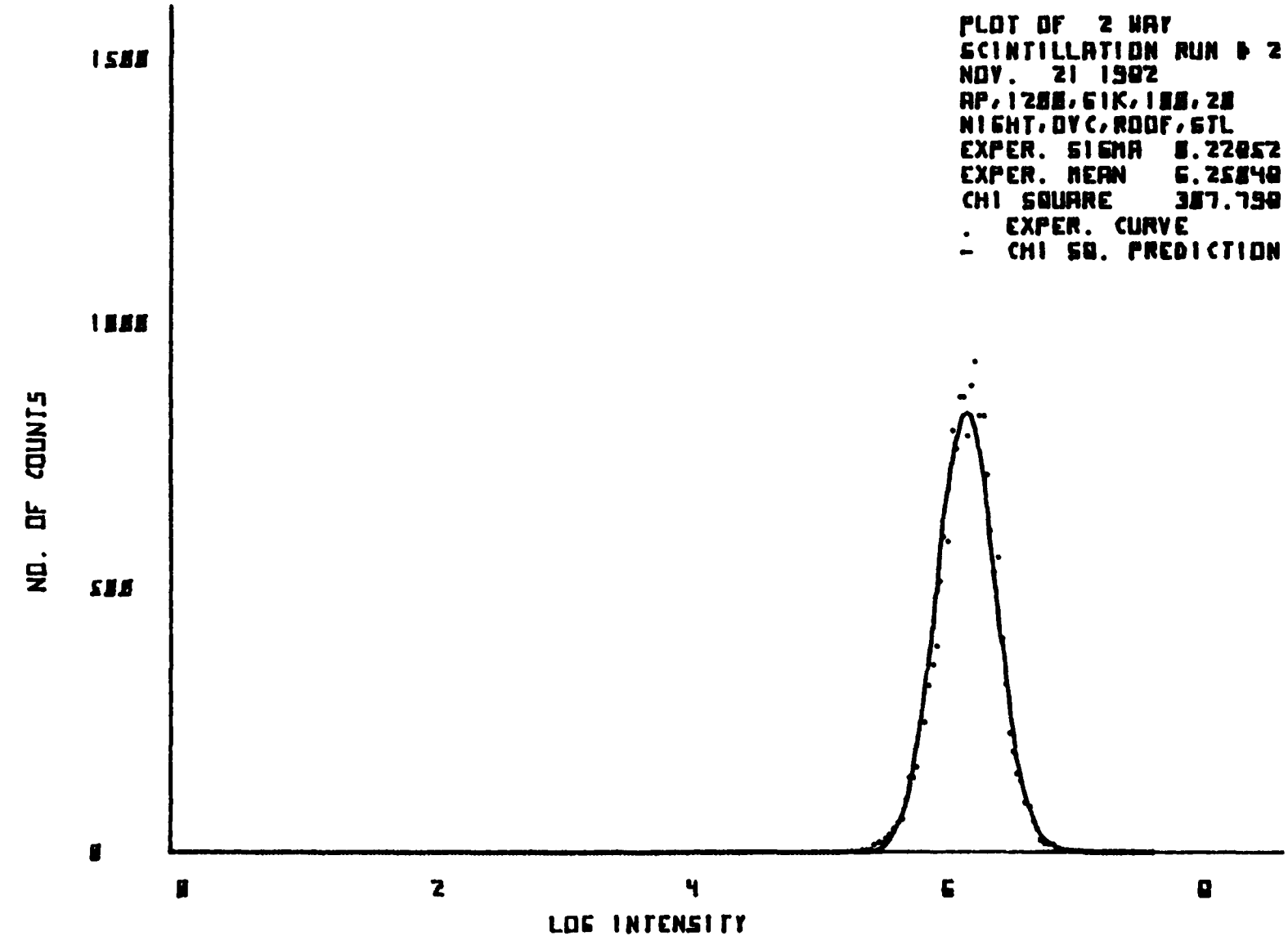

Figure 99. Scintillation Data and Theoretical Curve

NOV. 21 1982
Ap,1200,Glk,100,30
Night,ovc,root,stl
Wavelength= 6.33E-07 meters

Scintillation measurements of Sigma
16384 samples for each measurement
Fixed range= 40 meters

# pts	Sigma	Chi Square
1:15834	0.1801	2.35E 02
1:15835	0.2612	2.96E 02**
2:15850	0.2050	1.97E 02
2:15856	0.3195	4.55E 02**
3:15847	0.2064	2.02E 02
3:15846	0.3202	2.27E 02
4:15841	0.2070	1.83E 02
4:15841	0.2943	2.56E 02

Figure 100. Scintillation Statistics

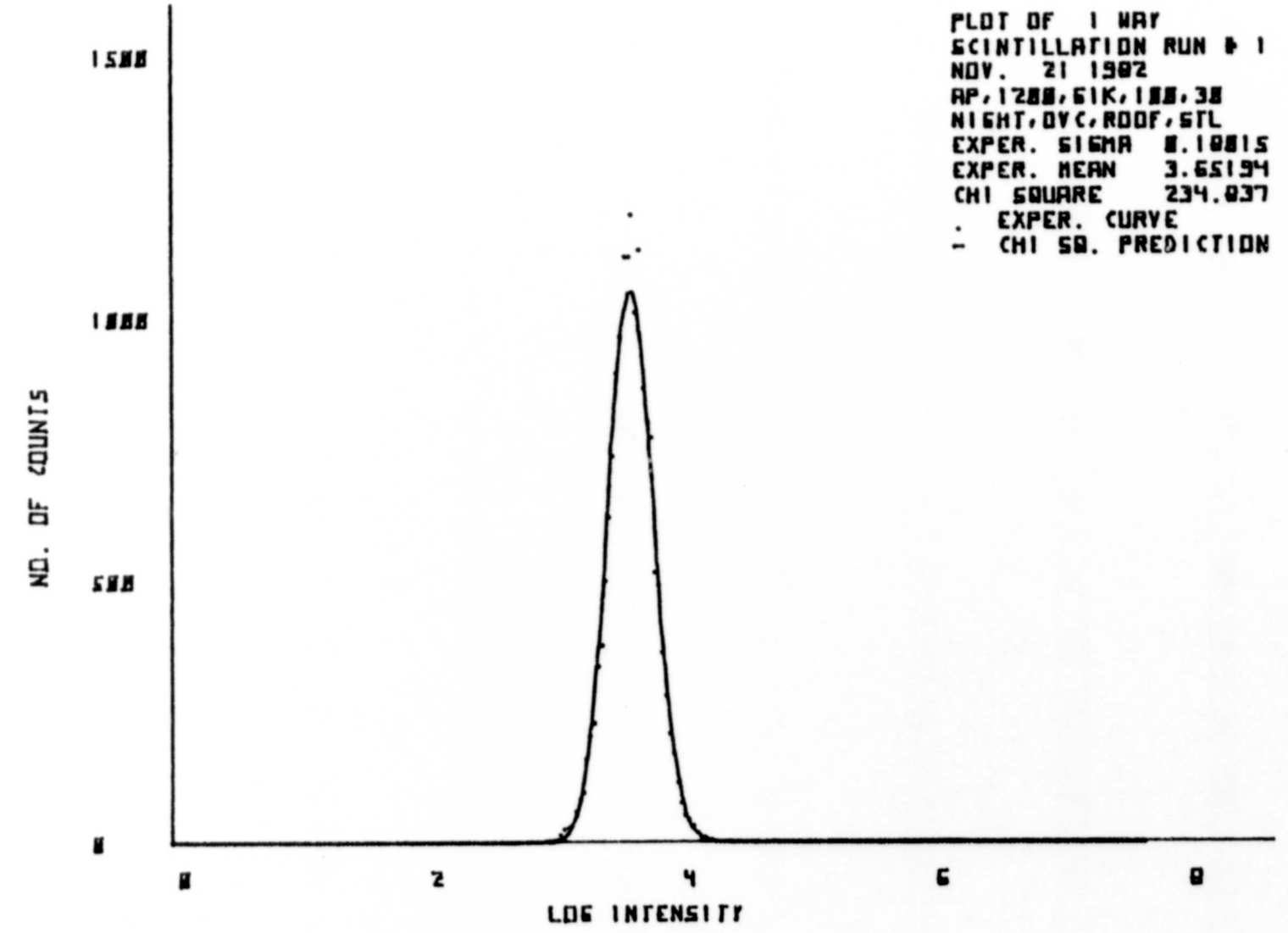

Figure 101. Scintillation Data and Theoretical Curve

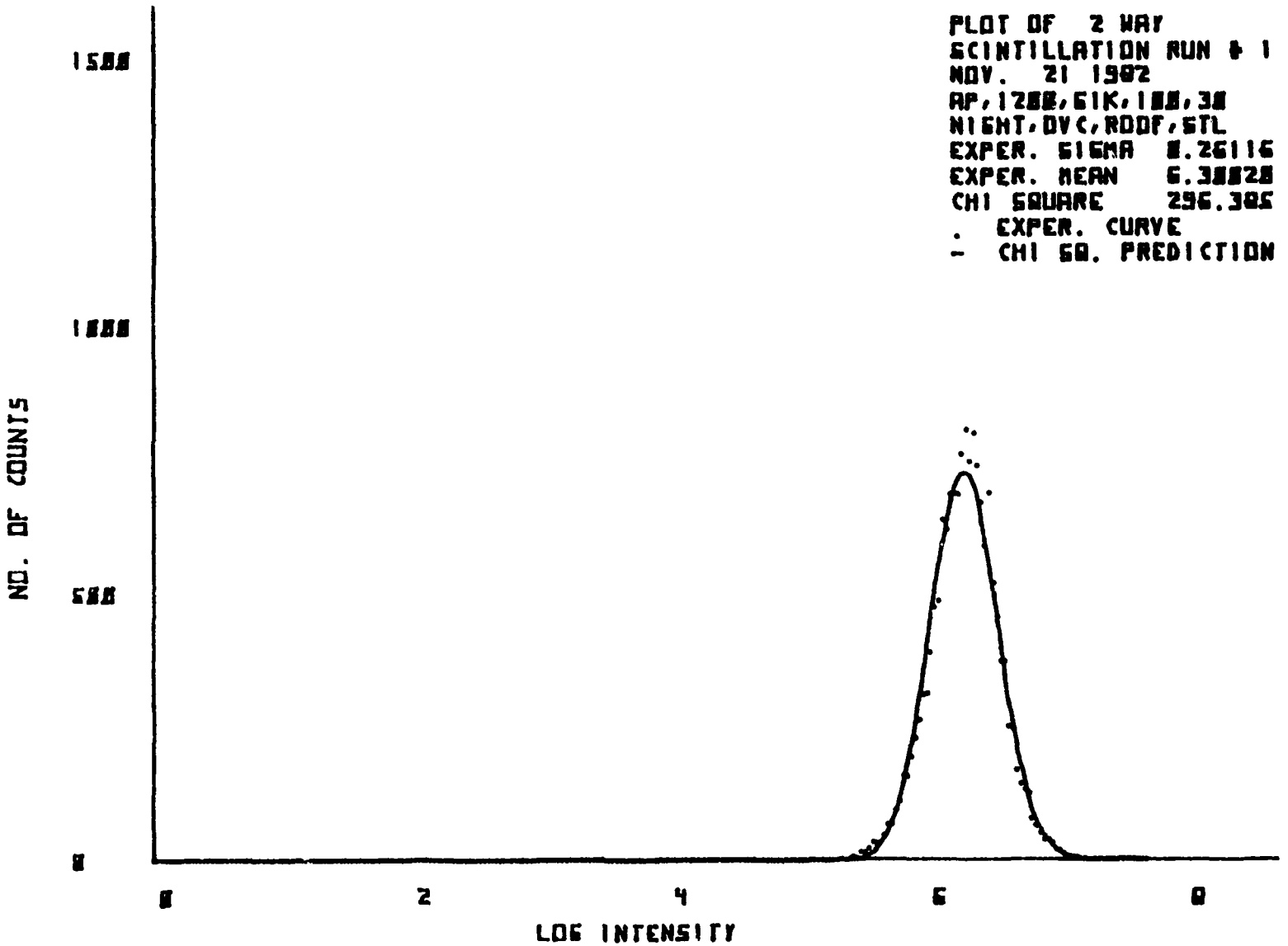

Figure 102. Scintillation Data and Theoretical Curve

NOV. 21 1982
Ap,1200,Glk,100,40
Night,ovc,rocr,stl
wavelength= 6.33E-07 meters

Scintillation measurements of Sigma
16384 samples for each measurement
Fixed range= 40 meters

# pts	Sigma	Chi Square
1:15851	0.2309	3.62E 02**
1:15850	0.2859	1.97E 02
2:15855	0.2383	4.22E 02**
2:15854	0.2826	1.53E 02
3:15851	0.2208	2.42E 02
3:15851	0.2773	3.13E 02**
4:15851	0.2244	8.09E 02**
4:15853	0.2703	6.08E 02**

Figure 103. Scintillation Statistics

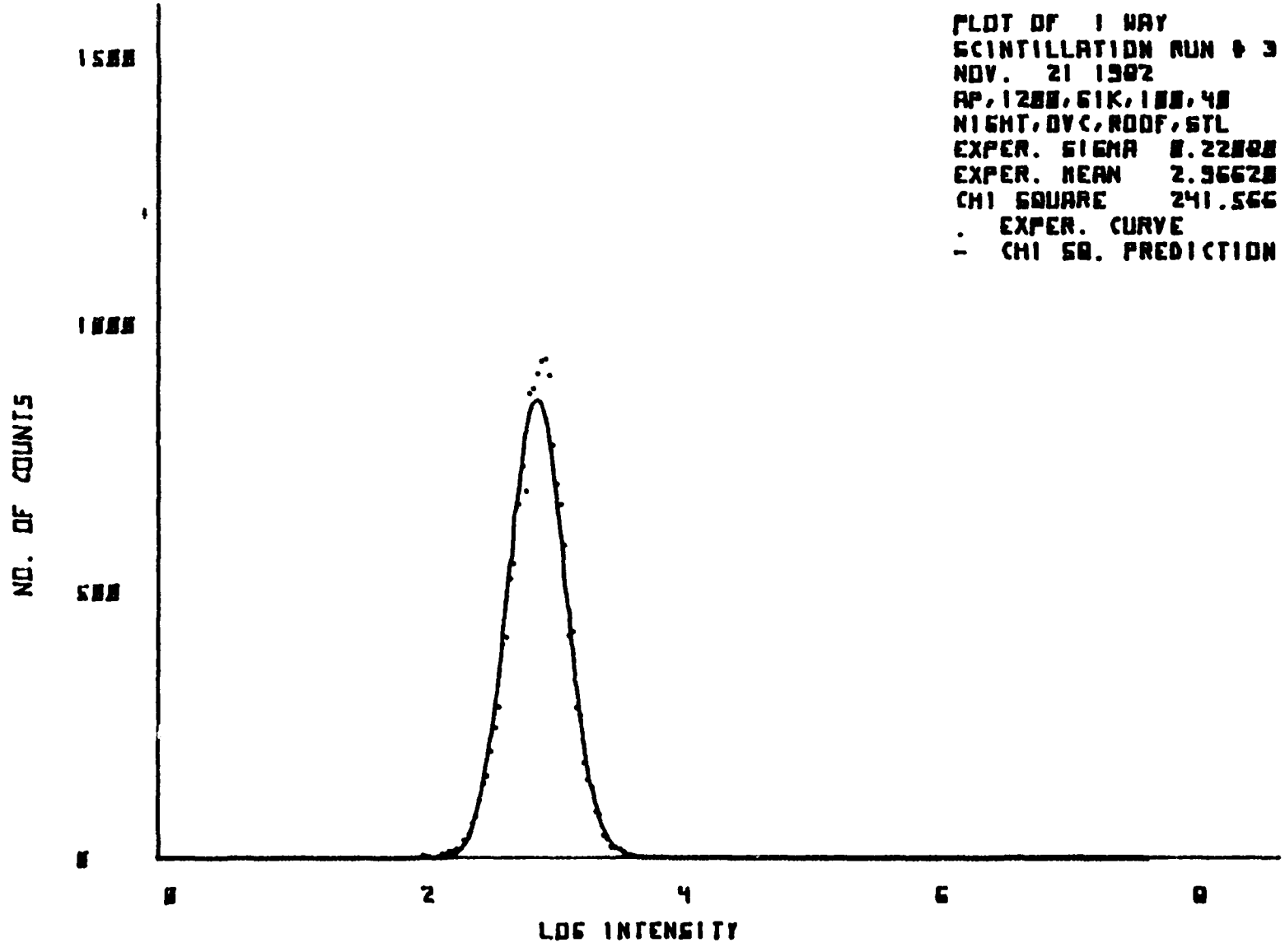

Figure 104. Scintillation Data and Theoretical Curve

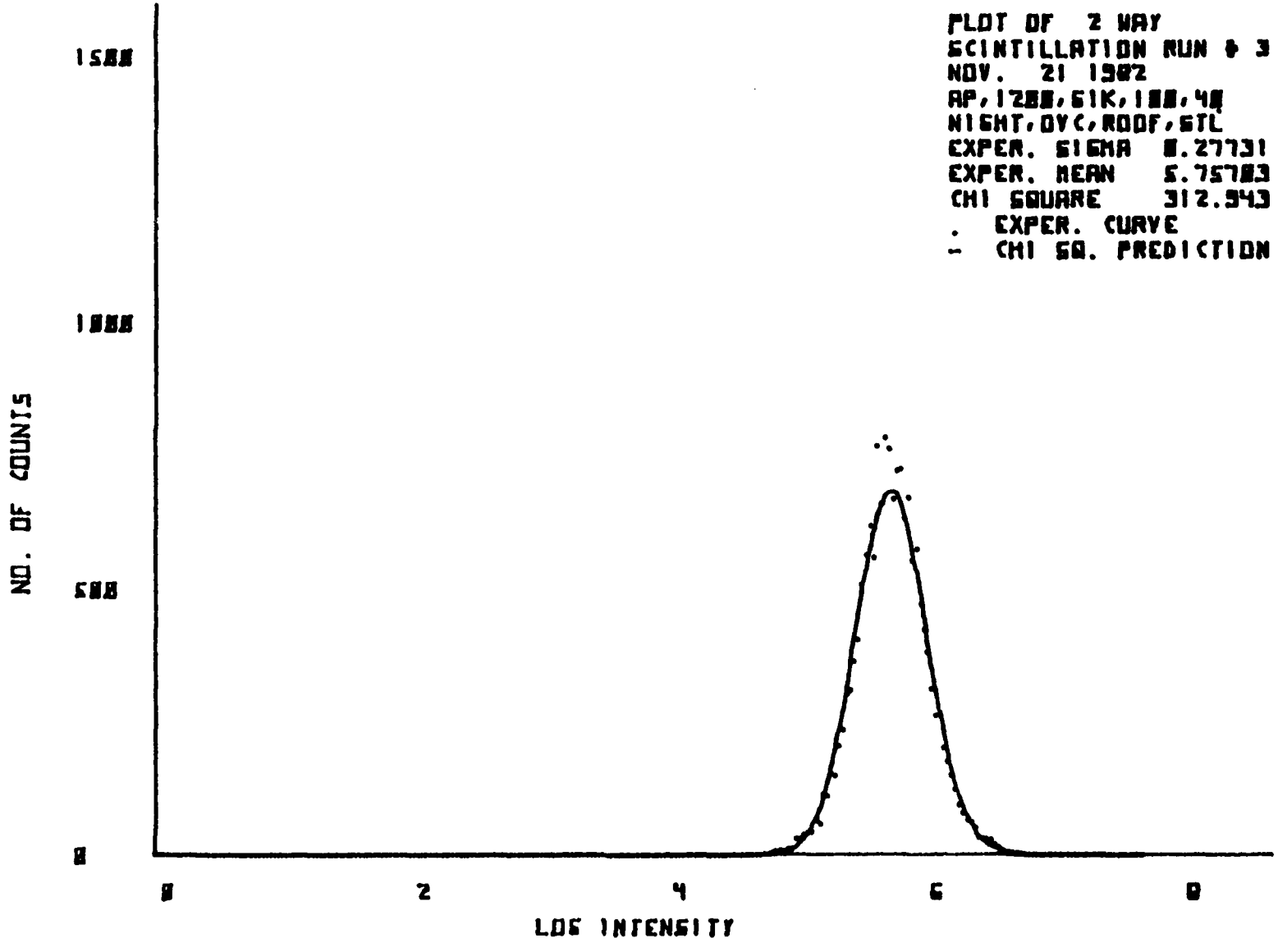

Figure 105. Scintillation Data and Theoretical Curve

LIST OF REFERENCES

1. Ze'evi, Avihu, Optical Scintillation Along Folded Paths, Ph.D. Thesis, Naval Postgraduate School, Monterey, March 1982.

2. Strohbehn, J. W., gen. ed., Topics in Applied Physics, v. 25, Springer-Verlag, 1978, "The Classical Theory of Wave Propagation in a Turbulent Medium", by S. F. Clifford.

3. Tatarski, V. I., The Effects of the Turbulent Atmosphere on Wave Propagation, Keter Press Binding, Israel, 1971.

4. Tatarski, V. I., Wave Propagation in a Turbulent Medium, McGraw-Hill, 1961.

5. Clifford, S. F., Ochs, G. R. Lawrence, R.S., "Saturation of of Optical Scintillation by Strong Turbulence", JOSA, v. 64, pp. 148-149, February 1974.

6. Hodgini, Thomas J., Optical Scintillation Measurements for Single and Folded Paths, Master's Thesis, Naval Postgraduate March 1982.

7. Larson, Harold J., Introduction to Probability Theory and Statistical Inference, Wiley, 1969.

INITIAL DISTRIBUTION LIST

		No. Copies
1.	Defense Technical Information Center Cameron Station Alexandria, Virginia 22314	2
2.	Library, Code 0142 Naval Postgraduate School Monterey, California 93940	2
3.	J. N. Dyer, Chairman, Code 61Dy Department of Physics Naval Postgraduate School Monterey, California 93940	2
4.	E. C. Crittenden, Jr., Code 61Ct Department of Physics Naval Postgraduate School Monterey, California 93940	2
5.	Professor E. A. Milne, Code 61Mn Department of Physics Naval Postgraduate School Monterey, California 93940	2
6.	G. W. Rodeback, Code 61Rk Department of Physics Naval Postgraduate School Monterey, California 93940	2
7.	LT B. A. Speer 6703 Verde Ridge Road Rancho Palos Verdes, California 92074	3
8.	LT F. H. Parker 339 Castlewood Ct. Hampton, Virginia 23669	3